IMPROVING PERFORMANCE OF WATER-BASED DRILLING FLUID BY OPTIMIZATION OF BARITE NANOPARTICLE SIZE AND CONCENTRATION

By

SAMAN AKHTARMANESH

Bachelor of Science in Petroleum Engineering
Amirkabir University of Technology
Tehran, Iran
2009

Master of Science in Drilling and Production Engineering
Amirkabir University of Technology
Tehran, Iran
2012

Submitted to the Faculty of the
Graduate College of the
Oklahoma State University
in partial fulfillment of
the requirements for
the Degree of
DOCTOR OF PHILOSOPHY
May, 2018

IMPROVING PERFORMANCE OF WATER-BASED DRILLING FLUID BY OPTIMIZATION OF BARITE NANOPARTICLE SIZE AND CONCENTRATION

Dissertation Approved:

Dissertation Adviser – Dr. Geir Hareland

Dr. Josh Ramsey

Dr. Prem Bikkina

Dr. Brian R. Elbing

ACKNOWLEDGEMENTS

I would like to express my sincere gratitude to my advisor Prof. Geir Hareland for the continuous support of my Ph.D study and my research, for his patience, motivation, and immense knowledge. His guidance helped me in all the time of research and writing of this thesis. I could not have imagined having a better advisor and mentor for my Ph.D study.

Name: SAMAN AKHTARMANESH

Date of Degree: JULY, 2018

Title of Study: IMPROVING PERFORMANCE OF WATER-BASED DRILLING FLUID BY OPTIMIZATION OF BARITE NANOPARTICLE SIZE AND CONCENTRATION

Major Field: CHEMICAL ENGINEERING

Abstract: This study investigates the influence of adding barium sulfate nanoparticles (NPs) on the performance of water based drilling fluids. Fluid loss, lubricity, fracture pressure and the performance of lost circulation materials (LCM) with the use of NPs were the main domains that were studied. One of the main objectives was to investigate the effect of NPs size distribution and concentration in different weighted water-based drilling fluid systems to minimize filtration into the different porous media. Filtration behavior was studied by changing different variables to develop a model for three drilling fluid compositions, and a predictive model was developed to predict fluid loss. Based on the results of hydraulic fracturing, a predictive model was developed to predict fracture pressure based on permeability and fluid loss reduction. The coefficient of friction of the water based drilling fluids was studied with and without NPs and the results show that using barite NPs improves lubricity. Barite NPs in water based drilling fluid also improve the performance of LCM in the presence of other solid materials. The overall findings demonstrate that improvement of water based drilling fluid performance is achievable by adding barite NPs even at the low concentrations.

TABLE OF CONTENTS

Chapter Page

LIST OF TABLES

Table Page

Table Page

LIST OF FIGURES

Figure Page

Figure Page

CHAPTER I

INTRODUCTION

Drilling fluid plays many important roles in accomplishing a successful drilling operation in a safe manner. Drilling fluid is used to facilitate the drilling process by serving different functions such as cutting transport (transferring cuttings from bottom hole to surface), suspending cuttings (during connecting drill pipe stands or other drilling fluid circulation halts), cooling off and lubricating drill bit and bottom hole assembly (BHA), providing hydrostatic pressure and support to avoid wellbore instability. In troublesome formations such as shales and fractured zones, it is important to choose and design the drilling fluid system properly to avoid costly wellbore instability and other fluid loss consequences. Besides formation lithology, wellbore geometry, in situ stresses, and formation fluid properties, might dictate special design for the drilling fluid system. Wellbore instability and fluid loss are two major problems that occur due to poor drilling fluid system design in troublesome formations. Drilling fluid loss could occur as a partial or as a complete loss, and in addition to the cost of mud; serious consequences are expected due to the filtrate absorption by the formation. To solve these problems, drilling fluids are normally formulated with fluid loss control (FLC) materials. FLCs are used in drilling fluid to reduce or prevent partial fluid loss into the permeable formations. FLCs, by increasing viscosity and generating a barrier on the surface of formation, reduce the filtration rate and volume of drilling fluid invasion into some native formations, micro fractures or larger openings in permeable formations. Lost circulation materials (LCM) on the other hand, are designed to reduce drilling fluid loss by physically plugging or sealing off macro fractures or larger pore openings.

Unfortunately, these solutions do not work for shale formations due to the very low permeability and low pore throat size of shale. Due to the physicochemical properties of these micro and macro-sized FLC and LCM additives, these materials do not reduce filtrate invasion into the shales. To tackle the above-mentioned problem, many studies have been performed on both improving chemical potential of drilling fluid/shale (by reducing water activity of drilling fluid) as well as the physical plugging mechanism. Shale membrane efficiency is defined as the capability of shale in preventing ions from moving through its pores, while providing a path for water molecules to go through it from one side to the other side. Al-Bazali et al., (2006) tested four different shale samples using different salts and concentrations. The authors concluded that membrane efficiency for the shale samples ranged from 0.18 to 4.23 %. By conducting pressure transmission tests, Osuji et al. (2008), concluded that Atoka shale membrane efficiency ranged from 0.4 to 13 percent. More than 85% of the reported results show membrane efficiencies of less than 7 percent, which indicates shale membrane significantly deviates from the ideal membrane. Very low shale membrane efficiency directed researchers to focus on physical plugging capacity on solving water invasion problem in shales. Due to their small size and large surface area to volume ratio, nanoparticles (NPs) were selected to be used in drilling fluid to mitigate shale problems. NPs could also help to bridge empty gaps between macro FLCs and LCMs, and therefore provide an effective seal to the formation with larger pore throat size. Sensoy et al. (2009) suggested that using NPs to seal off pore throats of shales, and subsequently minimizing fluid penetration into these water-sensitive formations, can result in better wellbore stability. Therefore, NPs could be a promising option for the development of drilling fluids to provide effective sealing, bridging, and cementing properties, resulting in the reduction of porosity and permeability of the wellbore formations, and thereby preventing the loss of fluid. In an over-balanced drilling condition, by reducing filtrate invasion into a formation, the pore pressure build-up rate decreases, and subsequently compressive and tensile strength increase. The process of increasing the wellbore pressure containment using engineered drilling fluids is called “wellbore strengthening”.

Although many studies have been conducted to investigate the application of NPs in drilling fluids to control shales, there are very limited studies on possible benefits of using a combination of NPs and FLCs or LCMs in wellbore strengthening of rocks with higher permeability. The process of permeability reduction using a combination of NPs and FLCs or LCMs has not been understood and correlated, and fracture pressure increase has not been modeled based on permeability and fluid loss reduction.

The primary objective of this study was to investigate the effect of nanoparticles (NPs) size and concentration in different weighted water-based drilling fluid systems to minimize filtration into different porous media. Based on permeability and pore throat size, appropriate NPs size and concentration were studied and optimized. Hence, this study could be a key part of actual drilling fluid system pre-planning, especially in off-shore and deep-water drilling projects. The second objective was to develop a new correlation between the permeability of different filter media as a function of time and filtrate flow when they come in contact with water-based drilling fluids containing NPs. The model includes the initial medium permeability and will predict permeability as filter-cake is being generated on the medium. The third objective was to develop a model to predict break down pressure as a function of permeability and fluid loss volume. This goal focuses on the wellbore strengthening criteria. Based on the presented wellbore strengthening model, it is possible to increase the fracture gradient using a small concentration of barite NPs to generate a wider mud window. Having a wider mud window could result in a reduced number of casing strings required to complete a well, which can reduce the total cost of drilling a well. The forth objective of this study was to study the effect of combining barite NPs and LCMs on the sealing pressure. This goal focuses on controlling a lost circulation situation by adding LCM and NPs to the drilling fluid. The number of needed casings decrease by sealing off fractures and highly permeable intervals and providing higher sealing pressure during drilling operation. This approach can reduce total drilling time and cost as well as proving a wider bore hole at the target formation.

This thesis consists of six chapters. More specifically, chapter one provides an introduction to the topics and objectives of the thesis. Chapter two includes background and literature review of previously published research about shale membrane efficiency and NPs application in water-based drilling fluid systems. This chapter also discusses permeability models developed for porous media and filter-cake permeability. A thorough literature review of the fracture initiation pressure models and fracture gradient pressure criteria is also discussed in this chapter. Chapter three expounds the methodology of experimental procedures related to synthesizing NPs, designing the base drilling fluids, static and dynamic filter press tests, and lubricity tests, as well as statistical analysis of the data using an artificial neural network (ANN) and a differential evolution algorithm to find optimal model parameters. In Chapter Four, experimental results are presented. Chapter Five discusses analyzing and validating the newly developed models for permeability and breakdown pressure prediction. An offshore oil well in Gulf of Mexico was studied to investigate the effect of reducing fluid loss using NPs and possibility of using less number of casing while ensuring a safe path to the target formation. Chapter six presents the conclusion of this study and provides suggestions for future works.

CHAPTER II

BACKGROUND AND LITERATURE REVIEW

2.1 Objective formations

Non-productive shale formations could be a potential threat to borehole stability and integrity. Shales hydrate easily when exposed to water, and water absorption is the main cause of shale instability for both soft and hard shales. Shale may swell or slump, which can result in a tight hole, poor hole conditions, or a stuck drill string. Water adsorption by sloughing shales causes a reduction in compressive and tensile strength, and leads to ultimate shale failure. Clays are the basic constituent of shales, and some of the clay minerals such as Montmorillonite and Illite, have a chemically active nature. Active clay particles may disperse in the drilling fluid and contaminate it, which could result in drill bit balling up and low-quality well logging and cementing jobs.

Typically, oil-based muds are the easiest choice to overcome shale instability for two reasons. First, the hydrocarbon molecules are bigger than water molecules, and therefore need higher capillary pressure to enter small shale pores and invert emulsion muds. As long as the emulsion is stable, a good osmotic membrane exists (Ewy and Morton, 2008). Second, hydrocarbon molecules are non-polar and do not cause shale swelling problems. Oil-based muds have functional advantages over the conventional water-based muds for drilling shale formations, and are considered as the desired option for drilling directional wells when handling wellbore instabilities that are more complicated. However, the easiest solution comes with expensive consequences. Fluid loss of oil-based mud can today cost drilling operators up to 200 USD per barrel. Due to environmental protection regulations,

oil-based mud and oily drilled cuttings have to be treated and decontaminated to zero-oil discharge standard before disposal.

Drilling fluid loss is defined as the partial or complete loss of drilling fluid during the drilling operation. Besides the cost of the drilling fluid system, loss of drilling fluid can cause serious problems if drilling fluid circulation is lost. Hence, preventing near-wellbore pore pressure increase is always an important deliberation for mud engineers when designing drilling fluid systems. Figure 1 illustrates how hydrated clay will stick to the bottom hole assembly (BHA) and the drill bit, which could then obstruct the drilling operation.

Figure 1. Hydrated clay sticks to BHA and results in a balled up bit

Other than oil-based muds, the better option is to use improved water-based drilling fluid systems, which have the required properties to deal with shale instability while being environmentally acceptable. Using different types of polymers such as partially hydrolyzed polyacrylamide (PHPA), polyanionic cellulose (PAC), or polyethylene glycol (PEG), and other soluble salts such as NaCl,

calcium chloride ($CaCl_2$) or sodium silicate are important steps in improving water-based drilling fluid systems to compete with oil-based mud in handling the shale instability problem.

Other permeable formations such as sandstones, calcite, and dolomite, or even fractured zones are also considered as objective formations of this study, because mud filtration into these permeable zones could result in thick mud cake that may cause differential pressure sticking and stuck pipe problems. Figure 2 shows the mechanical wellbore instabilities in different types of formations.

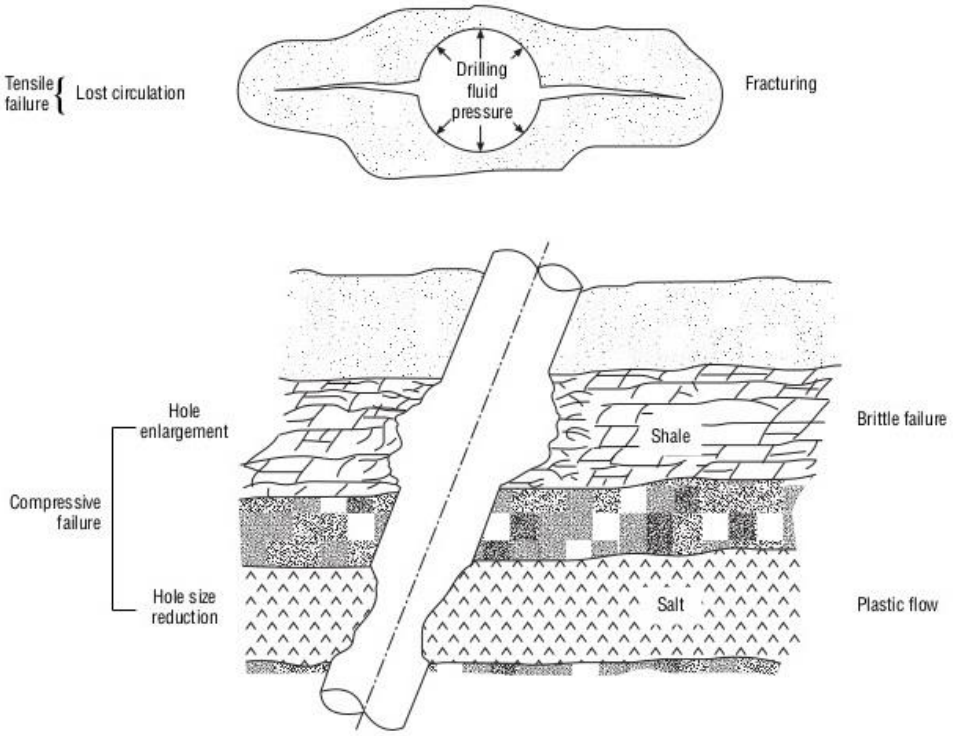

Figure 2. Mechanical wellbore instabilities (MI SWACO drilling fluid manual)

Drilling fluid filtration into permeable formations causes an increase in pore fluid pressure. According to the tensile fracturing criterion, increasing pore fluid pressure reduces fracture initiation pressure, which can result in tensile failure of the wellbore and formation breakdown. All of the mentioned problems are directly or indirectly related to fluid loss, which dictates minimizing filtration to achieve better wellbore stability and avoid more expense.

2.2 Osmosis and chemical potential

Shales are made of clay minerals that are stacked on top of each other and are compressed under the overburden pressure. The molecular structure of clay minerals is like thin sheets made by lattices of alumina and silica, and usually displays negative electrical surface charges when dry. When clay minerals come in contact with water, Al^{3+} ions can be exchanged by cations such as Ca^{2+}, Mg^{2+}, K^{+}, and H^{+} that are present in the aqueous solution when these cations flow between exchange sites on the clay lattice. This cation exchange capacity (CEC) is responsible for the positive surface charge of wet clay. Figure 3 illustrates how reducing water activity could mitigate hydration of bentonite (montmorillonite).

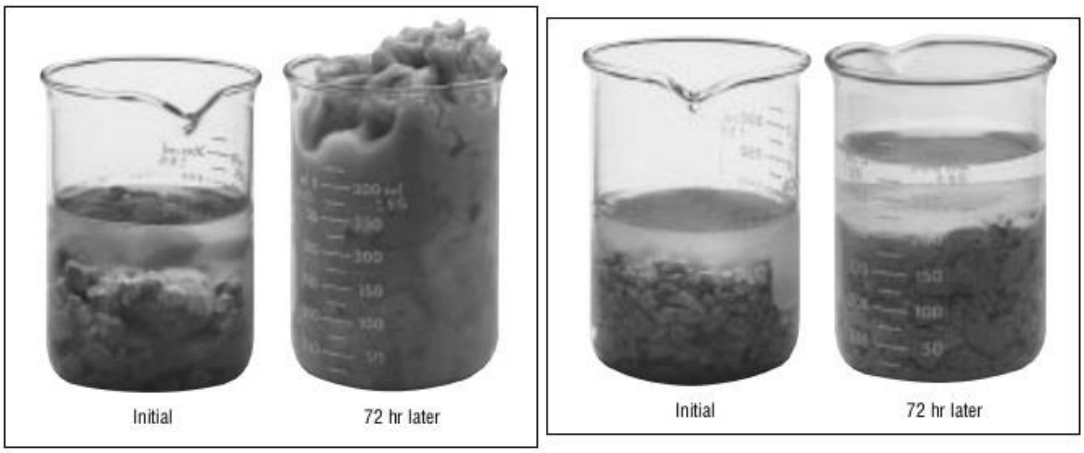

(a) (b)

Figure 3. Hydration of bentonite: (a) freshwater; (b) salt water (MI SWACO drilling fluid manual)

The CEC value indicates the concentration of compensating cations (Al^{3+}) on the clay surface that can be exchanged with other cations available in the aqueous solution. If this cation exchange happens between clay mineral and water molecules (H^{+}), clay starts to swell. However, if the cation exchange happens between clay and higher positive valence cations like Ca^{2+} or Mg^{2+}, the swelling will be limited. Shales display a non-ideal semi-permeable membrane behavior, which means some ions can move through them as well as water molecules. Scientists defined the reflection coefficient (as well as shale membrane efficiency) to explain the non-ideality of shale membrane systems. A pressure transmission test was used to measure the membrane efficiency of the shale-fluid systems

(Van Oort et. al, 1996). They suggested that the initial pressure drop, between two sides of shale, happens because of the osmosis phenomenon, and the subsequent pressure build-up can be explained by the diffusion phenomenon. They concluded that silicate-based drilling fluids can increase shale membrane efficiency to use the maximum osmotic effect. The paradigm of this approach is that shale borehole instability can be curbed by using inhibitive additives (soluble salts such as sodium chloride, sodium silicate, etc.) in water-based drilling fluids to develop effective osmotic forces. Al-Bazali et al. (2006) conducted a series of experiments to evaluate the performance of different water based and oil based drilling fluids when they come in contact with shale samples. They concluded that osmosis phenomenon plays a big role in shale inhibition while using high water activity drilling fluid. A pressure transmission test was used to measure membrane efficiency of each shale sample. The experiments were conducted using different salt concentrations in drilling fluid samples to evaluate the chemical potential capacity of shale samples. Based on the results, membrane efficiency of the shale samples was very low when exposed to different salt solutions. This means that the induced osmotic pressure is generally low, and shale samples can be considered as leaky membranes. Furthermore, the authors concluded that oil-based mud can generate much higher membrane efficiency than water-based mud. However, they disputed other researchers who had claimed a perfect (100%) membrane efficiency of oil-based muds. Ewy and Morton (2009) conducted a series of tests using actual water-based drilling fluids (not only different salts or brine, but also polymeric fluids) to evaluate different additives' performance in ensuring wellbore stability through troublesome shale formations. The authors explained both chemical potential and physical plugging mechanisms. They used a pressure transmission test to evaluate overbalance pressure conditions for each actual water-based drilling fluid. Four different water-based muds were tested on a specified shale sample (preserved shale samples, not previously exposed to water or brine) and upstream and downstream pressure were collected as representatives for wellbore pressure and pore pressure respectively. Based on the results, comparing to the base case (brine), some of the drilling fluids (especially polymeric water-

based drilling fluids) showed better performance keeping the overbalance pressure condition. The authors also measured the permeability of shale samples before and after exposing them to the testing muds, which demonstrated that using polymer-treated muds dramatically reduces shale permeability.

Tan et al., (2002) conducted several experiments to develop a novel water-based mud which was environmentally acceptable and ensures high membrane efficiency to keep shale formation from swelling and/or sloughing. Leaky membrane behavior of shale samples and osmotic flow were discussed in the background section. According to the methodology, the authors used Membrane Efficiency Screening Equipment (MESE), which uses a novel method to measure shale membrane efficiency. In this experiment, the authors used different fluids (with different salt concentration and water activity) at upstream to evaluate the performance of each fluid when in contact with different shale plugs. Based on the results, it was observed that some of the drilling fluids generated higher membrane efficiency. Moreover, the effect of different salts (such as sodium chloride and potassium chloride), and different concentration and combination of different salts have been studied. Additionally, the effect of different temperatures were investigated and the required amounts of each salt in the drilling fluid at different temperatures have been presented. The results suggest that improving drilling fluid by adding inhibitive materials such as soluble salts can reduce water molecules invasion into shale in some particular cases.

2.3 Physical plugging

FLCs are used in drilling fluid to reduce filtration into permeable formations, and to prevent additional fluid loss or lost circulation. They can limit or control mud filtration into the permeable formations and prevent wellbore instability. Therefore, FLCs can seal off microfractures or large openings at the wellbore wall, and decrease the amount of drilling fluid penetrating the formation.

However, using these existing FLCs is not always as effective as expected to cure loss of drilling fluid. Due to the physical and chemical properties of these micro and macro-sized fluid loss additives, these materials may fail to reduce fluid loss successfully, and cause increased non-productive drilling (NPT) time (Chenevert and Sharma, 2009; Fraser et al., 2003). For example, FLC materials with diameters in the range of 0.1 to 100 μm may be useful to plug pore throats in the range of 0.1 μm to 1 mm. However, these materials fail to reduce filtration into the shale formations with the size of pore opening in the range of 10 nm to 100 nm.

Shales have very small pore openings, mostly non-interconnected porosity which result in very low permeability (~10 nanodarcy). The size of pore openings in shale formations is in the range of 10 nm to 100 nm. Hence, micro and macro-sized LCM and FLC materials show very limited success in reducing filtrate penetration into the shales. Therefore, mud cake can not be created on the shale surface. Consequently, standard FLC materials are useless to prevent filtration into shale. Common drilling fluid additives such as bentonite and barite in the conventional drilling fluids have much larger particle diameters, ranging from 100 nm to more than 100 microns (Srivatsa, 2010). Mud filtrate penetrates into the clay structure gradually and may cause borehole instability both mechanically and chemically.

Besides adding soluble salts in water-based drilling fluids to reduce water activity and prevent shales from swelling, there have been a lot of efforts to reduce the shale and water contact by using physical isolation. For example, using PHPA in water-based drilling fluid increases rheological properties that can reduce filtration into porous media. PHPA also could encapsulate shale cuttings and prevent them from sticking to the BHA or drill bit. Another example is poly ethylene glycols (PEG) that come out of aqueous solution at their specific cloud point temperature and cover shale surface and lower water/shale exposure. PEGs usually are effective in saline (especially KCl) aqueous systems. The environmental protection regulations and cost of further treatment make PEG

systems undesirable for shallow formations or offshore drilling. Brady at al. (1998) introduced a new PEG system that provides a high level of shale inhibition in freshwater and low-salinity WBM.

Using NPs is also another step in this approach. NPs are defined as particulate dispersions or solid particles with a size in the range of 1 to 100 nm (Zakaria et al., 2011). Due to their size and large surface area to volume ratio properties, NPs can be used as a fluid loss additive (Amanullah et al., 2011; Abdo and Haneef, 2010).

Amanullah and Al-Tahini (2009) defined nanofluids as any fluids (including drilling fluids, drill-in-fluids, etc.) used in the exploitation of oil and gas that contain at least one additive with a particle size in the range of 1 to 100 nm. They also classified nanofluids as simple nanofluids and advanced nanofluids. Simple nanofluids contain NPs of only one dimension, whereas advanced nanofluids are ones with multiple nano-size additives. NPs can help bridge empty gaps between macro FLCs and LCMs, and therefore, provide an effective seal to the formation with larger pore opening size. Sensoy et al. (2009) used silica NPs to plug pore throats of different shale samples. By using higher concentrations of silica NPs, they minimized fluid penetration into these water-sensitive shale samples. They also measured the initial and final permeability of the sample and concluded that NPs were significantly effective in reducing shale permeability. Based on the results, using NPs in WBM systems provides effective sealing, bridging and cementing properties, resulting in the reduction of near wellbore porosity and permeability of the formations, thereby preventing the loss of fluid.

Adding NPs to drilling fluid can help other additives to seal off the pore openings in shales. In a drilling operation, it is preferable to plug the rock pores or fractures externally with a minimal damage to the formation to avoid consequent problems. Figure 4 shows the schematic of drilling fluid interaction with a porous formation with and without NPs.

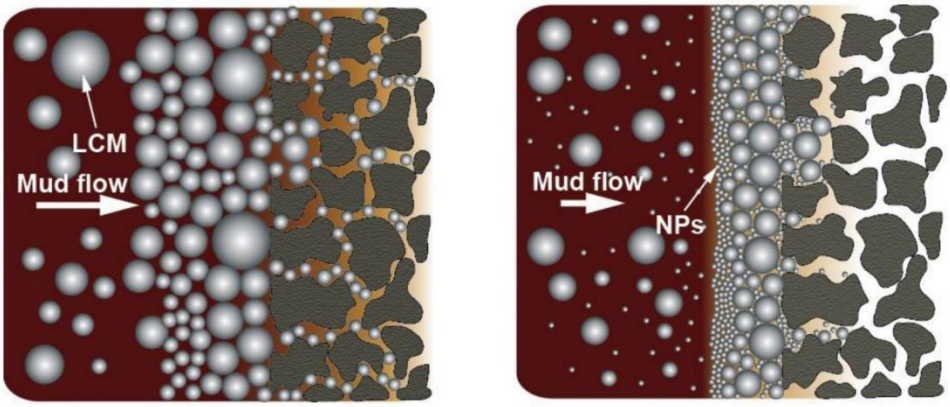

Figure 4. Left: Conventional LCM, Right: NPs and conventional LCM (Zakaria et al., 2011)

Chenevert et al. (2009) used different NPs in WBM to investigate their effect on the permeability reduction in Atoka and Gulf of Mexico shale samples. The NPs size in the range of 1-500 nm was selected from silica, iron, aluminum, titanium or other metal oxides. According to their results, the minimum NPs concentration required to detect any reduction in the fluid penetration is 10 weight percent. The results showed a drastic reduction of absorbed water and potential for collapse if a higher concentration of NPs was used.

A few more studies have been done on using NPs in drilling fluid to improve the functional characteristics described earlier (Cai et al., 2012; Srivatsa, 2010; Abdo and Haneef, 2010; Chenevert and Sharma, 2009; Sensoy, 2009; Agarwal et al., 2009). Kanj et al. (2009) suggested that small particles of high concentrations might bridge across the pore throat and smaller particles aggregate around larger ones, filling the tinier spaces and hence effectively plugging the pore opening spaces. Particle size and surface characteristics of NPs can be easily manipulated in water-in-oil emulsions in a similar fashion to those formed in water/oil (w/o) micro-emulsions (Husein and Nassar, 2012 a&b).

2.4 Filter-cake and permeability

Permeability is a measure of the capacity of a porous medium to transmit fluids. Permeability is considered as a property of the porous medium. A general rule of thumb for estimating the permeability (in md) is to calculate the square of the pore throat diameter (microns). Fluid flow in porous media has been studied by many researchers. Darcy's law is one of the first empirical equations to model fluid flow in porous media, however, it does not consider filter-cake formation or any interaction between the fluid and porous media. Figure 5 illustrates schematic of experimental design that Darcy used in his study.

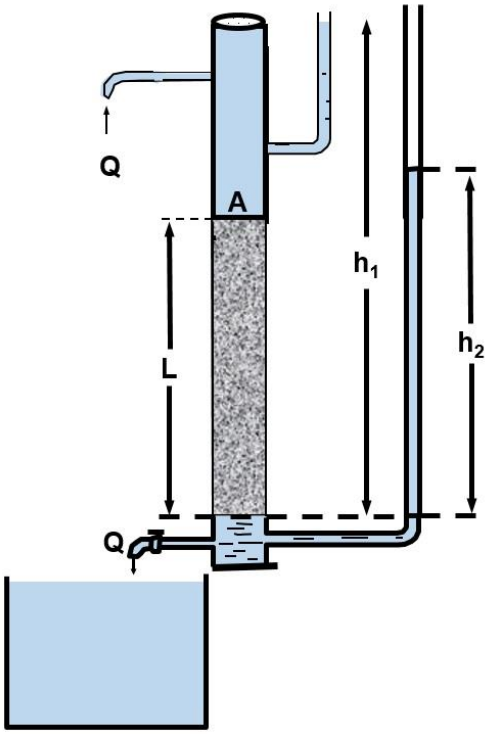

Figure 5. Schematic of experimental design to measure the permeability of a porous medium

Darcy's law for an incompressible single-phase flow in a porous substance with negligible inertial and gravitational effects is given by the following equations:

$$v = -K\frac{\Delta P}{\mu L} \qquad \text{Eq. 1}$$

$$K = -\frac{QL\mu}{A.\Delta P} \qquad \text{Eq. 2}$$

The initial permeability of the qualitative filter papers can be measured by equation 3:

$$K = -\frac{L\mu}{A.\Delta P}\frac{dV}{dt} \qquad \text{Eq. 3}$$

K: Permeability of the porous media, Darcy (m^2)

v: Fluid average velocity, (m/s)

ΔP: Pressure drop across the porous media, Pa

Q: fluid flow rate (m^3/s)

A: Cross section area of the porous media, m^2

μ: Viscosity of the mud filtrate, Pa.s

L: the length of porous media, (m)

During the drilling operation, due to the positive differential pressure between the drilling fluid and formation pore pressure, the drilling fluid (or its filtrate) invades the formation. The invaded zone can be significant for formations with high permeability. Because of the size of solid materials or electrical charge of some large polymers, some of the suspended solids or polymers cannot enter into the pores. These solid materials start to deposit on the surface of the rock and build a filter cake. The filter cake acts as a barrier against the flow, and decreases the rate of filtrate invasion. There are several studies regarding measuring the permeability of filter-cake. High filter cake permeability results in thicker filter cakes that could cause technical problems such as excessive rotational torque and axial drag, high swab and surge pressures, and differential pressure sticking. Burgoyne (1991) presented a model to calculate the cake permeability for static filtration. Based on the laboratory data, he found cake permeability is a function of cumulative filtrate volume and time:

$$V_f = \sqrt{2K\Delta P\left(\frac{\varepsilon_{sav}}{\varphi_s} - 1\right)}\ A\frac{\sqrt{t}}{\sqrt{\mu}} \qquad \text{Eq. 4}$$

K: Permeability of the filter cake, Darcy

V_f: Cumulative filtrate volume, cm^3

ΔP: Pressure drop across the mud cake, atm

φ_s: Volume fraction of solids in the mud

ε_{sav}: Volume fraction of solids in the cake

A: Area of the filter disk, cm^2

t: Time of filtration, s

μ: Viscosity of the mud filtrate, cp

Khatib (1994) conducted a series of experiments using different types of solid materials including iron sulfide, iron hydroxide, iron hydroxide/bentonite mixture, calcium carbonate, and calcium sulfate in drilling fluids to investigate permeability of the combined matrix and filter cake. He suggested that particle size distribution of the solid materials and pore throat size play important roles in the rate of filtrate invasion and filter cake permeability. The type of solid materials and the presence of oil have a significant effect on the permeability of filter cake. Khatib correlated permeability/porosity data for different solid materials to obtain the permeability of the filter cake based on porosity.

$$K = a(1 - \phi_c)^b \qquad \text{Eq.5}$$

K**:** Permeability of the mud cake, md

ϕ_c: Porosity of the filter cake, dimensionless

a and b: empirical constants for solid materials including iron sulfide, iron hydroxide, $CaCO_3$, $CaSO_4$, and silt/clay particles.

Mahesh (2000) developed a new model to measure the permeability of the filter cake. Using this model, the volume of filter cake should be measured indirectly.

$$K = Q_w Q_c \frac{\mu}{2t.\Delta P.A^2} \quad \text{Eq.6}$$

K : Permeability of the filter cake, darcies

Q_w: Filtrate volume in cm^3

Q_c: Volume of the cake in cm^3

μ : Viscosity of the filtrate in cp

t: Time in second

ΔP: Differential pressure in atm

A: Area of the filter cake in cm^2

Studying on a leaf filter system for chloride separation, Martinez et al. (2000) presented the following equation to predict the filter cake permeability.

$$\frac{\Delta P.t}{\mu.v} = \left(\frac{1}{2K}\right) L + R_m \quad \text{Eq.7}$$

K: Permeability of the filter cake, m^2

v: Volume of filtrate per unit area, m^3/m^2

L: Filter cake thickness, m

R_m: Resistance of filter medium, 1/m

ΔP: Differential pressure, Pa

t: Time, s

μ: Filtrate viscosity, Pa.s.

Tiller (2002) developed the following equations to calculate the filter cake permeability by considering the fraction of solid materials in the filter cake.

$$c = \frac{\varphi_s}{1-\frac{\varphi_s}{\varepsilon_{sav}}} \quad \text{Eq.8}$$

$$\frac{\Delta P.dt}{\mu.dv} = \alpha_{av}.c.v + R_m \quad \text{Eq.9}$$

$$\alpha_{av}.K.\varepsilon_{sav} = 1 \quad \text{Eq.10}$$

K: Permeability of the filter cake, m^2

v: Volume of filtrate per unit area, m

ε_{sav}: Volume fraction of solids in filter cake

R_m: Resistance of filter medium, 1/m

ΔP: Differential pressure, Pa

t: Time, s

μ: Filtrate viscosity, Pa.s.

φ_s: Volume fraction of solids in the slurry

Li et al. (2005) developed a new test method that studied fluid flow through the already formed cake in each filtration test. They calculated the permeability of filter cake based on Darcy's Law for liquid flow through the already formed filter cake and the filter media.

$$R_t = R_c + R_m \quad \text{Eq.11}$$

$$\Delta P_t = \Delta P_c + \Delta P_m \quad \text{Eq.12}$$

Flow rate q = rate through cake = rate of flow through filter media

Flow rate q = rate through filter cake = $K_c \frac{\Delta P_c}{\mu L_c}$

Flow rate q = rate through filter media = $K_m \frac{\Delta P_m}{\mu L_m}$

R_t: Total resistance

R_c: Resistance of cake

R_m: Resistance of filter media

q: Filtrate rate, $m^3/m^2.s$

K_c: Permeability of the filter cake, m^2

K_m: Permeability of the filter medium, m^2

L_c: Thickness of the filter cake, m

L_m: Thickness of the filter medium, m

ΔP_t: Total pressure drop, Pa

ΔP_c: Pressure drop across the filter cake, Pa

ΔP_m: Pressure drop across the filter medium, Pa

μ: Filtrate viscosity, Pa.s.

Dewan and Chenevert (2001) studied filtration for more than 100 water-based muds. They used Darcy's equation to measure filter cake permeability.

$$K_{mc} = 14700 \frac{QT_{mc}\mu}{\Delta P_{mc}} \qquad \text{Eq.13}$$

K_{mc}: Permeability of the filter cake, md

Q: Filtration rate, cm3/sec

T_{mc}: Filter cake thickness, cm

μ: Viscosity of the filtrate, cp

ΔP_{mc}: Pressure across filter cake, psi

Although many researchers focused on developing new models to predict permeability and fluid loss, none of them investigated the effect of NPs influence on permeability. The use of NPs in

drilling fluids can reduce permeability and fluid loss. Sensoy et al. (2009) used a drilling fluid containing silica NPs in a pressure transmission test to plug the pore throats of Atoka shale samples. Based on their results, a suspension of 29% wt. silica NPs reduced the shale permeability by 98% without creating an observable filter-cake on the surface of the shale. Previously discussed models cannot predict permeability behavior of filter cake and porous media when NPs are being used in drilling fluid. Loggins et al., (2017) studied the effect of using NPs on filtration reduction in different permeable media. They observed that filtration reduces when a very small concentration of NPs is used in water based drilling fluid.

2.5 Mud weight window

During the drilling operation, it is important to select safe mud weight with lower and upper limits. In order to establish the minimum safe mud weight, the goal is to minimize the risk of complete hole collapse and kick, while hole cleaning is being effectively implemented.

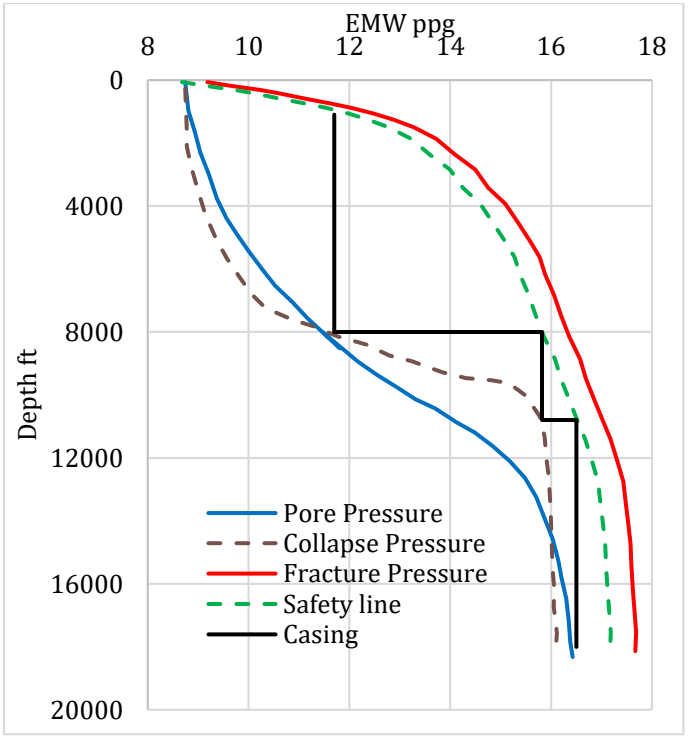

Figure 6. Upper and lower limits of mud weight window

Figure 6 illustrates the concept of mud weight window. The lower limit of safe mud weight is dictated by either pore pressure or collapse pressure, whichever is higher. The breakout zones are the intervals that collapse pressure profile and are higher than pore pressure. The intervals with higher pore pressure than collapse pressure increase the risk of kick. The upper limit is defined by the fracture pressure gradient in each depth. Induced fractures start to appear when the breakdown pressure is infringed.

It is important to keep the mud weight in the safe region to avoid serious consequences of trespassing both lower and upper limits. Exceeding the formation fracture pressure during drilling operations can result in high fluid losses, lost circulation, loss in mud hydrostatic pressure potentially resulting in a kick, which could lead to a blowout. As a well deepens, the mud safe window range narrows due to the convergence of the pore and formation fracture gradient. Therefore, it is crucial to choose a mud weight to stay in the mud weight safe window.

2.6 Wellbore Strengthening

Wellbore strengthening (WS) is a process of increasing the wellbore pressure containment using engineered drilling fluids. WS can be achieved by preventing drilling fluid penetration into the formation and limiting the local increase of formation pore pressure around the wellbore. WS has been studied by many researchers and different procedures and techniques have been suggested. WS is applied to prevent or treat lost circulation with the goal of decreasing or limit the drilling fluid from entering the formation. WS methods include the use of different additives in drilling fluids, heating the wellbore to change in situ rock stresses around the borehole, and use of pills for temporarily isolating troublesome zones.

Nayberg et al., 1987 showed that adding thermoset rubber in both water-based and oil-based drilling fluid systems reduced mud loss into simulated fractured formations. Morita et al., 1990

conducted hydraulic fracturing tests on sandstone samples and found that the fracture pressure increased when using bridging materials. Similar results were shown by Fuh et al., 1992 which proved that using certain size and specific gravity lost-prevention materials (LPMs) increases fracture breakdown pressure. Aston et al., 2004 designed a mud system which increased fracture pressure by forming a stress cage using bridging solid materials in a low fluid loss mud system for both shale and sandstone intervals in three field tests. They concluded that wellbore strengthening is a better approach than treating lost circulation events.

Soroush et al., 2006 studied different methods and suggested strategies to stabilize the wellbore. They concluded that using methods like grouting, bridging balls, and high-power laser glazing can reduce permeability and increase strength. Growcock et al., 2009 reviewed different wellbore stabilization technologies available in the industry, and concluded that drilling fluid selection and optimization of mud properties are key factors in preventing wellbore instability.

Nwaoji et al., 2013 used iron hydroxide NPs in combination with granular graphite in water-based mud (WBM) to increase fracture pressure up to 70 %. They also found the including calcium carbonate NPs and graphite oil-based mud (OBM) can increase fracture pressure by 36 %. Contreras et al., 2014a continued this work and used NPs and graphite in an invert emulsion mud system to increase breakdown pressure. They conducted hydraulic fracturing and HPHT filtration tests on Roubidoux sandstone samples. The results showed 65 percent increase in breakdown pressure can be achieved if 2.5 % wt. NPs and 0.5 % wt. graphite is used in the invert emulsion mud. Contreras et al., 2014b also conducted fracturing and HPHT filtration tests on Catoosa shale samples. The results showed 30 percent increase in breakdown pressure can be achieved if 2.5 % wt. NPs and 2.0 % wt. graphite is used in invert emulsion mud. Cedola et al., 2016 conducted hydraulic fracturing tests to investigate the effect of using barite NP on fracture gradient pressure increase. Their results showed an increase in fracture breakdown pressure of more than 12 % if 3% wt. barite NP was used in water-based drilling fluids.

Based on the tensile fracturing criterion, fracture initiates when the tangential (hoop) stress around the well (σ_θ) equals the rock tensile strength (T_R).

$$\sigma_\theta = -T_R \quad \text{Eq.14}$$

Based on Kirsch equations, hoop stress around the borehole can be estimated using the in-situ stress state. When the wellbore is vertical and perfectly circular without hydraulically conductive fractures and a non-penetrating fluid, the fracturing gradient of the formation can be estimated using the equation below.

$$P_{ini} = 3\sigma_h - \sigma_H + T_R - P_0 \quad \text{Eq.15}$$

where P_{ini} is the fracturing pressure, σ_h is the minimum horizontal stress, σ_H is the maximum horizontal stress and P_0 is the pore pressure.

When the fluid is permeable, the formation becomes weakened by the fluid penetration. The equation below may be applied for such conditions.

$$P_{ini} = \frac{3\sigma_h - \sigma_H + T_R - 2\eta P_0}{2(1-\eta)} \quad \text{Eq.16}$$

where η can be calculated as

$$\eta = \frac{1-2\upsilon}{2(1-\upsilon)} \quad \text{Eq.17}$$

Fluid penetration into formation increases pore pressure and therefore, decreases the rock fracture initiation pressure. It also changes the porochemoelastic properties of the rock due to the physiochemical reactions between filtrate and pore fluid.

2.7 Lost Circulation Material (LCM) and NPs

Lost circulation is the other challenging situation when a fractured or a highly permeable formation is being drilled. The related consequences include losing valuable drilling fluid that increases the well construction cost, with potential for kick and blowout in severe lost circulation conditions due to loss of hydrostatic pressure. Lost circulation can be prevented using a proper drilling fluid to deal with permeable or fractured zones. Reducing the mud weight, and treating the mud with granular bridging materials, fibrous, flake materials, or a combination of these materials are primary attempts to control lost circulation. The type of lost circulation zone and the severity of the losses are important factors in selecting the appropriate LCMs. LCMs such as nutshells, mica, cottonseed hulls, sized graphite, cellulose fibers and plastic chips are used to seal outflows in fractured zones and pore throats in permeable formations.

Chemical and mechanical ways are two approaches to control lost circulation and have previously been studied by many researchers. Vidick et al. (1988) used a solid-free silicate drilling fluid system to treat lost circulation. They studied the performance of their drilling fluid system based on different parameters including gelation time, plugging capability and long-term stability. The reported results show successful application of their silicate system for cores with different permeability.

Burton et al. (2001) used cross-linking polymers in combination with fibrous LCMs to control drilling fluid loss into a cavernous formation. They reported that drilling fluid loss successfully stopped after chemically activated cross-linked pills were injected and set.

Whitfill et al. (2007), used different size distributions of resilient graphite carbon and ground marble to produce deformable-viscous-cohesive drilling fluid systems, which successfully controlled lost circulation in depleted sand formations in a well in the Gulf of Mexico.

Mata and Veiga, (2004) designed two crossed link cements to cure severe lost circulation in fractured zones and to minimize formation damage in highly-permeable productive zones. Lecolier

et al. (2005) used chromium acetate as a cross-linker agent in PHPA to develop a nanocomposite gel to control severe circulation loss.

Whitfill and Miller (2008) suggested using either particle plugging test apparatus (PPA), or a High Pressure High Temperature (HPHT) fluid loss test apparatus that is fitted with slotted/tapered metal discs or ceramic discs to measure the fluid loss volume at a constant 1000 psi overbalance pressure condition to evaluate the performance of LCM treatments.

Hettema et al. (2007) designed a new fracture test apparatus to study the effects of solids bridging in the fractured media. They tested different synthetic-based and water-based mud treated with different LCMs. They concluded that LCM with a broad distribution of particle sizes can seal fractures better than a narrow size distribution. They concluded that concentration of the solid materials plays a big role in increasing sealing fracture pressure. Kumar and Savari (2011) used tapered slots (TS) which physically resemble a wedge-shaped fracture in PPA. They suggested that selecting proper particle size distribution of LCM is an important parameter in lost circulation control and wellbore strengthening.

Savari et al. (2014) defined plug breaking pressure as the maximum differential pressure that LCM plug over a tapered slot can withstand before breaking. They used a tapered slot with 2500 microns opening width, which tapers down to 1000 microns over the length of 1.4 inches. The maximum measured sealing pressure was 2100 psi when a combination of resilience graphite carbon and four kinds of fibers was used as lost circulation material.

Al-saba et al. (2014) evaluated the performance of conventional LCM performance on different width-opening size tapered slots. They also measured sealing pressure for different LCM concentrations and temperatures. The highest measured sealing pressure for 50ppb nutshells was 714 psi for a 2000 microns fracture width tapered slot. They concluded that because of swelling of nutshell particles at a higher temperature, the sealing efficiency increases more than 50 %. Although the performance of different conventional and unconventional LCMs has been evaluated

by many researchers, the effect of using nanoparticles alongside with LCM in water-based mud has not been investigated.

CHAPTER III

METHODOLOGY

3.1 Barite NPs synthesizing: Ex-situ procedure

This research adopted a (w/o) micro-emulsion technique to prepare barite NPs in drilling fluids. To avoid any hazardous liquid phase such as diesel or kerosene, a linear alpha olefin was selected to be part of the micro-emulsion. 1- hexadecene is already being used in formulating synthesized oil-based muds (SBM) as a substitution for hazardous hydrocarbons in drilling fluid. The thin layer of a surfactant around NPs prevents their growth and aggregation and hence, preserves the suspension stability. Stability of colloidal particles is founded on the net between the repulsive and the attractive forces when particles approach each other due to Brownian motion or other external forces. The colloidal suspension remains stable when repulsive forces dominate, while aggregation and precipitation occur when attractive forces dominate. Van der Waals force is an attractive type of interaction and is inversely proportional to the sixth power of the distance between the surfaces of the particles (Husein and Nassar, 2008; Nassar and Husein 2007a, 2007b; Kostansek, 2003). Microemulsions (w/o) are thermodynamically stable systems and are different in nature from the kinetically stable invert emulsions typically used in drilling operations. The entropy of dispersion is a very important parameter for the formation of microemulsion systems. The entropy of dispersion contributes to very effective mixing of water pools and, hence very high rate of inter-micellar exchange dynamics compared to invert emulsion systems. This high rate is indispensable for the formation of NPs in (w/o) micro-emulsions (Husein and Nassar, 2008).

Chemically generated barite NPs were synthesized by a reaction of two precursors. An aqueous emulsion of dissolved potassium sulfate (K_2SO_4) in water and 1-hexadecene was the first precursor mixture. The second emulsion of dissolved barium chloride ($BaCl_2$) in water and 1-hexadecene was the second precursor used in the NPs synthesizing process. Each precursor contained 10 ml of 1-hexadecene and 165 ml of water containing a specific amount of surfactants such as Tween-20, SDS, or CTAB. The desired reaction is shown below.

$$K_2SO_4\,(aq) + BaCl_2\,(aq) \longrightarrow BaSO_4(s) + 2\,KCl\,(aq)$$

The two emulsions were mixed by a high RPM mixer at 25°C for 5 minutes to ensure all reactants were dissolved properly. After the 5-minute mixing period, the $BaCl_2$ was added to the K_2SO_4 and was mixed for an additional 5 minutes to ensure the reaction completely took place. The reaction produces a certain amount of barium sulfate ($BaSO_4$) and potassium chloride (KCl) based on the specified amount of reactants.

To ensure consistency in the comparison between different mud samples, the amount of $BaSO_4$ NPs that was produced from the reaction was being taken into consideration when the other mud additives were added to the fluid as a whole. In other words, as the concentration of barite NPs increased, the amount of normal barite and KCl were reduced to ensure the fluid system had a constant overall concentration of barite and KCl. This ensured the rheology was consistent and comparable for all tests. After synthesizing barite NPs, various tests were conducted to better characterize the NPs. A dynamic light scattering (DLS) apparatus was used to obtain the NPs particle size distribution, as well as the variance in the size distribution. The following list summarizes the process of ex-situ barite NP preparation:

- Calculate the needed amount of reactants, based on the desired concentration of barite NPs.

- Solubilize the calculated amount of barium chloride in 165 ml deionized water (dispersion phase). Stir it using a mixer for 5 minutes.
- Solubilize the calculated amount of potassium sulfate in 165 ml deionized water. Stir it using a mixer for 5 minutes.
- Add 10 cc of the selected dispersed phase fluid (1-hexadecene) and 0.2 gr surfactant to both aqueous samples and mix to have a stable emulsion.
- Then, add (dropwise or at once) aqueous barium chloride to the prepared solution of potassium sulfate. Stir it using a mixer for 5 minutes.
- In this step, you can take it for size analysis or add other additives to it to prepare desired mud.

The produced barite NPs were centrifuged and dried in order to be analyzed for their purity. Figure 7 shows the X-ray diffraction (XRD) analysis for the chemically synthesized barite NPs. Due to the high purity of the reagents, the XRD graph for the generated barite matches the analysis for pure barium sulfate.

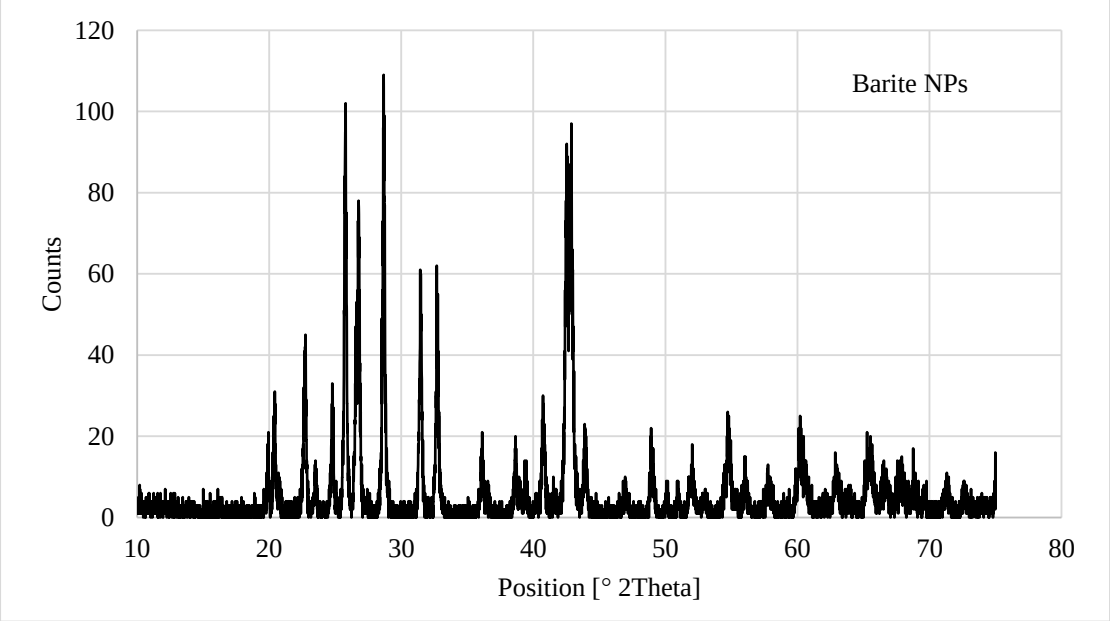

Figure 7. XRD analysis for the chemically synthesized barite NPs

3.2 Surfactants and dispersed phases

Utilizing ex-situ method makes it possible to control the range of particles size distribution using different types of surfactant as well as different dispersed fluids. Surfactants decrease the interfacial tension, and this causes a reduction in droplet size. The HLB number, developed by Griffin (1954), is a semi-empirical scale for selecting surfactants to prepare either O/W or W/O emulsions. The HLB number of a surfactant represents the relative percentage of hydrophilic to lipophilic (hydrophobic) groups in the surfactant molecules. The HLB concept is the best-known method to select an appropriate surfactant for an application. The HLB number is assigned to a surfactant according to its chemical structure. HLB numbers range from 1 to 40. For instance, if a surfactant has an HLB value of 1, it is considered very oil soluble, while a surfactant with an HLB value of 15 is considered to be water-soluble. The HLB number is particularly useful to select the suitable surfactants for oil and water emulsification. To have stable micro-emulsion, different combinations of two surfactants were used in this study. Table 1 shows the HLB value range for different applications.

Table 1. HLB values for particular application

HLB value	Application
<10	Lipid soluble (or water-insoluble)
>10	Water Soluble
4-8	Antifoaming
7-11	Water-in-oil emulsion
12-16	Oil-in-water emulsion
11-14	Good Wetting
12-15	Good detergency
16-20	Stabilizing

In order to obtain a better understanding of fluid loss results, the barite NPs size distribution was studied using a dynamic light scattering (DLS) apparatus. The intensity fluctuation of light scattered from suspended particles can be used to determine particle size. Peak intensity distribution gives a reliable measurement of effective particle size. Figure 8 shows the barite NPs size distribution when CTAB (Hexadecyltrimethylammonium bromide) was used to generate 1-

hexadecene in water emulsion. The effective diameter of barite NPs is 744 nm. CTAB has a HLB value of 10 that indicates it is not a suitable choice for oil in water emulsion.

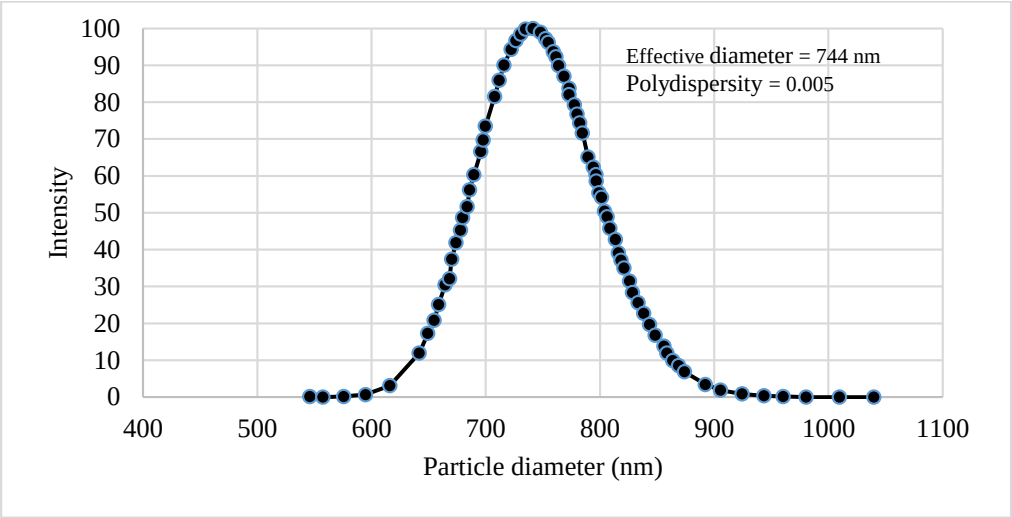

Figure 8. Barite NPs size distribution when CTAB and 1-hexadecene are being used to generate an emulsion

Figure 9 illustrates barite NPs size distribution when CTAB was used to generate to generate diesel in water emulsion. The effective diameter of barite NPs is 54 nm. CTAB worked better with diesel compared to the 1-hexadecene.

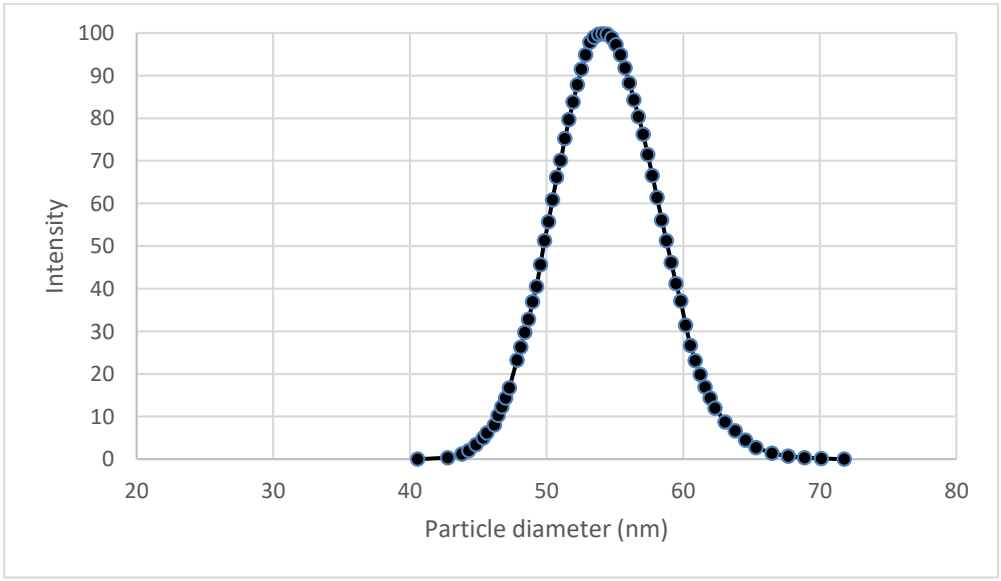

Figure 9. Barite NPs size distribution when CTAB and diesel are being used to generate an emulsion

Due to the toxicity of diesel and the waste disposal cost of using diesel, it was decided to discard diesel from the formulation of the emulsion. To generate microemulsion of 1-hexadecene in water, Tween 20 and SDS were used to generate barite NPs. Figure 10 shows the barite NPs size distribution when above mentioned anionic surfactants were used to create microemulsion. The effective diameter is 62 nm.

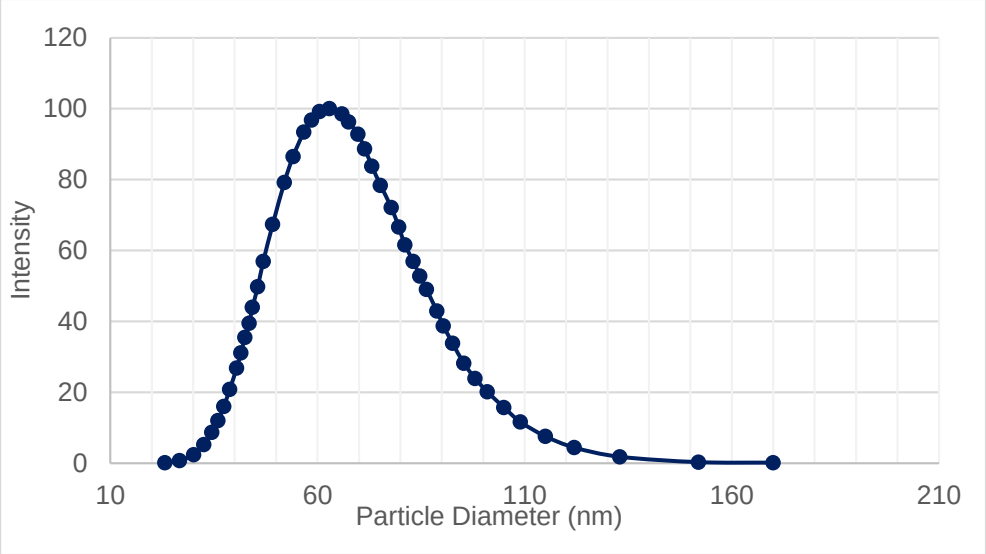

Figure 10. Barite NPs size distribution when Tween 20, SDS and 1-hexadecene are being used to generate an emulsion

3.3 Mechanical Grinding of Fine Barite

Barite NPs were also prepared mechanically using a high energy ball grinder. For this purpose, a specific amount of standard barite was seived using a 38-micron mesh to separate finer from coarser barite particles. The high-speed ball grinder is used to prepare barite nano-micro particles mechanically. Using 2 millimeter-diameter stainless steel balls, the ball grinder milled 10 grams of seived barite for 6 hours at a speed of 1000 RPMs. The milled barite was used instead of normal barite in the mixture to have the desired percentage of barite nano-micro particles at the end. Figure 11 shows the high-speed ball grinder which is used to produce nano-scale particles.

Figure 11. High-Speed Ball Grinder

Figure 12 illustrates barite micro and NPs size distribution prepared using high-speed ball grinder. The graph shows the particles have a very wider range of size from 500 nm to 3 microns.

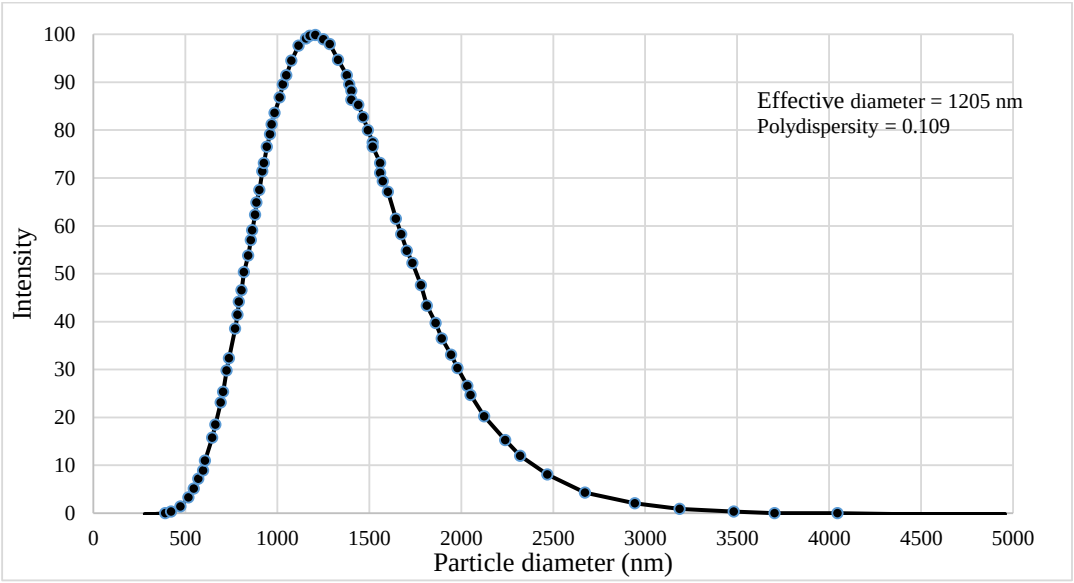

Figure 12. Particle size distribution for ground barite (Mechanically prepared barite NPs)

In order to obtain an understanding of the shape of generated barite NPs, transmission electron microscopy (TEM) was used to provide an additional visual aid. To do so, a centrifuge machine was used to take NPs out of suspension and then NPs were washed with an organic solvent three times and were placed on the carbon coated Cu TEM grid to dry. Figure 13 shows a TEM image taken from barite NPs generated by the chemical reaction.

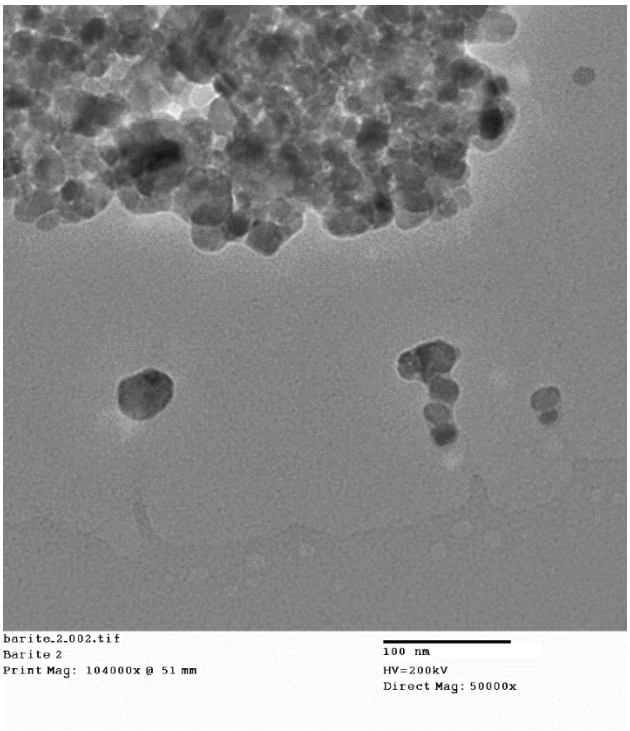

Figure 13. TEM image of chemically generated barite NPs

The same procedure was used to prepare mechanically generated barite NPs. Figure 14 shows the shape and size of barite micro and nano-sized particles generated by milling the sieved barite. Mechanically generated barite NPs contains small particles (as small as 40 nm) and larger particles (as large as 12 microns); however, the effective diameter is to be 1205 nm based on the DLS intensity change analysis.

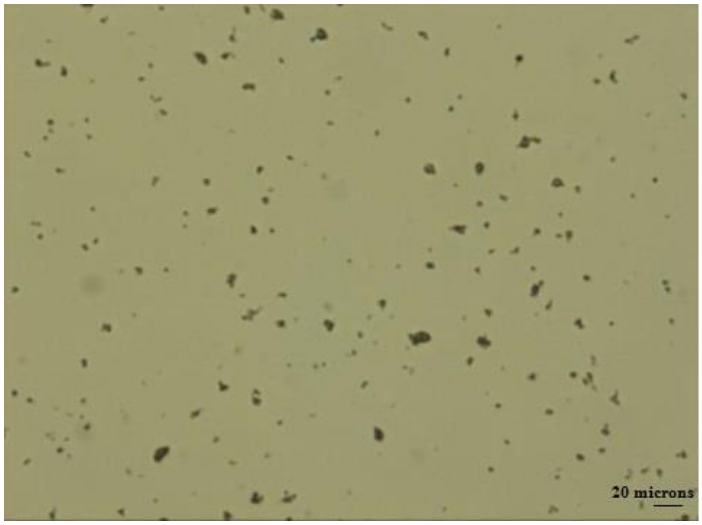

Figure 14. Microscopic image of mechanically generated barite NPs

3.4 Drilling fluid preparation

Four different drilling fluids were formulated and tested in this research to investigate the influence of different parameters in the performance of NPs in drilling fluid. In this section, the composition and properties of each formulation are presented. Drilling fluid case 1 was designed to investigate if a drilling fluid containing barite NPs can reduce filtration for a 2-25 micron opening sizs.

3.4.1 Drilling fluid case 1

This mud formulation was designed to evaluate the performance of up to 5 % wt. of barite NPs when there is none or a very small amount of other solid materials. The main objective of designing this mud was to study the performance of barite NPs in plugging higher pore opening sizes. Table 2 and 3 shows the composition and properties of the drilling fluid case 1.

Table 2. The composition of the drilling fluid case 1

Components	Amount (gr)
Water	330
1-Hexadecene	20
Surfactant	1
Barite	19
KCl	13

Table 3. Properties of the drilling fluid case 1 at 25 C

Properties	Value
MW	8.7 ppg
PV	5 cp
YP	2 lb/100ft^2
CoF	0.3

The amount of barite NPs for each designed concentration was calculated based on $BaCl_2$ and K_2SO_4 reaction and substitute normal barite in the mud. Therefore, the same amount of KCl and barite were present in drilling fluid in each case. The only difference was the size of barite particles that were used in the mud. Figure 15 and 16 illustrate plastic viscosity (PV) and yield point (YP) values that were measured using the FANN 35A apparatus. Error bars indicate standard error of the collected data.

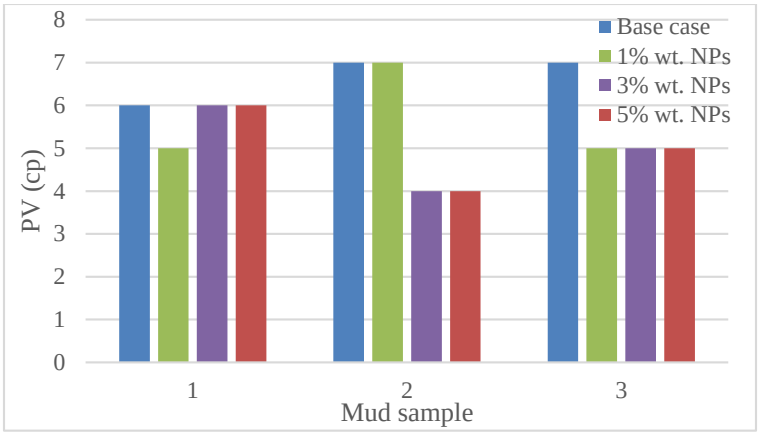

Figure 15. Measured PV for the mud samples of case 1 with and without NPs

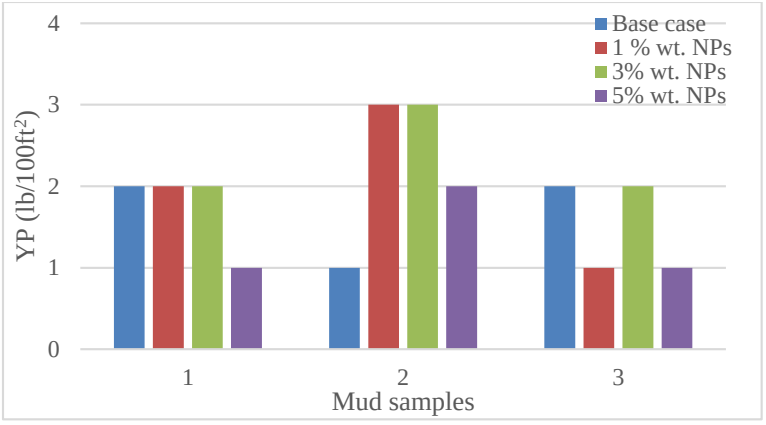

Figure 16. Measured YP for the mud samples of case 1 with and without NPs

3.4.2 Drilling fluid case 2

This mud formulation was designed to evaluate the performance of up to 4 % wt. of Barite NPs in the presence of other solid materials as well as polymers. The objective of designing this mud was to investigate the effectiveness of NPs in high plastic viscosity and yield point. High yield point drilling fluids are being used in horizontal intervals drilling when cutting suspension is crucial. Table 4 and 5 shows the composition and properties of the base case 2.

Table 4. The component of the drilling fluid case 2

Components	Amount (gr)
Water	330
1-Hexadecene	20
Surfactant	1
NaCl	80
Xanthan Gum	0.5
PAC LV	3
$CaCO_3$	80
Barite	100
KCl	20

Table 5. Properties of the drilling fluid case 2 at 25 C

Properties	Value
MW	11.6 ppg
PV	39 cp
YP	50 lb/100ft2
CoF	0.38

As presented in table 4 and 5, this case contains solid materials as well as polymers, which makes the final product a weighted mud with high plastic viscosity and yield point. Using solid materials in drilling fluid is necessary to enable it to plug the pore opening and reduce fluid loss. Figure 17 and 18 illustrate the collected PV and YP results for the drilling fluid case 2 with and without barite NPs.

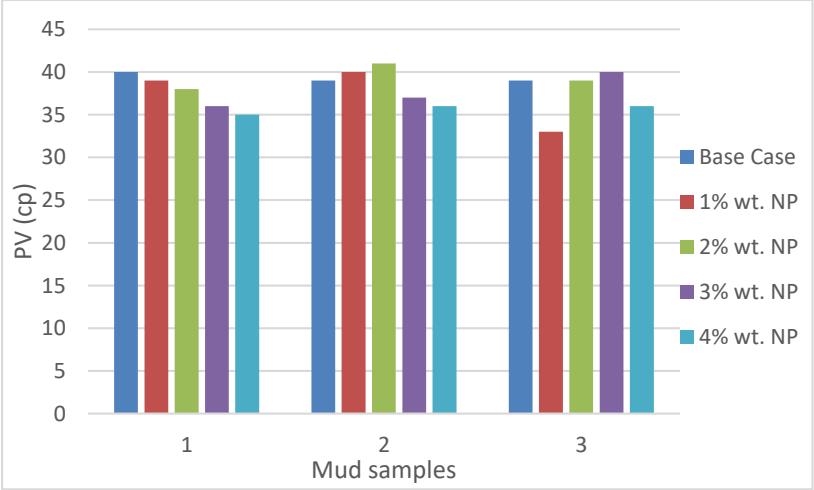

Figure 17. Measured PV for the mud samples of case 2 with and without NPs

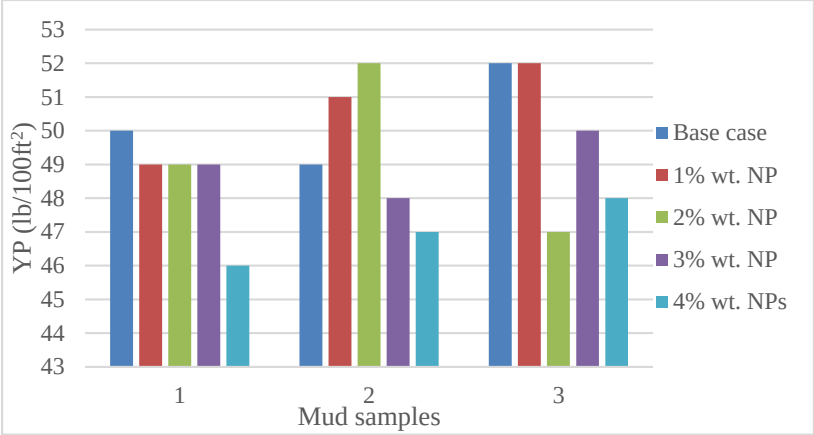

Figure 18. Measured YP for the mud samples of case 2 with and without NPs

3.4.3 Drilling fluid case 3

This mud formulation was designed to evaluate the performance of Barite NPs in the presence of other solid materials as well as polymers when pressure is higher than normal. The other objective of designing this mud was to investigate the effectiveness of NPs in high temperature and pressure condition. Drilling fluid case 3 can be used for vertical and deviated intervals. Tables 6 and 7 show the composition and properties of the drilling fluid case 3.

Table 6 Composition of the base case 3

Components	Amount (gr)
Water	330
1-Hexadecene	20
Surfactant	1
NaCl	40
PAC LV	2
Barite	100
KCl	20

Table 7 Properties of the base case 3 at 25 C

Properties	Value
MW	10.5 ppg
PV	29 cp
YP	10 lb/100ft^2
CoF	0.34

As presented in table 7, mud rheology is in the range of a typical drilling fluid. By adding soluble salt, the value of YP was reduced to remain in acceptable range. Figure 19 and 20 illustrate the measured PV and YP for the sample muds for the case 3 with and without NPs at 25C.

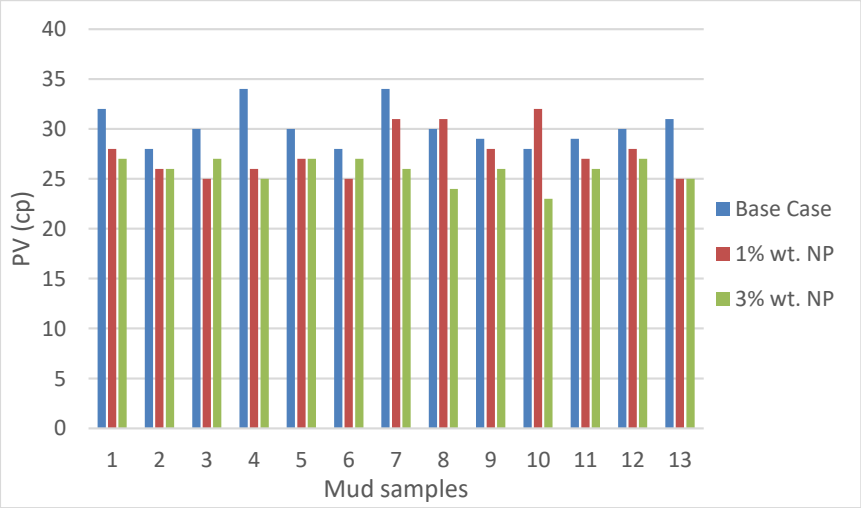

Figure 19. Measured PV for the mud samples of case 3 with and without NPs

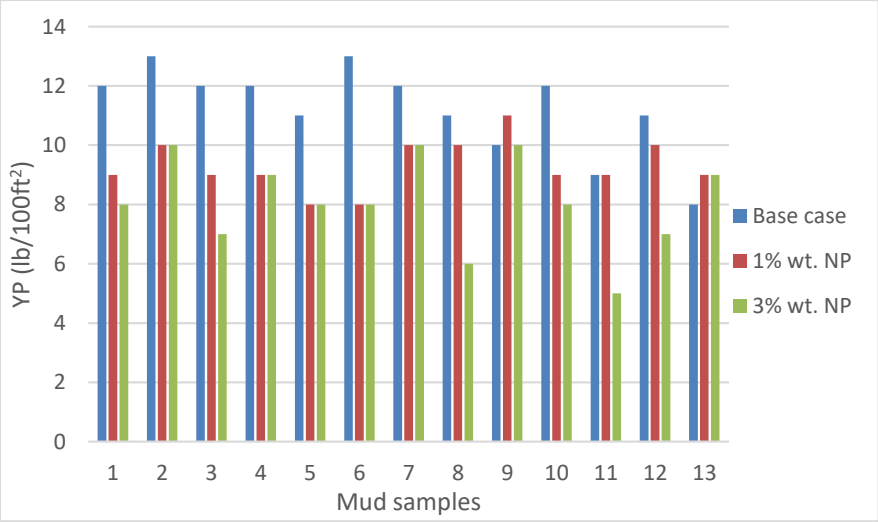

Figure 20. Measured YP for the mud samples of case 3 with and without NPs

3.4.4 Drilling fluid case 4

This mud formulation was designed to evaluate the performance of different size Barite NPs in the presence of other solid materials as well as polymers. The objective of designing this mud was to investigate the performance of NPs size in plugging different pore opening sizes and to provide more information for statistical analysis. Drilling fluid case 4 can be used in shallow to medium depth vertical intervals. Tables 8 and 9 show the components and properties of drilling fluid case 4.

Table 8 Composition of the drilling fluid case 4

Components	Amount (gr)
Water	330
1-Hexadecene	20
Surfactant	1
NaCl	50
PAC LV	2
Barite	70
KCl	20

Table 9 Properties of the drilling fluid case 4 at 25 C

Properties	Value
MW	10.5 ppg
PV	19 cp
YP	5 lb/100ft^2
CoF	0.3

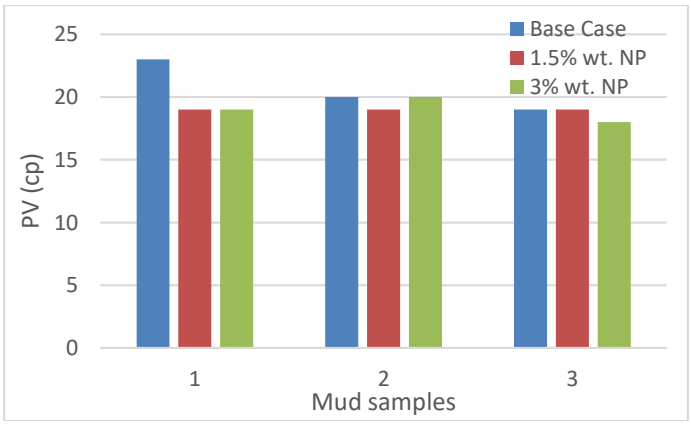

Figure 21. Measured PV for the mud samples of case 4 with and without NPs

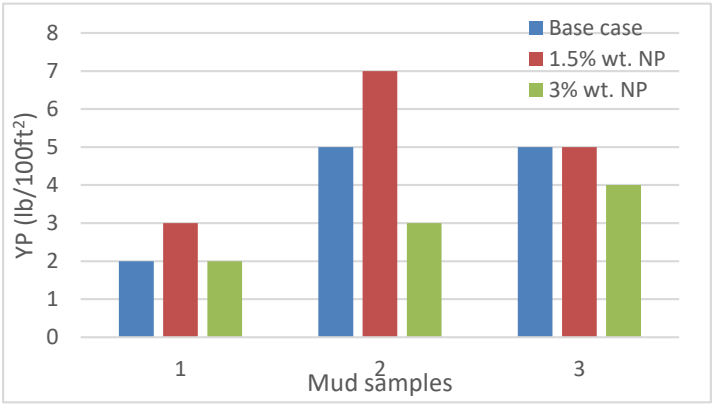

Figure 22. Measured YP for the mud samples of case 4 with and without NPs

In this case, YP and PV were reduced by adding more salt and reducing the solid content. Figure 21 and 22 illustrate the measured PV and YP for the sample muds for case 4 with and without NPs at 25C.

3.5 LPLT and HPHT filtration tests

All samples were tested using a standard API fluid loss apparatus or HPHT filtration tester. Three different qualitative filter papers and one type of ceramic disk were used to simulate porous media. Four different pressures and three different temperatures were selected to evaluate the performance of different mud samples. After preparing each drilling fluid sample, mud weight and rheological properties were measured and recorded. Figure 23 shows a standard API fluid loss tester.

Figure 23. The standard API fluid loss tester

The filtration test was conducted by filling the testing cup with the mud sample and placing it within the support structure. Then, the pressure cap with an attached pressure regulator was tightened via a T-screw handle. The desired pressure was provided using a CO_2 cartridge. A graduated cylinder was used to collect filtrate, and the cumulative volume of the filtrate was recorded at 5 or 2-minute intervals for 30 minutes.

A FANN HPHT filter press (series 387) was used to measure filtration at higher temperatures and pressure. The upstream pressure of 600 psi was applied when a backup pressure of 100 psi was used in downstream. The area of the filter paper used in the HTHP filter press was half of the area of the standard API filter press. Figure 24 shows a FANN HPHT filter press apparatus that was used in this study.

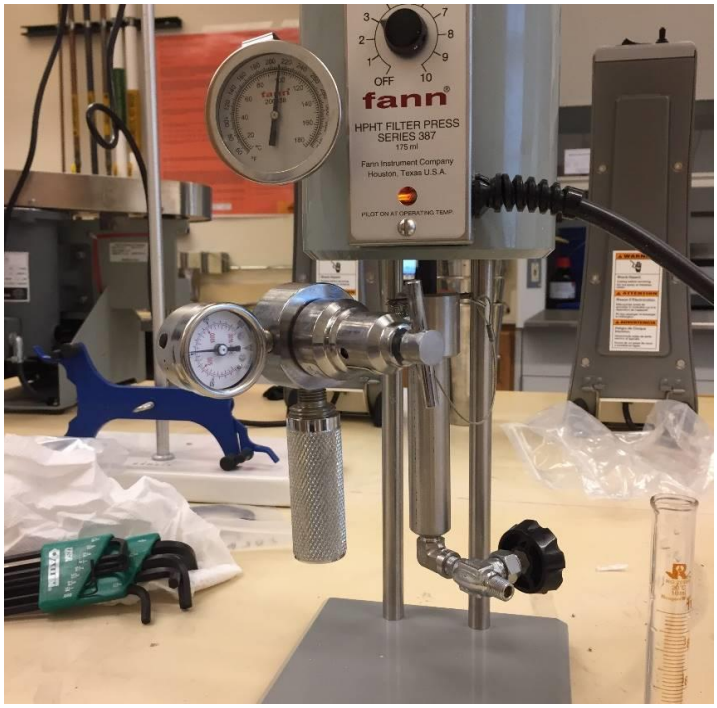

Figure 24. HPHT filtration apparatus

3.6 Lubricity tester

The lubricity test is designed to measure the coefficient of friction by simulating friction between the drill string and the wall of the borehole. Caldarola et al., (2016) and Alshubbar et al., (2017) studied the use of NPs in water based drilling fluid, and its influence on the lubricity. They concluded that using barite NPs in the water based drilling fluid decrease the CoF and based on the axial tension and torque analysis, it would be possible to drill a longer horizontal interval by extending the reach hundreds of meters with the same drillstring input power at surface. In this study, a FANN Lubricity Tester was used to evaluate lubricity property of the NPs-containing drilling fluid at 150 inch-pounds of torque at 60 RPM rotational speed as shown in Figure 25.

Figure 25. FANN Lubricity Tester

The ring and block are completely immersed in the mud sample. The apparatus runs at 60 RPM for 5 minutes in order to coat the surface of the ring and block with the drilling fluid. After that, 150 inch-pounds of torque is needed to be applied using the torque adjustment handle. Friction coefficient reading is recorded after a 5-minute stabilization period. The coefficient of friction is equal to meter reading divided by 100. The coefficient of Friction (CoF) is used to quantify the friction between surface slide in the presence of drilling fluid. CoF directly affects the rotational torque and axial drag.

3.7 High-pressure LCM test unit

Akhtarmanesh et al., (2016) investigate the use of NPs and LCM in drilling fluid and their effect on sealing pressure. A high-pressure LCM test unit was used to evaluate the sealing capabilities of the prepared drilling fluid samples. Nutshells were added to the prepared water-based drilling fluid samples in a 50 ppb concentration. Figure 26 shows a schematic of the high-pressure testing apparatus. As shown in Figure 26, the plastic accumulator is used to fill the high-pressure metal accumulator with drilling fluid. The syringe pump provides the required pressure (up to 10,000 psi) to inject drilling fluid into the test cell. A 2000-micron tapered disc was used in the testing cell for the purpose of simulating a wide fracture opening.

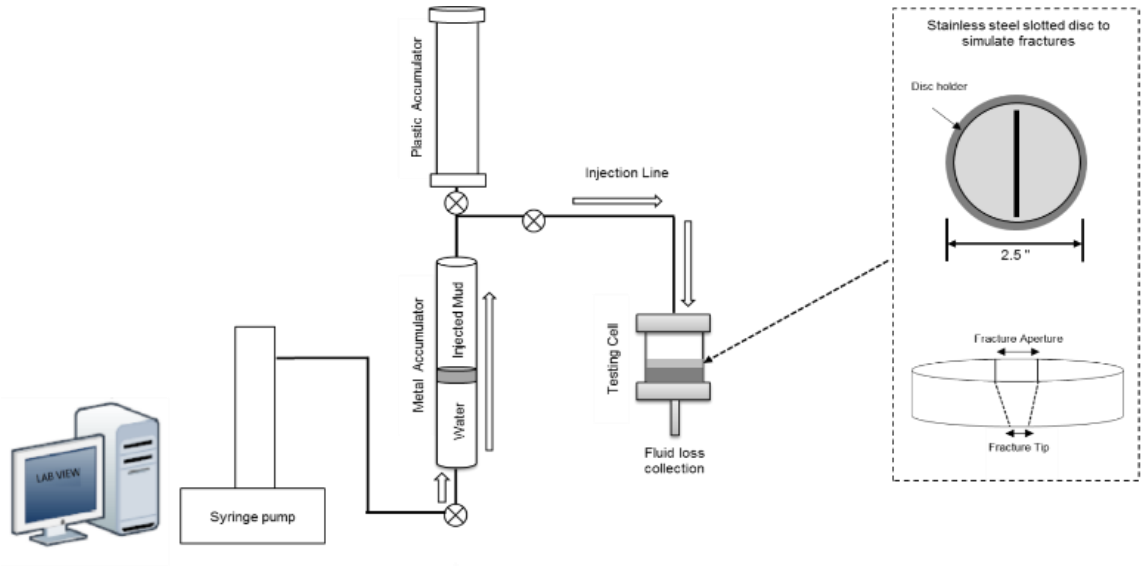

Figure 26. Schematic of the high-pressure testing apparatus

The test starts by injecting the drilling fluid into the testing cell at a flow rate of 25 ml/min while pressure is monitored. Drilling fluid injection continues to observe an increase in the injection pressure, which indicates that a seal has been formed on the fracture. Drilling fluid injection continues at the same flow rate until a rapid decrease in injection pressure occurs, which indicates the seal has been broken. After the seal breaks, since LCMs tend to re-form the seal after each

breaking, the test is repeated to measure the reopening sealing pressure. Figure 27 shows the high-pressure LCM test unit.

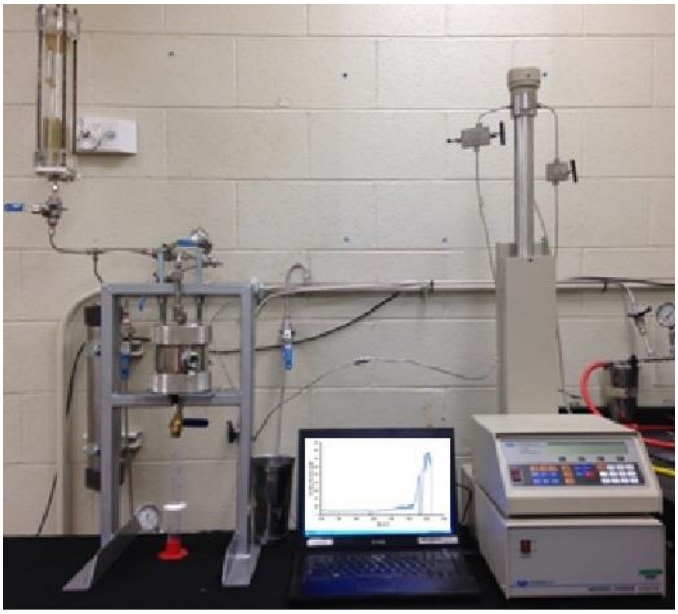

Figure 27. High-pressure LCM test unit

CHAPTER IV

EXPERIMENTAL RESULTS

This chapter presents the results of different experiments using graphs. Please see the appendix of this document to get detailed experimental data.

4.1 LPLT Filtration test

Different sizes of barite NPs (62, 744, 1205 nm) at different concentrations (up to 5% wt.) were used in four different drilling fluids. Three different qualitative papers with the pore opening sizes (2-5, 5-10 and 20-25 microns) were used in the LPLT filtration test. Although the majority of LPLT tests were conducted at the pressure difference of 100 psi, some of the experiments were conducted at 20 psi and 130 psi pressure difference.

4.1.1 Results for drilling fluid case 1

As mentioned in chapter 3, drilling fluid case 1 was designed to study the performance of barite NPs in reducing filtration in presence of none or limited solid content. Due to the high rate of filtration, the tests were conducted at 20 psi upstream pressure, and cumulative fluid losses were recorded at two-minute intervals. Figure 28 illustrates the fluid loss results when barite NPs (size = 62 nm) at concentrations of 1%wt., 3% wt., and 5% wt. are used. The results show that a mud sample containing 5% wt. barite NPs underperforms the base case. The visual result of filtrate color also suggested that the barite NPs were transmitted through the pore opening and no mud cake was formed on the filter paper. The mud samples containing 1% wt. and 3% wt. barite NPs

outperformed the base case by reducing filtration, because only a part of the total amount of barite content was NPs and the rest of it was normal barite.

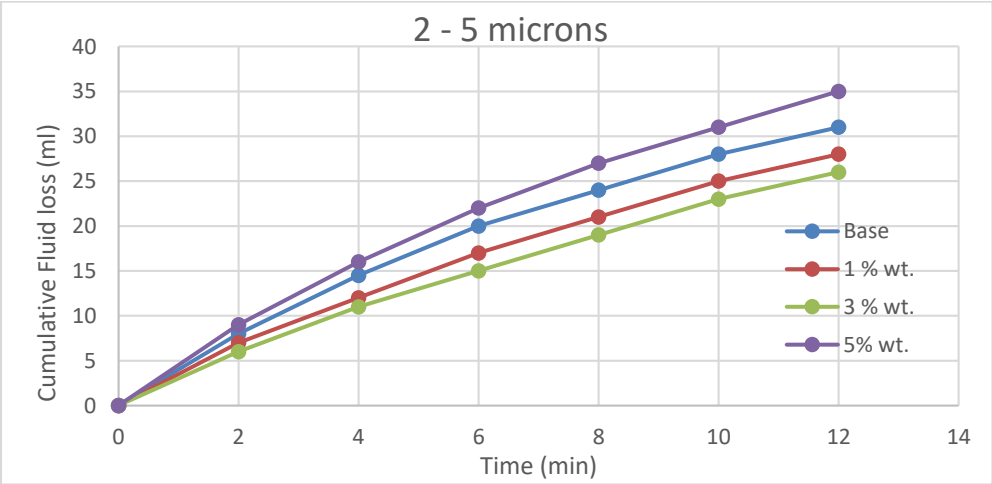

Figure 28. Fluid loss results using 2-5 micron filter paper at $\Delta P = 20$ psi

Even though drilling fluid case 1 does not seem to be practical mud in the real drilling operation, FLC materials such as PAC LV or starch were not used in the drilling fluid case 1 to minimize the influence of other additives. Figures 29 and 30 show the performance of drilling fluid case 1 for the higher pore opening size filter paper.

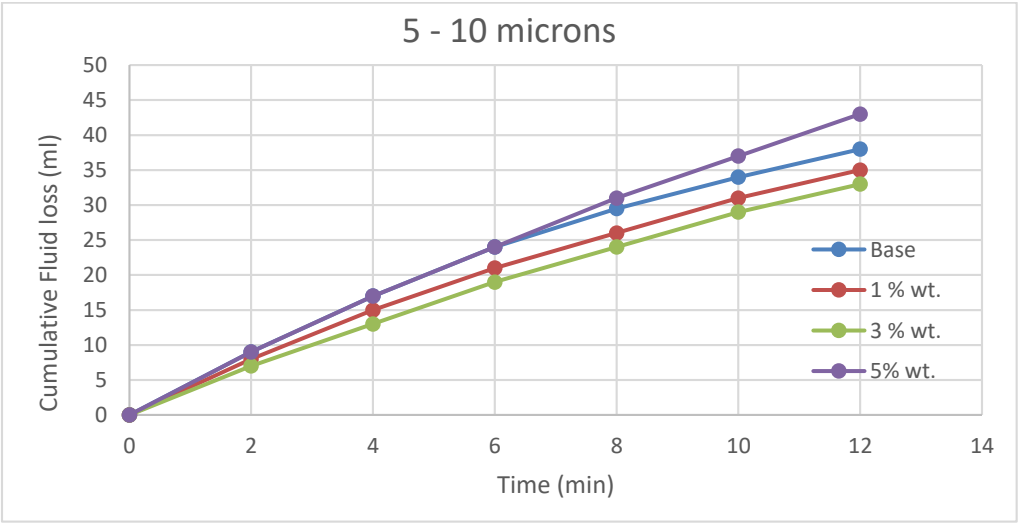

Figure 29. Fluid loss results using 5-10 micron filter paper at $\Delta P = 20$ psi

The results for 5-10 and 20-25 microns suggests that mud samples without normal barite fail to create filter cake and in these sizes of pore opening, discarding bigger particles is not recommended. Even in the presence of small amount of normal barite, mud samples containing a very small amount of barite NPs perform better than base case.

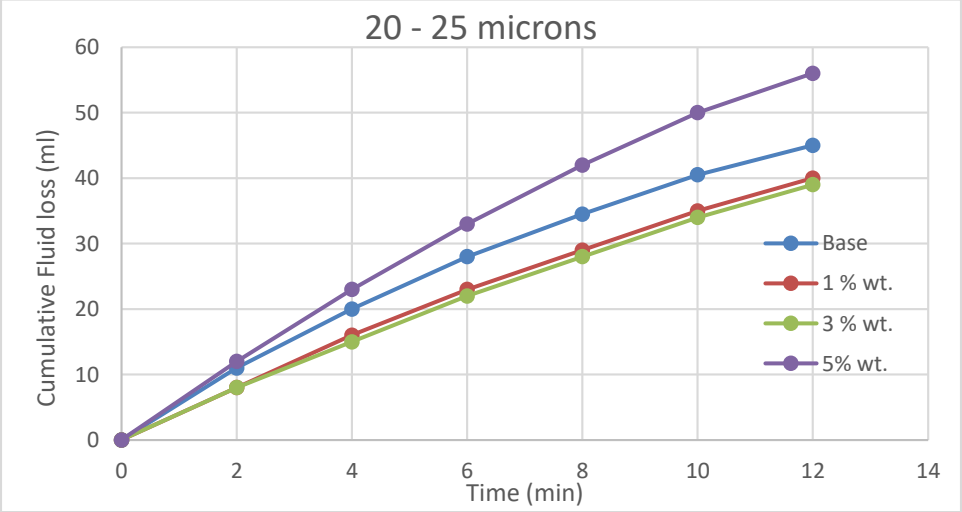

Figure 30. Fluid loss results using 20-25 micron filter paper at $\Delta P = 20$ psi

To compare fluid loss reduction for each sample mud, the final cumulative fluid losses were compared to the base case of each qualitative filter paper. The results are presented in figure 31.

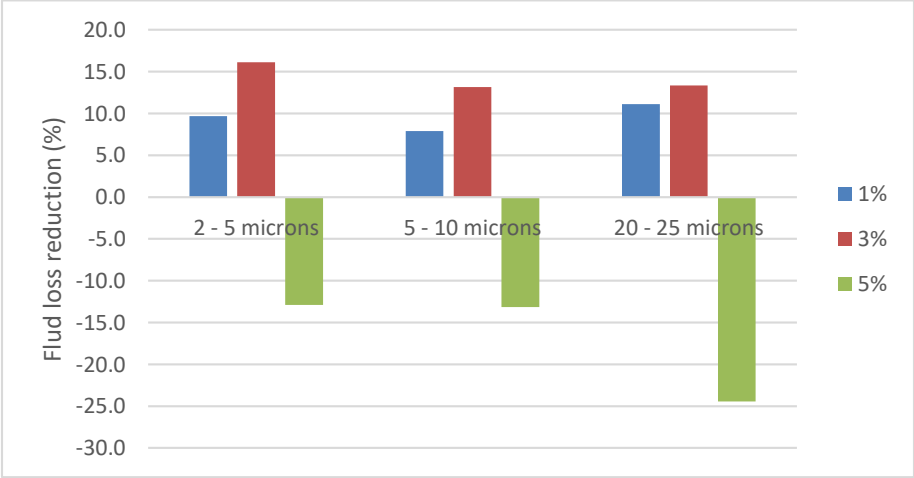

Figure 31. Fluid loss reduction comparison for different NPs concentrations for each qualitative filter paper

The results suggest that the performance of barite NPs with the size of 62 nm is better in reducing filtrate for smaller pore openings. However, using a combination of the different sizes of the solid particle can reduce filtrate even in larger pore opening sizes.

4.1.2 Results for drilling fluid case 2

As mentioned in chapter 3, drilling fluid case 2 was designed to study the performance of barite NPs on filtration reduction in presence of high solid content and polymers. Solid content helps to establish mud cake as well as FLC materials such as PAC LV. Polymers like xanthan gum increase YP and keep the solids suspended in the mud. All tests were conducted at 100 psi upstream pressure and 25 C temperature, and cumulative fluid loss was recorded at five-minute intervals. Figure 30 illustrates the fluid loss results when barite NPs (size = 744 nm) at concentrations of 1%wt., 2% wt. and 4% wt. are used. The results show that mud samples containing barite NPs outperform the base case.

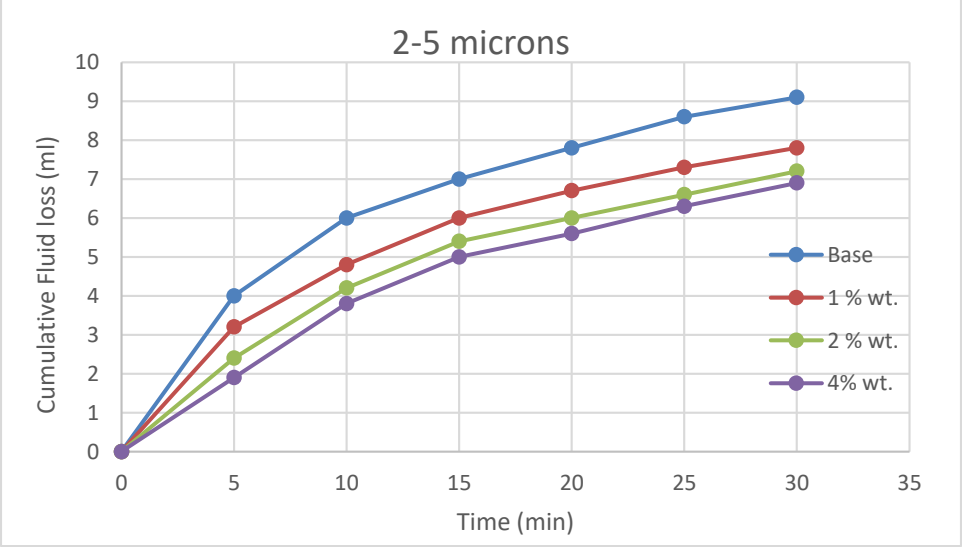

Figure 32. Fluid loss results using 2-5 micron filter paper at $\Delta P = 100$ psi

Even though drilling fluid case 2 contains a large amount of solid content (MW = 11.6 ppg), the high YP value decreases the performance of barite NPs. In other words, high thixotropic property,

due to use of a large amount of xanthan gum, reduces the forming rate of a thin filter cake on the surface of porous media. Figures 33 and 34 show the performance of drilling fluid case 2 for the higher pore opening size filter paper.

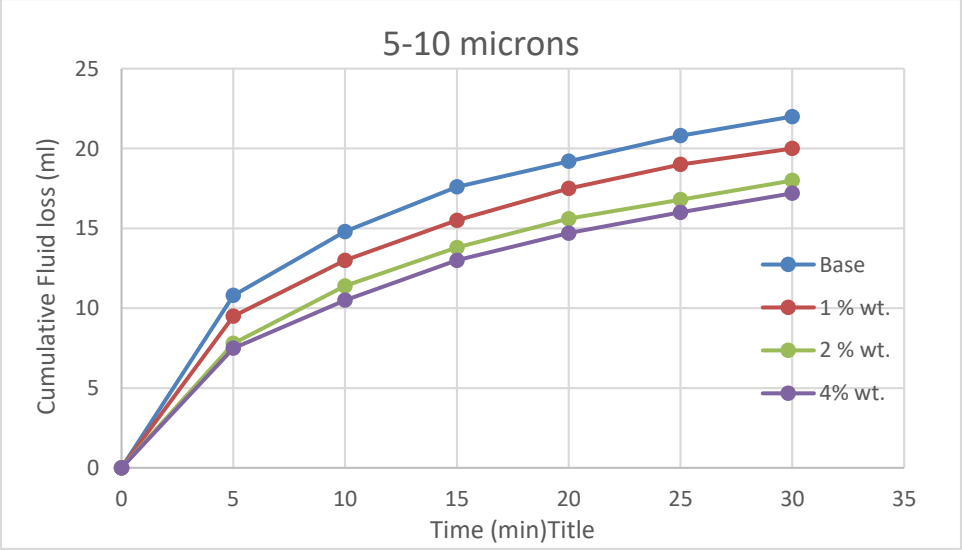

Figure 33. Fluid loss results using 5-10 micron filter paper at $\Delta P = 100$ psi

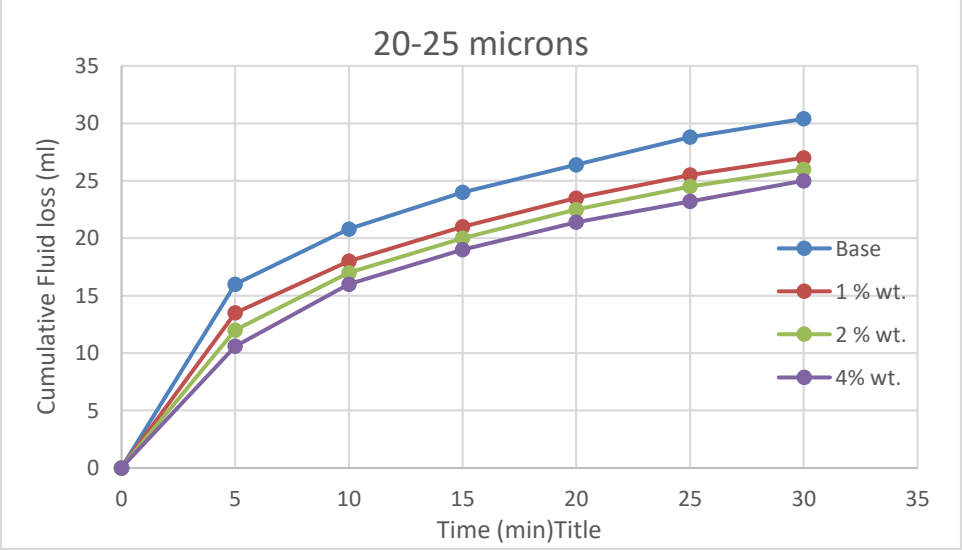

Figure 34. Fluid loss results using 20-25 micron filter paper at $\Delta P = 100$ psi

Considering the size of the used barite NPs (744 nm), results for 5-10 and 20-25 microns suggests that by increasing pore opening size (permeability), there is more likely to be a higher fluid loss even if barite NPs are used. In other words, better sealing can be achieved for smaller size pore

openings. For a better understanding of the fluid loss reduction results for each sample mud, the final cumulative fluid loss was compared to the base case of each qualitative filter paper. The results are presented in figure 35.

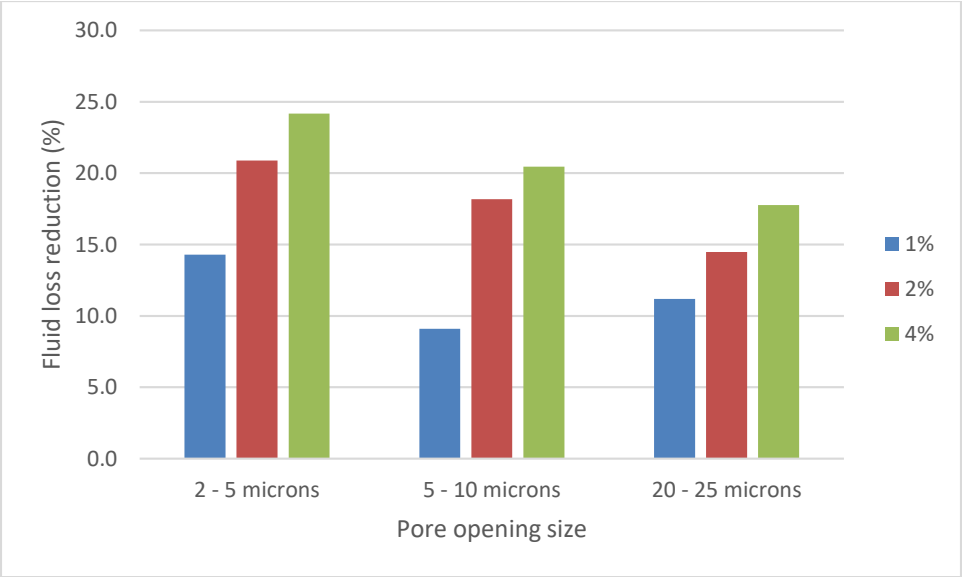

Figure 35. Fluid loss reduction comparison for different NPs concentrations for each qualitative filter paper

The results suggest that the performance of barite NPs with the size of 744 nm are better in reducing filtrate for smaller pore openings. However, using a combination of the different size of the solid particle is beneficial to reduce filtrate even in bigger pore opening sizes. It is important to notice that high YP can be blamed for a high amount of fluid loss. It is more likely that YP adversely influences the performance of barite NPs by preventing them from forming a thin filter cake at the first few minutes of the filtration test.

4.1.3 Results for drilling fluid case 3

As mentioned before, drilling fluid case 3 was designed to study the performance of different size of barite NPs on filtration reduction in the presence of solid materials and FLC. Solid content helps to establish mud cake as well as FLC materials such as PAC LV. To keep YP low, xanthan gum

was not included in formulation of drilling fluid case 3. All tests were conducted at 130 psi as upstream pressure and 25 C temperature, and cumulative fluid loss was recorded in five-minute intervals. Figure 34 illustrates the fluid loss results when barite NPs1(64 nm) and barite NPs2 (1205 nm) at concentrations of 1%wt. and 3% wt. are used. The results show that mud samples containing barite NPs outperform the base case.

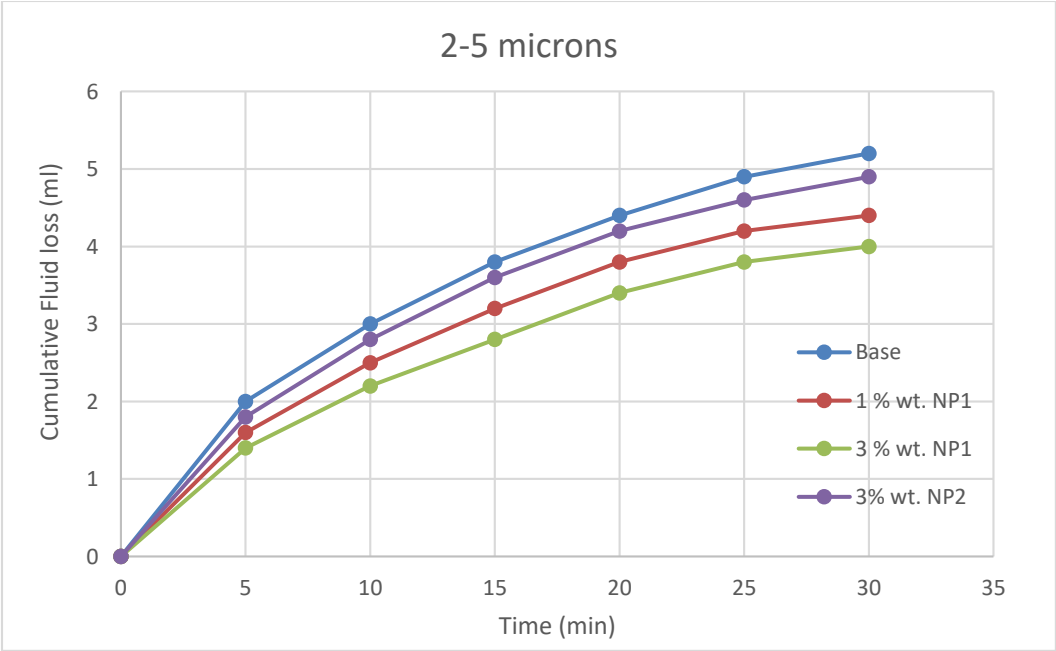

Figure 36. Fluid loss results using 2-5 micron filter paper at $\Delta P = 130$ psi

Drilling fluid case 3 contains a high amount of solid content (MW = 10.5 ppg) and shows low YP value that is beneficial toward the performance of barite NPs. As shown in figure 36, the volume of fluid loss is low and using barite NPs in drilling fluid caused clear reduction of fluid loss. Figure 37 and 38 show the performance of drilling fluid case 3 for the higher pore opening size filter paper.

Considering the size of the used barite NPs (62 nm and 1205 nm), results for 2-5 and 5-10 microns filter paper suggest that the performance of barite NPs with the size of 62 nm outperform barite NPs with the size of 1205 nm. The results for 20-25 micron also confirmed the better performance of smaller NPs sizes.

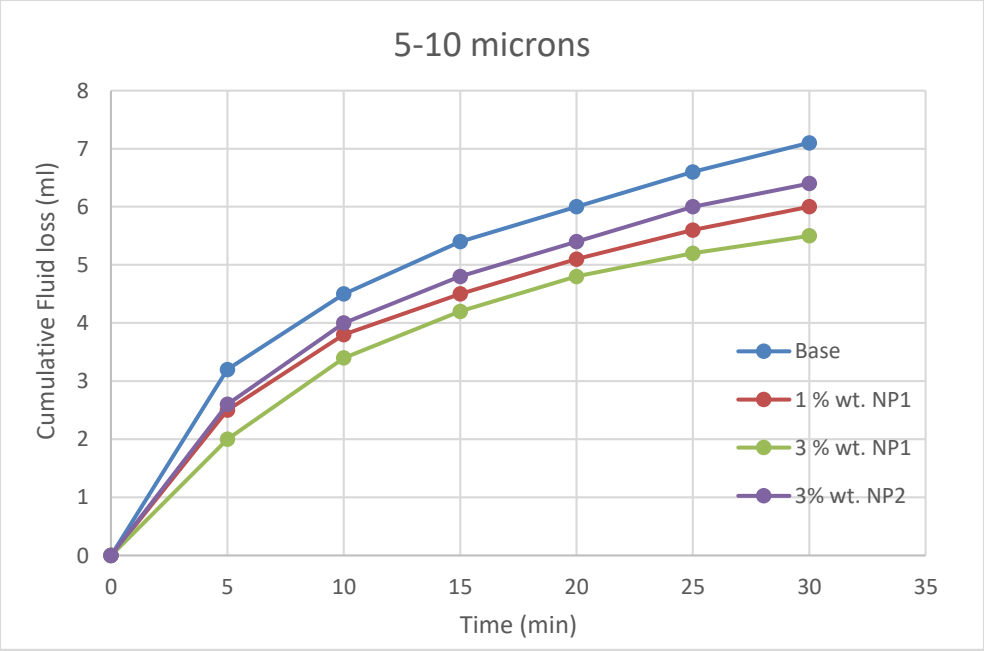

Figure 37. Fluid loss results using 5-10 micron filter paper at $\Delta P = 130$ psi

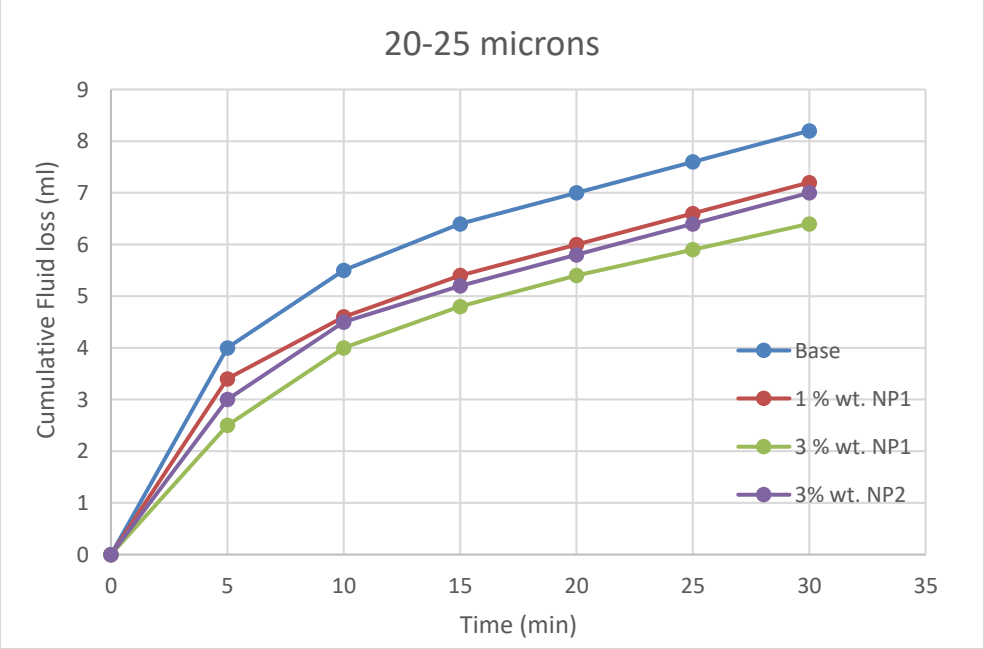

Figure 38. Fluid loss results using 20-25 micron filter paper at $\Delta P = 130$ psi

The results suggest that better sealing can be achieved for smaller size barite NPs. For a better understanding of the fluid loss reduction results for each sample mud, the final cumulative fluid

loss was compared to the base case of each qualitative filter paper. The results are presented in figure 39.

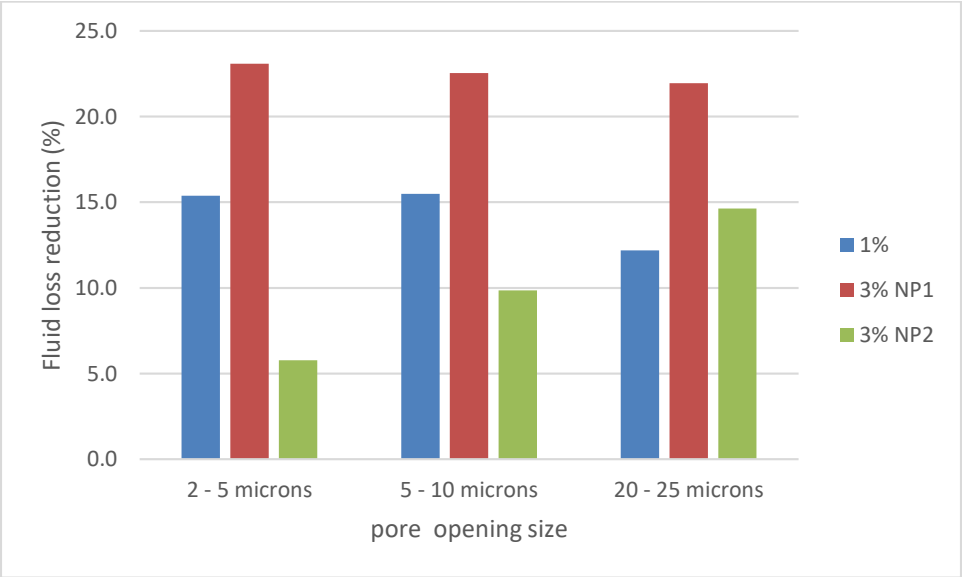

Figure 39. Comparison of Fluid loss reduction for different NPs concentrations and sizes for each qualitative filter paper

4.1.4 Results for drilling fluid case 4

As mentioned before, drilling fluid case 4 was designed to study the performance of different sizes of barite NPs on filtration reduction in the presence of solid materials and FLC. All tests were conducted at 100 psi as upstream pressure and 25 C temperature, and cumulative fluid loss was recorded in five-minute intervals. Figure 38 illustrates the fluid loss results when barite NPs1 (62 nm) and barite NPs2 (1205 nm) at concentrations of 1.5% wt. and 3% wt. are used. The results show that mud samples containing barite NPs outperform the base case. Some of the tests were repeated to make sure that results were reproducible.

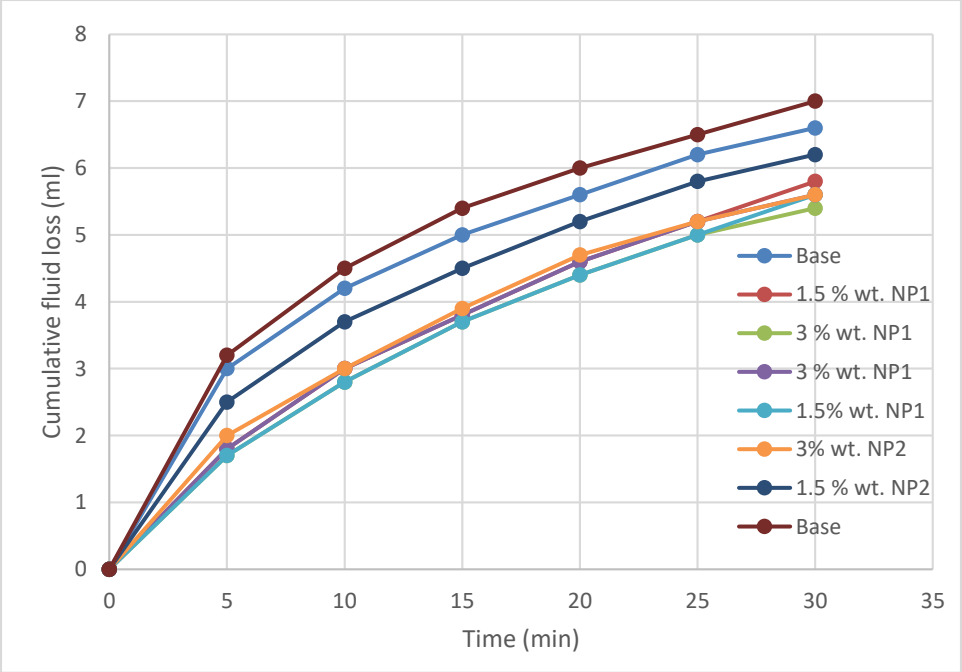

Figure 40. Fluid loss results using 2-5 micron filter paper at $\Delta P = 100$ psi

For a better understanding of the fluid loss reduction results for each sample mud, the final cumulative fluid loss was compared to the base case of each qualitative filter paper. The results are presented in figure 41.

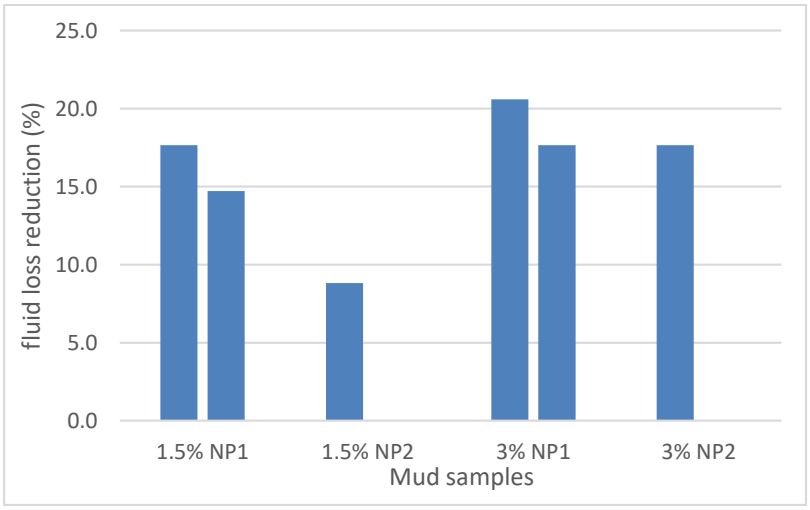

Figure 41. Comparison of Fluid loss reduction for different NPs concentrations and sizes

4.2 HPHT filtration result

To investigate the effect of higher temperature and pressure, HPHT tests were conducted using drilling fluid case 3 at two different NPs concentrations using NP1 (62 nm) and NP2 (1205 nm). The tests were conducted at 90C and 120C temperatures, and 500 psi differential pressure. Figure 42 shows the results of the HPHT filtration test using different size and concentration of NPs.

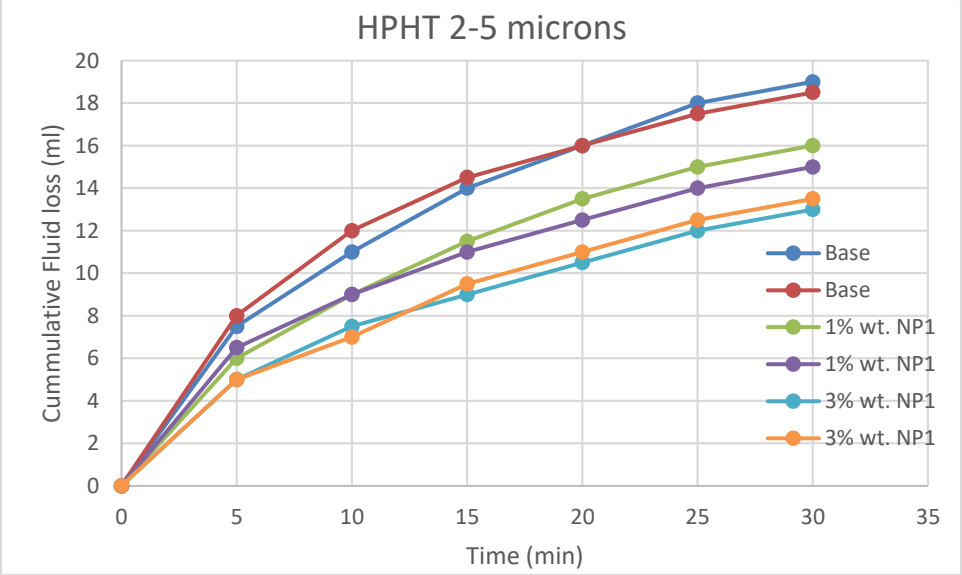

Figure 42. Fluid loss results using 2-5 micron filter paper at ΔP=500 psi

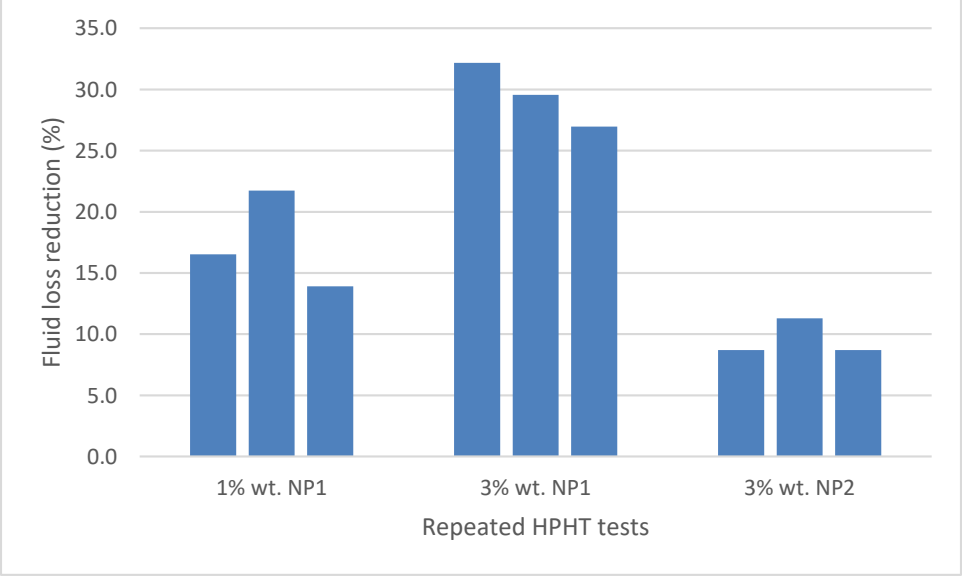

Figure 43. Comparison of Fluid loss reduction for different NPs concentrations and sizes

Figure 43 shows the performance of different sizes and concentrations of NPs in reducing HPHT filtration. To obtain a better insight of the NPs performance, a series of HPHT filtration tests were conducted using ceramic disks with the permeability of 775 md. Figure 44 shows a summary of the results using the ceramic disk as porous media in HPHT tests.

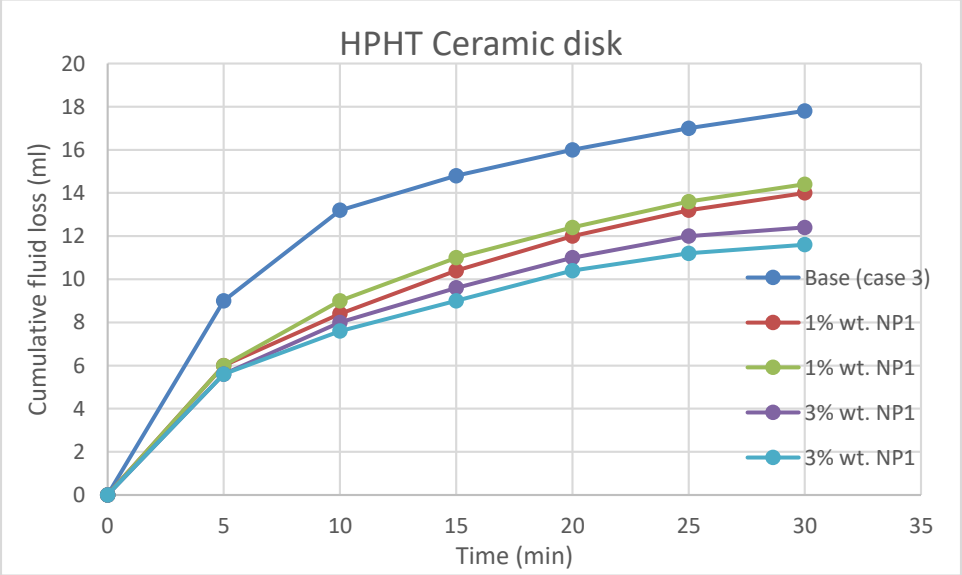

Figure 44. Fluid loss results using 775 md ceramic disks at ΔP=500 psi

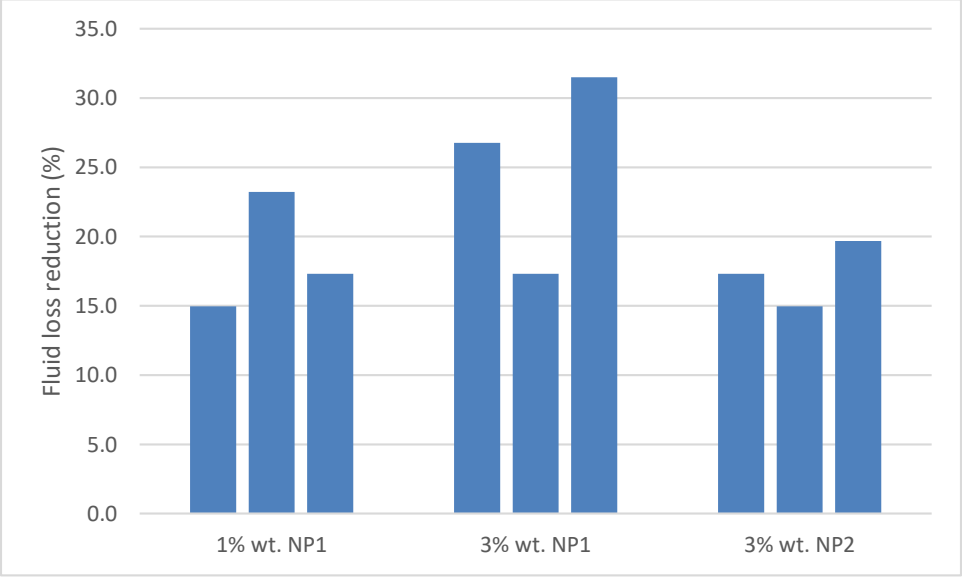

Figure 45. Comparison of Fluid loss reduction for different NPs concentrations and sizes

4.3 Particle plugging test

Due to the high suspension capacity of drilling fluid case 2, it was selected to investigate the effect of adding barite NPs on the performance of LCMs in fracture sealing pressure. Based on the previous experiments (Al-saba et al., 2014), 50 ppb nutshell and 2000 micron tapered discs were selected to evaluate the sealing efficiency of the drilling fluid case 2 with and without NPs.

As shown in Figure 46, the seal formed after about 3 minutes of drilling fluid injection. As injection continued at the same rate, upstream pressure increased rapidly. The formed seal on the fracture can stand this pressure before failure. Using the base mud containing 50 ppb nutshells, the formed seal broke at 1096 psi overbalance pressure and a sharp decrease at upstream pressure was observed.

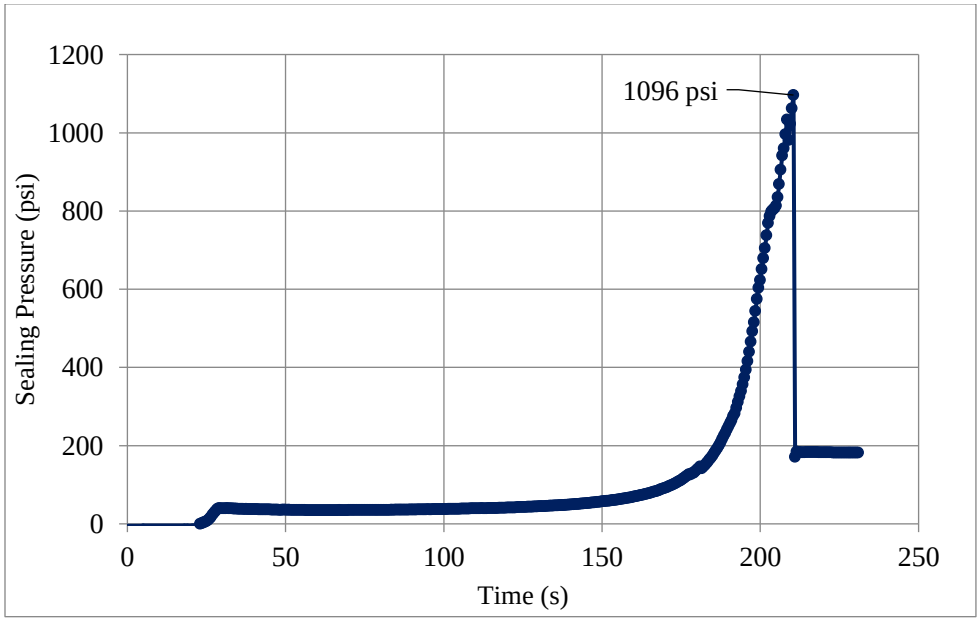

Figure 46. Particle plugging test for the base mud case 2

Figure 47 shows the top view of the formed plug when the base sample of drilling fluid case 2 was used comprising 50 ppb nutshells. The diameter of the tapered slot shown in figure 45 is 2.5 inches and the thickness of the slot is a quarter inch. The fracture opening is 2000 microns and the fracture length is 2 inches.

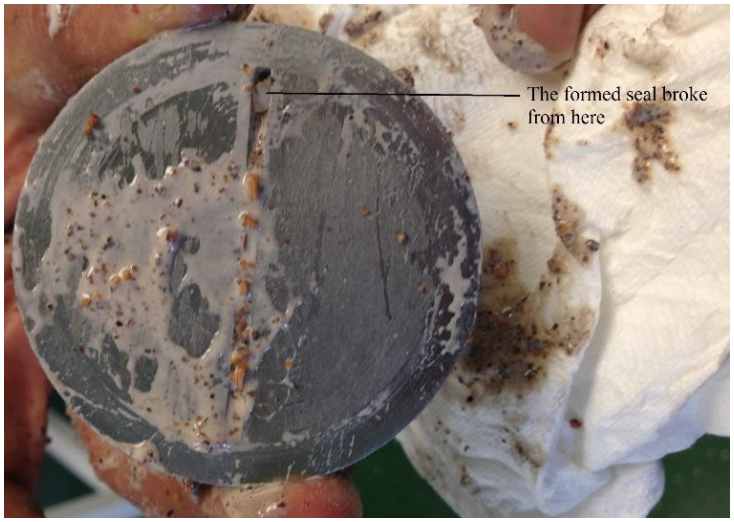

Figure 47. Top view of formed plug using the base mud containing 50 ppb nutshells

Figure 48 shows the particle plugging test data when the drilling fluid containing 3% wt. of 744 nm barite NPs and 50 ppb nutshells was used. The maximum sealing pressure was recorded to be 1761 psi.

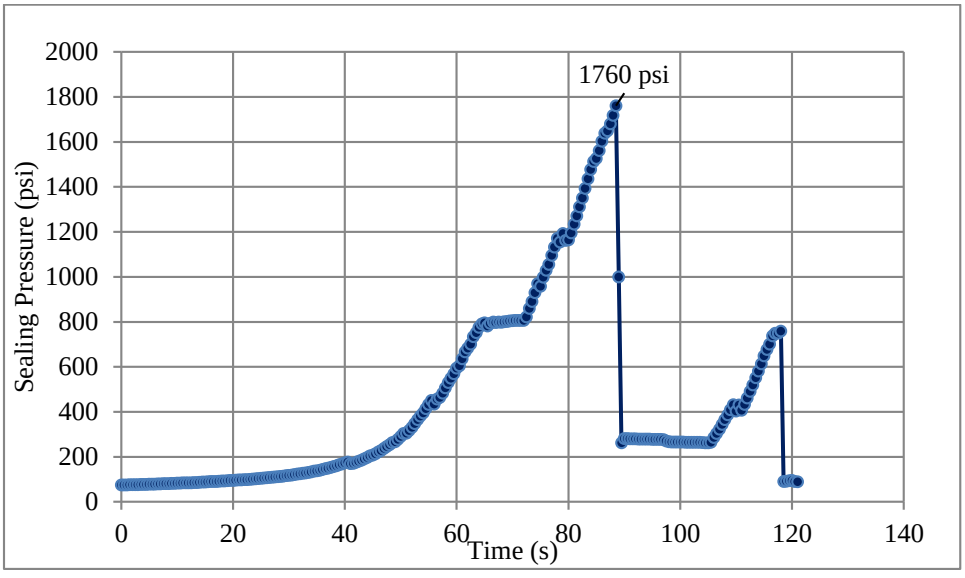

Figure 48. Particle plugging test for the chemical-barite nanoparticle mud

The particle plugging test was also conducted using the drilling fluid containing 3% wt. of 1205 nm barite nano-micro particles and 50 ppb nutshells. Figure 47 shows the results depicting the sealing pressure for drilling fluid case 2 containing mechanically-made barite nano-micro particles.

During the first cycle, the maximum recorded sealing pressure was 1677 psi. After the seal plug re-formed, the test was repeated. The second cycle shows very high sealing pressure, and achieved sealing pressure as high as 3347 psi.

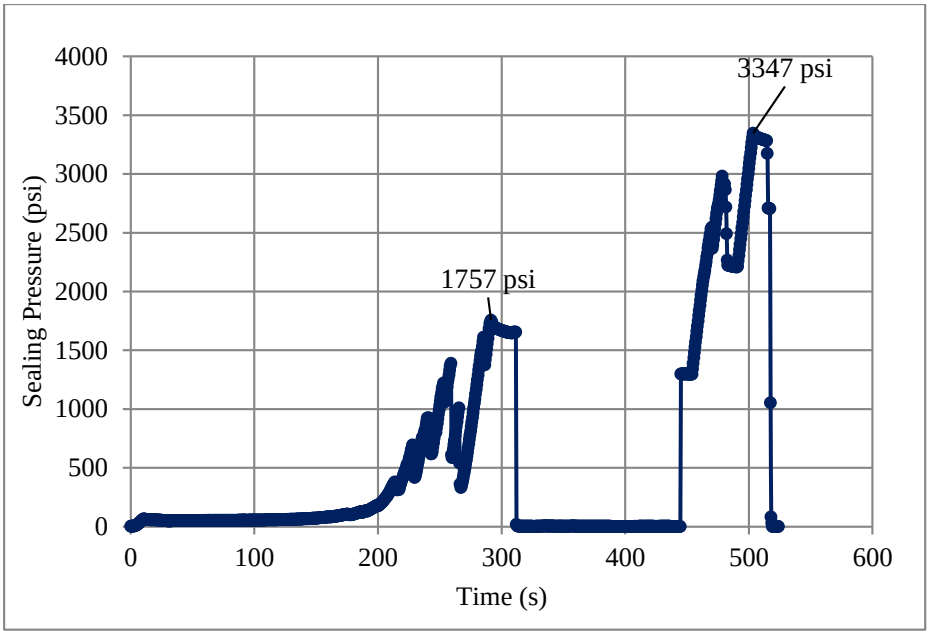

Figure 49. Particle plugging test for the 1205 nm barite particles

The results suggest that even for a 2000 microns opening, using NPs is beneficial if a combination of different size solids is used in formulating the drilling fluid. Figure 50 summarizes the results of the maximum sealing pressure using different drilling fluid samples.

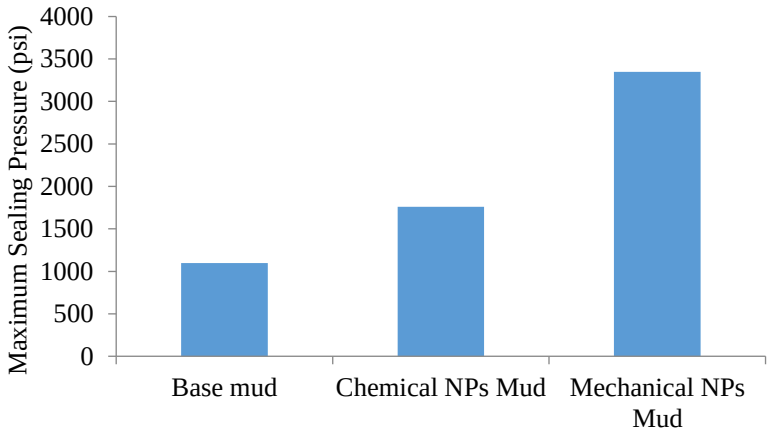

Figure 50. Maximum sealing pressure for different tested drilling fluids

4.4 Lubricity results

Friction causes rotational torque and axial drag between drillstring and wellbore. Reducing friction helps engineers to be able to design extended reach wells and longer horizontal sections using the same drilling rig. The CoF for two drilling fluid cases was measured using a FANN lubricity tester. The results are summarized in table 10. Results suggest that using barite NPs reduces the CoF for both cases.

Table 10. CoF results for drilling fluid case 3 and case 4

	Drilling fluid case 3	Drilling fluid case 4
Base	0.32	0.34
1.5% wt. NP1	0.26	0.29
3% wt. NP1	0.27	0.29
1.5% wt. NP2	0.28	0.32
3% wt. NP2	0.27	0.31

As shown in figure 50 the CoF reduces by adding barite NPs to the drilling fluid case 3 and case 4.

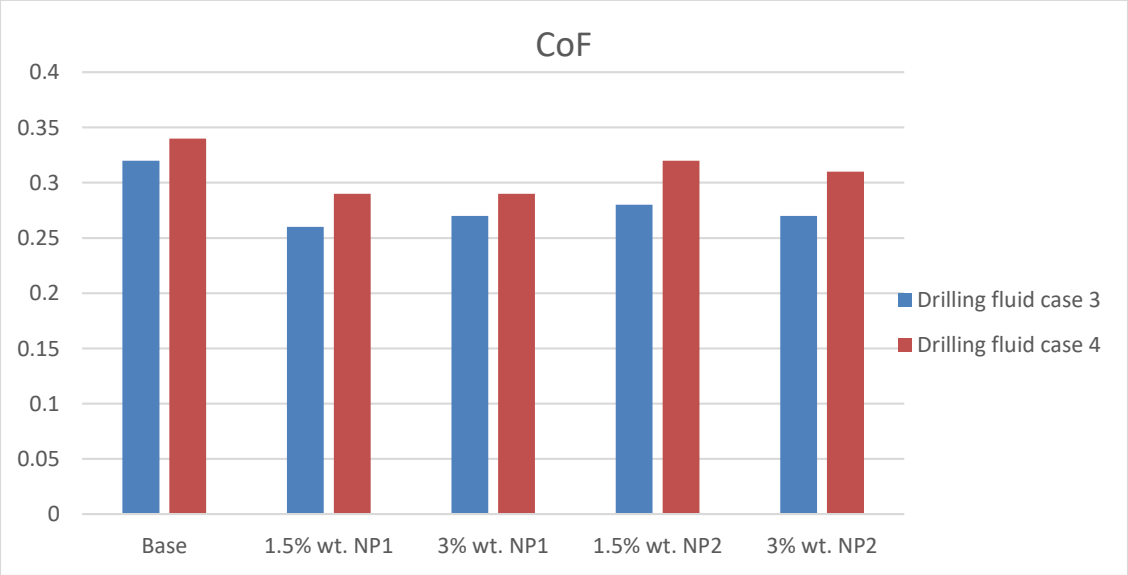

Figure 51. The CoF results for drilling fluid case 3 and case 4

CHAPTER V

STATISTICAL ANALYSIS AND PREDICTIVE MODELS

In this chapter, statistical analysis of the data, using different tools including SAS software and Microsoft Azure machine learning cloud computation, are presented. Boosted decision tree regression and neural network regression were used to model fluid loss reduction based on influencing parameters. The models were evaluated using test data, and statistical parameters such as Mean Absolute Error and Root Mean Squared error and R^2 were presented for each model. Based on the statistical analysis, differential evolution algorithm was used to generate a model for fluid loss reduction based on influencing parameters. This model can be used in combination with the breakdown pressure initiation model that has been presented in this chapter.

The collected data was prepared in the correct format and then analyzed statistically. Statistical Analysis Software (SAS) was used to evaluate variables. Table 11 shows summary statistics of the data. Q1 is a median in the lower half, and Q3 is a median for the upper half of the data. MAD stands for median absolute deviation.

Table 11. Summary statistics of the data

Summary Statistics						
Variable	Q1	Median	Q3	Mean	Standard deviation	MAD
Time	10	15	25	16.1875	8.8084	11.8608
NPC	1	3	3	2.2813	1.0013	0.7413
NPS	62	62	744	451.8	485.3	0
Perm	12	56	506	244.7	310.4	65.2345
DP	100	130	500	245.6	199.8	103.8
Temp	25	25	120	59.5	44.9194	0
Area	31.67	63.62	63.62	51.6388	15.4947	0
PV	21	26	29	25.0417	9.4856	4.4478
YP	6.5	9	10	14.9375	16.3359	2.9652
MW	10.3	10.5	10.5	10.4313	0.8059	0
Hmc	1	1	1.5	1.5625	1.0607	0
FLR	15.5903	21.9756	28.8127	22.9112	9.4524	9.779

Analysis of variance (ANOVA) uses F-tests to assess the equality of means in a group of variables. F-value of 76.64 indicates that the between-groups variance is 76.64 times the size of the within-group variance. In other words, the means of variables spread out more than the variability of the data within each variable. Table 12 shows a single F-test result on the collected data.

Table 12. Analysis of variance

Analysis of Variance					
Source	DF	Sum of Squares	Mean Square	F Value	Pr > F
Model	11	19318	1756.19028	76.64	<.0001
Error	276	6324.82708	22.91604		
Corrected Total	287	25643			

Univariate regression was used to model FLR based on different variables. Root MSE (RMSE) is the standard deviation of the error which is the square root of the Mean Square Residual. Dependent Mean is the mean of the dependent variable (FLR). Coeff Var is the coefficient of variation and is equal to the RMSE divided by the mean of the dependent variable. Table 13 illustrates overall model fit analysis.

Table 13. Overall model fit analysis

Root MSE	4.787	R-Square	0.7533
Dependent Mean	22.91	Adj R-Sq	0.7435
Coeff Var	20.89		

After the model had been fit, predicted and residual values were calculated. Figure 52 visually shows different statistical graphs including histogram of residuals, predicted value vs. residual,

residual-fit spread plot, and predicted value vs. actual value plot. The histogram of residuals (Percent vs. Residual plot) suggests that the residuals are normally distributed.

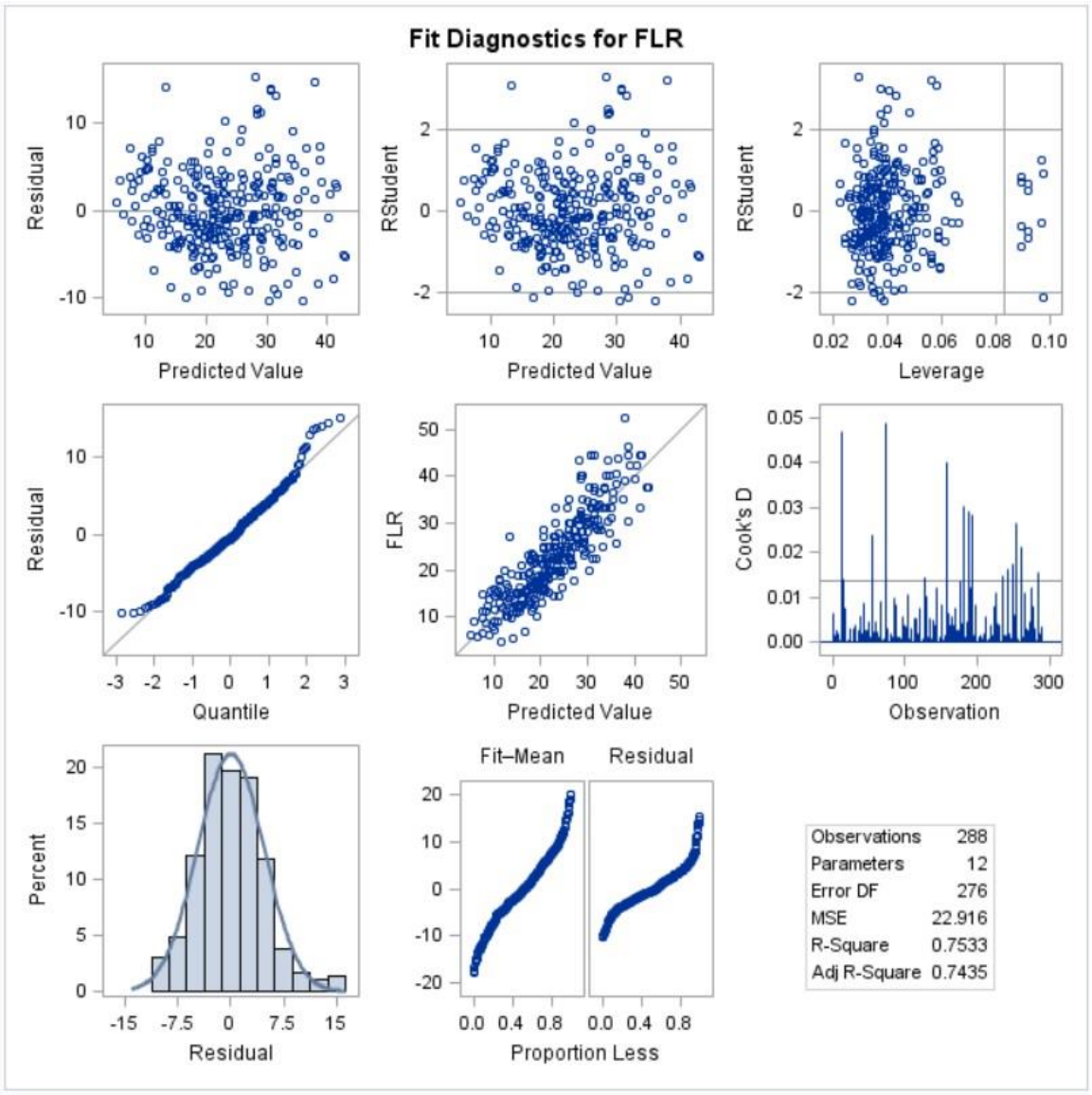

Figure 52. Goodness of the fit graphs for FLR

5.1 Statistical analysis

5.1.1 Fluid Loss reduction

Table 14 shows the results for the drilling fluid case 2 based on the changing variables. The investigated variables are permeability, NPC concentration, NPs size, differential pressure, temperature, plastic viscosity and yield point. A base case was selected for the comparison and also for sensitivity analysis.

Table 14. Changing variables for the drilling fluid case 2

Changing variable	Type	K (md)	NPC (%)	NPS (nm)	DP (psi)	T (C)	PV (cp)	YP ($lb/100ft^2$)	FL (ml)
	DF2	12	0	NA	100	25	40	50	9.1
	DE2	12	1	744	100	25	39	49	7.8
	DF2	56	4	744	100	25	36	47	17.2
	DF2	12	4	62	100	25	34	48	6.9
	DE2	56	0	NA	100	25	39	52	22
	DF2	56	1	744	100	25	40	51	20
NPS	DF2	56	3	744	100	25	36	49	17.5
Base	DF2	56	3	62	100	25	37	48	11
NPS	DF2	56	3	1205	100	25	40	50	15
DP	DF2	56	3	62	70	25	38	48	8
DP	DF2	56	3	62	130	25	38	50	14.5
T	DF2	56	3	62	100	90	26	32	23
T	DF2	56	3	62	100	130	21	25	26
K	DF2	506	3	62	100	25	36	46	26
K	DF2	12	3	62	100	25	38	49	7.2
NPC	DF2	56	1	62	100	25	33	52	18
NPC	DF2	56	4	62	100	25	36	46	10
	DF2	506	0	NA	100	25	39	49	30.4
	DF2	506	1	62	100	25	40	51	26
	DF2	506	4	744	100	25	35	45	25
	DF2	12	2	744	100	25	38	49	7.2
	DF2	56	2	744	100	25	41	52	18
	DF2	506	2	744	100	25	39	47	26
	DE2	506	1	744	100	25	39	49	27

The results suggest that by increasing temperature, rheology properties such as plastic viscosity and yield point decrease. Variables and corresponding fluid loss were normalized based on the selected base case to study the sensitivity analysis for the fluid loss and each variable. Table 16 shows the normalized fluid loss values for each corresponding variable. The influence of temperature on rheology properties is hidden in variable T. Increasing temperature reduces PV and

YP which effects fluid loss. Increasing the temperature reduces the cohesive forces in liquid phase that causes viscosity reduction. Table 15 shows the selected results for the sensitivity analysis.

Table 15. Normalized fluid loss for each variable

Parameter	value	Normalized	FL	Normalized FL
DP	70	0.70	8.0	0.73
	100	1.00	11.0	1.00
	130	1.30	14.5	1.32
T	25	1.00	11.0	1.00
	90	3.60	23.0	2.09
	130	5.20	26.0	2.36
NPC	1	0.33	18.0	1.64
	3	1.00	11.0	1.00
	4	1.33	10.0	0.91
NPS	62	1.00	11.0	1.00
	744	12.00	17.5	1.59
	1205	19.44	18.0	1.64
K	12	0.21	7.2	0.65
	56	1.00	11.0	1.00
	506	9.04	26.0	2.36

Figure 53 shows sensitivity analysis for fluid loss and affecting variables. The trending lines show that fluid loss has a direct relationship to the differential pressure. Increasing barite NPs concentration reduces fluid loss. In the studied range of NPs size, by increasing NPs size, fluid loss increases, even though NPs size is not a governing variable in the studied range of NPs concentration. Temperature shows an important influence on the fluid loss by reducing viscosity and yield point. Results show that increasing permeability reduces the NPs performance and increases the fluid loss.

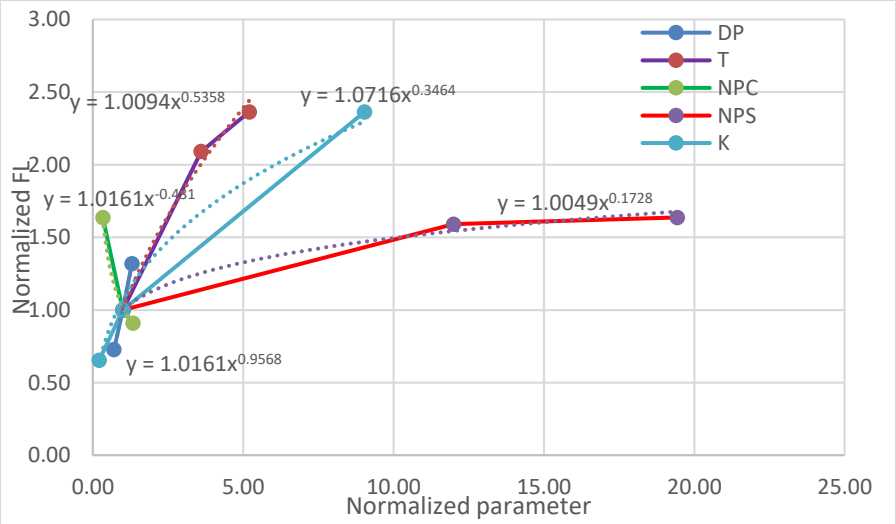

Figure 53. Sensitivity analysis for FL and influencing variables (case 2)

Based on the sensitivity analysis, the following equation was derived to simulate fluid loss reduction in the presence of barite NPs in base case 2.

$$\frac{FL}{FL_B} = 1.12 \times \left(\frac{DP}{DP_B}\right)^{0.95} \times \left(\frac{NPC}{NPC_B}\right)^{-0.431} \times \left(\frac{NPS}{NPS_B}\right)^{0.173} \times \left(\frac{K}{K_B}\right)^{0.346} \times \left(\frac{T}{T_B}\right)^{0.536} \quad \text{Eq.18}$$

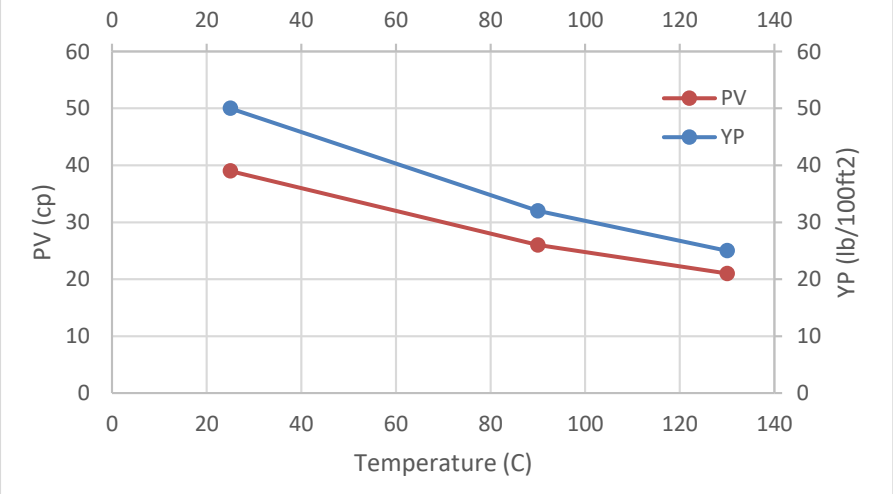

Figure 54. The effect of increasing temperature on PV and YP for mud case 2

The effect of changing plastic viscosity and yield point of drilling fluid is hidden in temperature term. In other words, increasing temperature causes reduction in plastic viscosity and yield point, which results in higher filtration.

Table 16 Changing variables for the drilling fluid case 3

Changing variable	Type	K (md)	NPC (%)	NPS (nm)	DP (psi)	T (C)	PV (cp)	YP ($lb/100ft^2$)	FL (ml)
	DF3	12	0	NA	100	25	32	12	4
	DF3	12	0	NA	130	25	28	13	5.2
	DE3	56	0	NA	100	25	30	15	5.8
	DF3	56	0	NA	100	25	34	12	5.5
	DF3	56	0	NA	130	25	30	15	7.1
	DF3	506	0	NA	100	25	28	13	6.3
	DF3	506	0	NA	130	25	34	12	8.2
K	DE3	12	3	62	100	25	27	8	3.1
K	DF3	506	3	62	100	25	26	10	6
NPC	DF3	56	1	62	100	25	31	10	5.8
NPC	DF3	56	4	62	100	25	30	9	3.8
Base	DF3	56	3	62	100	25	29	8	4.2
NPS	DF3	56	3	744	100	25	26	10	5.5
NPS	DF3	56	3	1205	100	25	30	10	6.2
T	DF3	56	3	62	100	90	15	6	10
T	DE3	56	3	62	100	130	12	5	12
DP	DF3	56	3	62	70	25	26	10	3
DP	DF3	56	3	62	130	25	26	10	5.8
	DE3	12	1	62	130	25	31	10	4.4
	DF3	56	1	62	130	25	28	11	6
	DF3	506	1	62	130	25	32	9	7.2
	DF3	12	3	62	130	25	29	8	4
	DE3	56	3	62	130	25	26	10	5.5
	DF3	506	3	62	130	25	28	9	6.4
	DE3	12	3	1205	130	25	29	10	4.9
	DF3	56	3	1205	130	25	27	8	6.4
	DF3	506	3	1205	130	25	26	10	7
	DF3	12	0	NA	500	120	30	11	7.6
	DF3	12	0	NA	500	120	29	10	7.4
	DE3	12	0	NA	500	93	28	12	8
	DF3	12	1	62	500	120	28	9	6.4
	DF3	12	1	62	500	120	26	10	6
	DF3	12	1	62	500	93	25	9	6.6
	DE3	12	1	62	500	120	26	9	5.2
	DF3	12	1	62	500	120	27	8	5.4
	DE3	12	1	62	500	93	25	8	5.6
	DF3	12	3	1205	500	120	27	7	7
	DF3	12	3	1205	500	120	25	9	6.8
	DF3	12	3	1205	500	120	27	8	7
	DF3	775	0	NA	500	120	29	9	17
	DF3	775	0	NA	500	120	30	11	16
	DE3	775	0	NA	500	120	31	8	17.8
	DF3	775	1	62	500	120	27	9	14.4
	DF3	775	1	62	500	120	28	10	13
	DF3	775	1	62	500	120	25	9	14
	DE3	775	3	62	500	120	24	6	12.4
	DF3	775	3	62	500	120	26	10	13.2
	DE3	775	3	62	500	120	23	8	11.6
	DF3	775	3	1205	500	120	26	5	14
	DE3	775	3	1205	500	120	27	7	14.4
	DF3	775	3	1205	500	120	25	9	13.6

Table 16 shows the results of drilling fluid case 3 based on the changing variables as described previously including permeability, NPs concentration, NPs size, differential pressure, temperature, plastic viscosity, and yield point. A base case similar to the previous case was selected for the comparison and also for sensitivity analysis.

As in the previous case, the results suggest that by increasing temperature, rheology properties, including plastic viscosity and yield point, diminish. Variables and corresponding fluid loss were normalized based on the selected base case to study the sensitivity analysis for the fluid loss and each variable. Table 17 shows the normalized fluid loss values for each corresponding variable. The influence of temperature on rheology properties is hidden in variable T. Increasing temperature reduces PV and YP, which affects fluid loss.

Table 17. Normalized fluid loss for each variable

Parameter	Value	Normalized	FL	Normalized FL
DP	0.7	70	3	0.71
	1.0	100	4.2	1.00
	1.3	130	5.8	1.38
T	1.0	25	4.2	1.00
	3.6	90	10	2.38
	5.2	130	12	2.86
NPC	0.3	1	5.8	1.38
	1.0	3	4.2	1.00
	1.3	4	3.8	0.90
NPS	1.0	62	4.2	1.00
	12.0	744	5.5	1.31
	19.4	1205	6.2	1.48
K	0.2	12	3.1	0.74
	1.0	56	4.2	1.00
	9.0	506	6	1.43

Figure 55 shows sensitivity analysis for fluid loss and affecting variables. The trending lines show that fluid loss has a direct relationship to the differential pressure. Increasing barite NPs concentration reduces fluid loss. In the studied range of NPs size, by increasing NPs size, fluid loss increases, even though NPs size is not a governing variable in the studied range of NPs concentration. Temperature shows an important influence on the fluid loss by reducing viscosity

and yield point. Results show that increasing permeability reduces the NPs performance and increases the fluid loss.

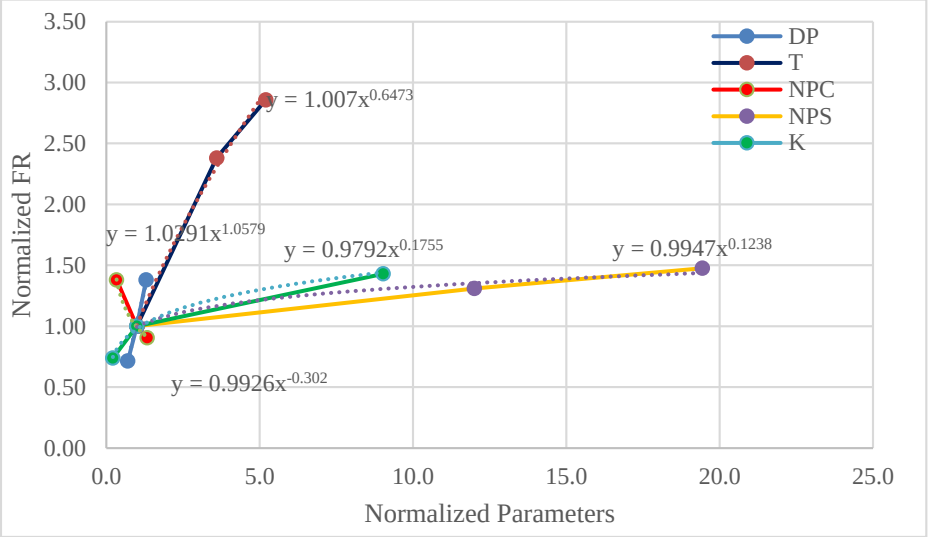

Figure 55. Sensitivity analysis for FL and influencing variables (case 3)

Based on the sensitivity analysis, the following equation was derived to simulate fluid loss reduction in the presence of barite NPs in base case 2.

$$\frac{FL}{FL_B} = 1.001 \times \left(\frac{DP}{DP_B}\right)^{1.058} \times \left(\frac{NPC}{NPC_B}\right)^{-0.302} \times \left(\frac{NPS}{NPS_B}\right)^{0.123} \times \left(\frac{K}{K_B}\right)^{0.175} \times \left(\frac{T}{T_B}\right)^{0.647} \qquad \text{Eq.19}$$

The effect of changing plastic viscosity and yield point of drilling fluid is hidden in temperature term.

The same procedure was used for case 4, and table 18 shows the results of drilling fluid case 4 based on the changing variables as described previously, including permeability, NPs concentration, NPs size, differential pressure, temperature, plastic viscosity and yield point. A base case similar to the previous case was selected for the comparison and also for sensitivity analysis.

Table 18 Changing variables for the drilling fluid case 4

Changing variable	Type	K (md)	NPC (%)	NPS (nm)	DP (psi)	T (C)	PV (cp)	YP ($lb/100ft^2$)	FL (ml)
NPS	DF4	56	3	744	100	25	19	2	12
Base	DF4	56	3	62	100	25	20	3	9
NPS	DF4	56	3	1205	100	25	18	4	13
DP	DF4	56	3	62	70	25	16	6	6.5
DP	DF4	56	3	62	130	25	19	2	12
T	DF4	56	3	62	100	90	12	3	14
T	DF4	56	3	62	100	130	11	2	16
K	DF4	506	3	62	100	25	18	5	14
K	DF4	12	3	62	100	25	16	7	5.6
NPC	DF4	56	1	62	100	25	19	5	11
NPC	DF4	56	4	62	100	25	17	6	8
	DF4	12	0	0	100	25	23	2	6.6
	DF4	56	0	0	100	25	20	5	7
	DF4	12	1.5	62	100	25	19	7	5.6
	DF4	12	1.5	62	100	25	19	5	5.8
	DF4	12	3	62	100	25	17	6	5.4
	DF4	12	1.5	1205	100	25	19	3	6.2
	DF4	12	3	1205	100	25	18	5	5.6

As in previous cases, the results suggest that by increasing temperature, rheology properties including plastic viscosity and yield point diminish. Variables and corresponding fluid loss were normalized based on the selected base case to study the sensitivity analysis for fluid loss and each variable.

Table 19. Normalized fluid loss for each variable

Parameter	Value	Normalized	FL	Normalized FL
DP	70	0.7	6.5	0.72
	100	1.0	9	1.00
	130	1.3	12	1.33
T	25	1.0	9	1.00
	90	3.6	14	1.56
	130	5.2	16	1.78
NPC	1	0.3	11	1.22
	3	1.0	9	1.00
	4	1.3	8	0.89
NPS	62	1.0	9	1.00
	744	12.0	12	1.33
	1205	19.4	13	1.44
K	12	0.2	5.6	0.62
	56	1.0	9	1.00
	506	9.0	14	1.56

Table 19 shows the normalized fluid loss values for each corresponding variable. The influence of temperature on rheology properties is hidden in variable T. Increasing temperature reduces PV and YP, which affects fluid loss. Figure 56 shows sensitivity analysis for fluid loss and affecting variables. The trending lines show that fluid loss has a direct relationship to the differential pressure. Increasing barite NPs concentration reduces fluid loss. In the studied range of NPs size, by increasing NPs Size, fluid loss increases, even though NPs size is not a governing variable in the studied range of NPs concentration. Temperature shows an important influence on the fluid loss by reducing viscosity and yield point. Results show that increasing permeability reduce the NPs performance and increase the fluid loss.

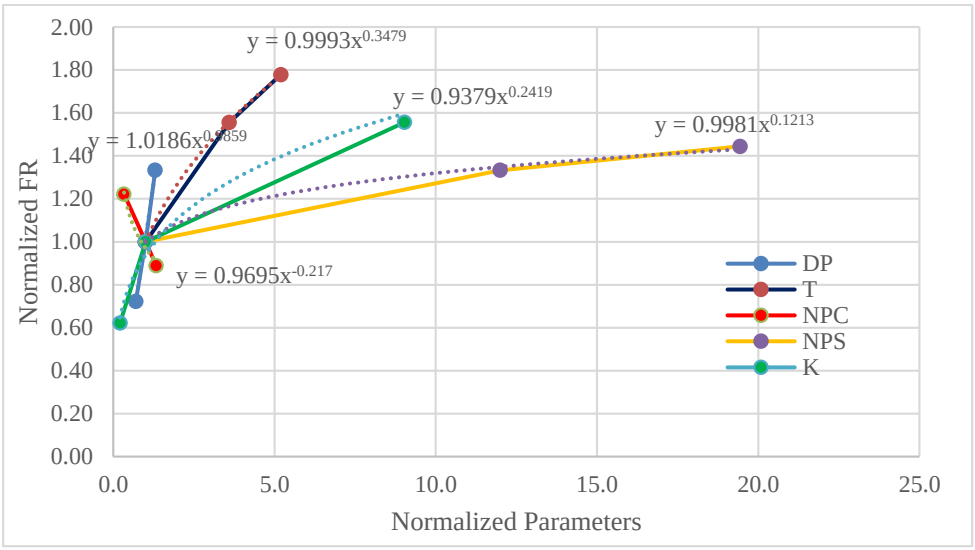

Figure 56 Sensitivity analysis for FL and influencing variables (case 4)

Based on the sensitivity analysis, the following equation was derived to simulate fluid loss reduction in the presence of barite NPs in base case 2.

$$\frac{FL}{FL_B} = 0.9238 \times \left(\frac{DP}{DP_B}\right)^{0.986} \times \left(\frac{NPC}{NPC_B}\right)^{-0.217} \times \left(\frac{NPS}{NPS_B}\right)^{0.123} \times \left(\frac{K}{K_B}\right)^{0.242} \times \left(\frac{T}{T_B}\right)^{0.348} \quad \text{Eq.20}$$

The effect of changing plastic viscosity and yield point of drilling fluid is hidden in temperature term.

Table 20 summarizes the findings for cases 2, 3 and 4. Similarities and discrepancies in some parameters indicate the independence or dependence of their corresponding variable to the composition of drilling fluid in each case. For example, the findings suggest that differential pressure is a dominant, independent factor in porous media filtration, while the influence of temperature on filtration is dependent to the composition of drilling fluid. By increasing differential pressure, filtration increases, and they show a linear direct relationship.

Table 20 summary of the parameters

	Case 2	Case 3	Case 4	Ave
Constant	1.120	1.002	0.924	1.015
DP	0.950	1.058	0.986	0.998
T	0.530	0.647	0.348	0.508
NPC	-0.431	-0.302	-0.217	-0.317
NPS	0.170	0.124	0.121	0.138
K	0.346	0.176	0.242	0.254

Temperature influences on plastic viscosity and yield point, which are dependent to the composition of the drilling fluid. The thermal instability of polymers in each drilling fluid influences the filtration. Equation 23 is based on the average values calculated for the three drilling fluid cases.

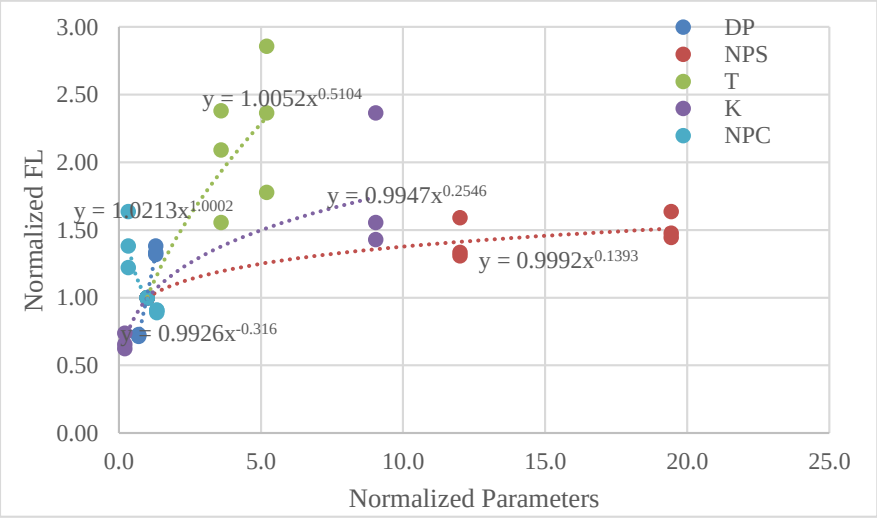

Figure 57 Sensitivity analysis for FL and influencing variables (all cases)

Equation 21 is based on the average values calculated for the three drilling fluid cases.

$$\alpha = \frac{\mathrm{FL}}{\mathrm{FL_B}} = 1.01 \times \left(\frac{\mathrm{DP}}{\mathrm{DP_B}}\right)^{1.000} \times \left(\frac{\mathrm{NPC}}{\mathrm{NPC_B}}\right)^{-0.316} \times \left(\frac{\mathrm{NPS}}{\mathrm{NPS_B}}\right)^{0.139} \times \left(\frac{\mathrm{K}}{\mathrm{K_B}}\right)^{0.254} 46 \times \left(\frac{\mathrm{T}}{\mathrm{T_B}}\right)^{0.510}$$

Eq.21

Fluid loss reduction can be calculated using following equation:

$$FLR = \frac{(\alpha \times FL_B - FL_{without\ NP})}{FL_{without\ NP}} \times 100 \qquad \text{Eq.22}$$

5.1.2 Wellbore strengthening using NPs (Differential evolution)

Storn and Price (1997) developed differential evolution algorithm (DE), which is used to find an optimum solution in big continuous spaces. DE, as a competitive stochastic real-parameter optimization algorithm, has been used to solve a large variety of engineering problems due to its boosted iteration search. The performance of DE is a function of the mutation strategy and control parameters, including mutation and crossover factors. The DE algorithm begins with initializing all candidate solutions with random positions in the search space. For each random candidate solution, three random vectors are chosen (X_1, X_2, X_3). (X_2 - X_1) gives a differential vector. The weighted difference vector F(X_2-X_1) is used to perturb the third random vector (X_3). Donor vector (V) is generated using the following equation:

$$V_{i,G+1} = X_{3,G} + F(X_{2,G} - X_{1,G}) \qquad \text{Eq.23}$$

The mutation factor or weighting factor (F) is a constant, mostly in the range of 0.5 to 2. The weighting factor determines the amplification of differential variation among candidates. The trial vector (U) is developed from the elements of the target vector and the elements of the donor vector (V).

$$U_{i,G+1} = \begin{cases} V_{i,G+1} & \text{if rand} \leq \mathrm{CR} \\ X_i, \mathrm{G} & \text{if rand} > \mathrm{CR} \end{cases} \qquad \text{Eq.24}$$

The crossover factor (CR) regulates the amount of recombination between candidates. Recombination incorporates successful solutions from the previous generation with current donors.

The fitness of trial vector is compared with the target vector and it is replaced if it is better. The DE algorithm repeats the mutation (weighting factor), recombination (crossover factor) and selection steps until a predetermined criterion is achieved.

The results of hydraulic fracturing tests conducted by Contreras et al. (2014) were used in this section for the base case and drilling fluid containing different nanoparticle types and concentrations. Fracture breakdown pressure was recorded for each case. These tests have been done for Roubidoux sandstone and Catoosa shale. HPHT filtration tests were conducted for the base case and drilling fluids containing different nanoparticle types and concentrations. Figure 54 shows the results of P_{fb} increase percentage and HPHT filtration reduction compared to the base case for Roubidoux sandstone samples. It can be observed that fracture breakdown pressure increases when HPHT filtration is reduced. Using iron hydroxide NPs and graphite caused a high reduction in HPHT filtration; it also shows that better sealing of the sandstone can be obtained if optimum concentrations of nanoparticle and graphite are used in oil base mud.

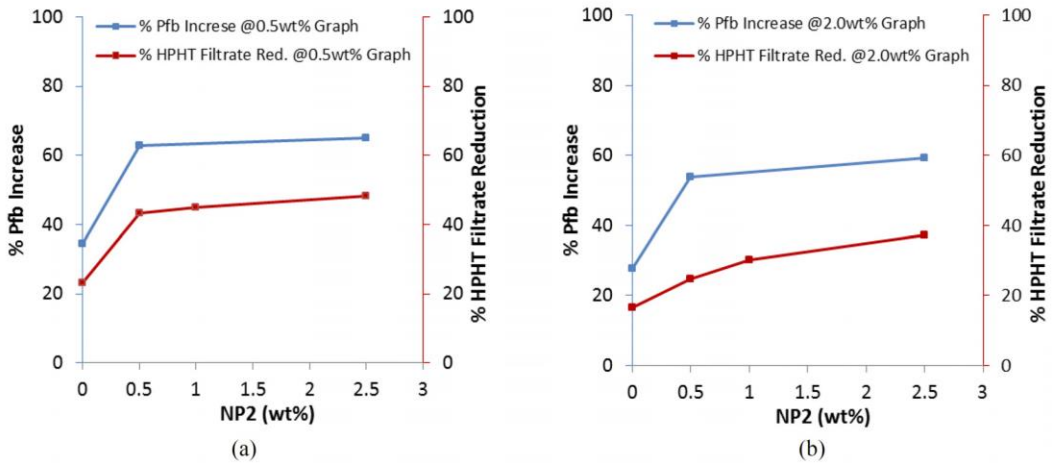

Figure 58. P_{fb} increase (left axis) compared to HPHT filtrate reduction (right axis) for NP2 blends at two graphite levels (a) 0.5 wt% and (b) 2.0 wt%. (Contreras et al., 2014a)

Figure 59 shows the results of P_{fb} increase percentage and HPHT filtration reduction compared to the base case for Catoosa shale samples. As it can be seen, fracture breakdown pressure increases when HPHT filtration is reduced. Using calcium carbonate NPs and graphite caused a high

reduction in HPHT filtration. A better sealing on the shale surface can be obtained if optimum concentrations of nanoparticle and graphite are used in oil base mud. Based on the results, it is seen that using a low concentration of NPs (0.5 % wt.) in the oil-based mud increases fracture pressure by 60 percent in Roubidoux sandstone and about 30 percent for Catoosa shale.

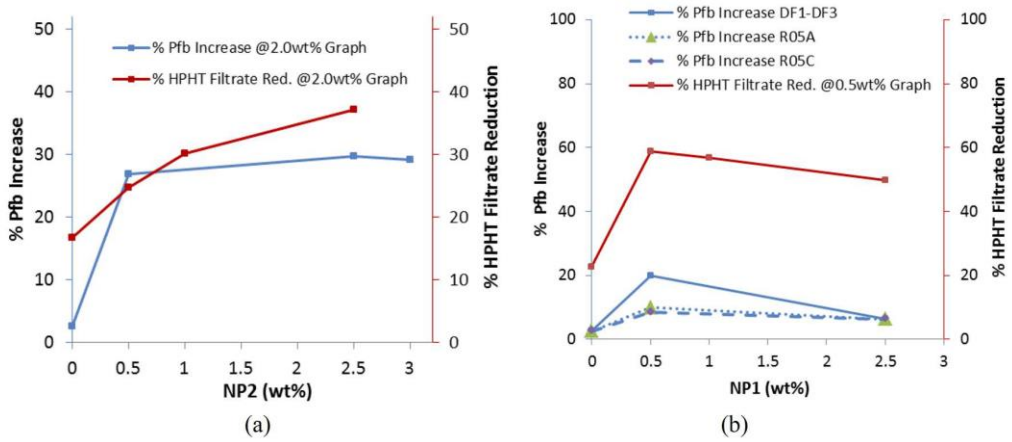

Figure 59. P_{fb} increase (left axis) compared to HPHT filtrate reduction (right axis) for (a) NP2 and (b) NP1. (Contreras et al., 2014b)

Test results including permeability (K), filtration reduction (FLR), and fracture breakdown pressure (P_{fb}) have been collected and inserted into the below equation:

$$P_{fb} = a \times FLR^{b} \times K^{c} \qquad \text{Eq.25}$$

Parameters a, b, and c were calculated using DE, and a best fit was found. Figure 60 shows the value for these parameters and the fitness value, as well as data comparison between test result and the correlation. Equation 22 can then be written as follow:

$$P_{fb} = 1.5149 \times FLR^{0.6489} \times K^{0.0790} \qquad \text{Eq.26}$$

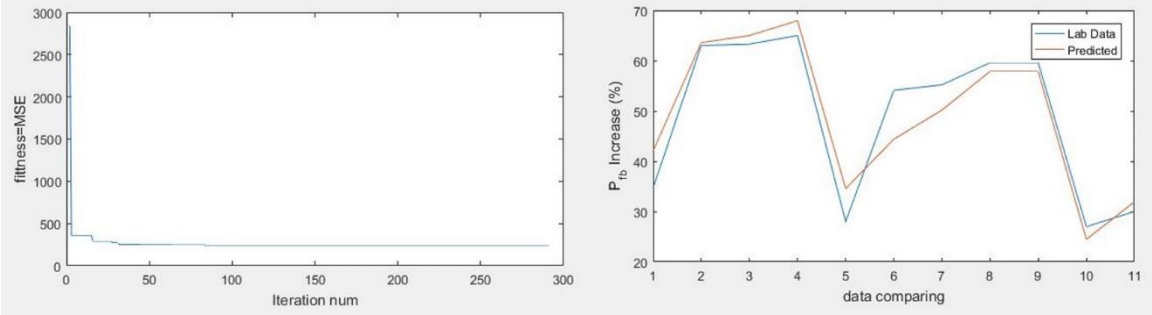

Figure 60. Equation fitness and data comparison

Comparing the effects of filtration reduction and permeability indicates that filtration reduction has a higher effect on wellbore strengthening. Table 21 shows the predicted P_{fb} increase and measured P_{fb} increase based on the filtration reduction and permeability.

Table 21. Result from tests and DE

Fluid loss Reduction (%)	Permeability (md)	P_{fb} Increase (%)	Predicted P_{fb} Increase (%)
23	12	34.7	42.04
43.5	12	63	63.58
45	12	63.3	64.99
48.2	12	65	67.95
17	12	28	34.55
25	12	54.1	44.38
30.2	12	55.2	50.17
37.63	12	59.6	57.87
24.75	0.007	27	24.47
37.29	0.007	30	31.93

Comparing measured and predicted fracture breakdown pressure shows that using DE algorithm is a promising tool for developing a WS prediction. Figure 61 shows predicted P_{fb} vs. measured P_{fb} in the laboratory. The accordance between predicted values and experimental data indicates that DE can effectively simulate and predict fracture breakdown pressure, based on the experimental results.

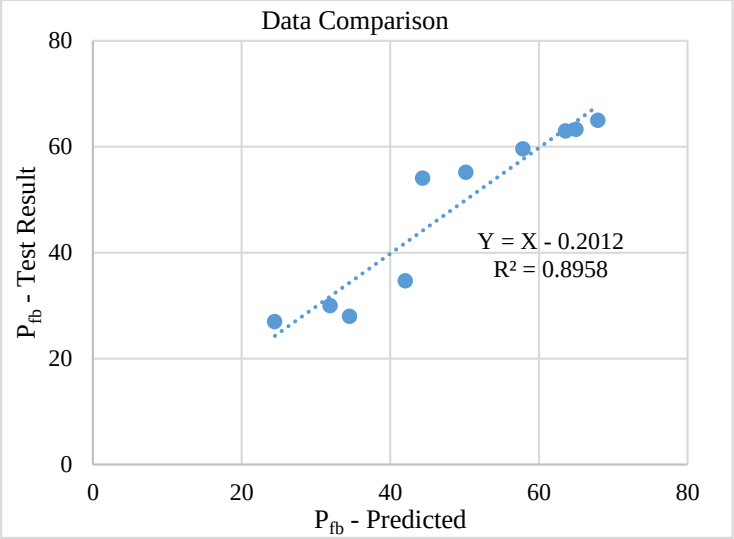

Figure 61. Data comparison of the test results and equation

Figure 62 shows the Sensitivity analysis for the equation.

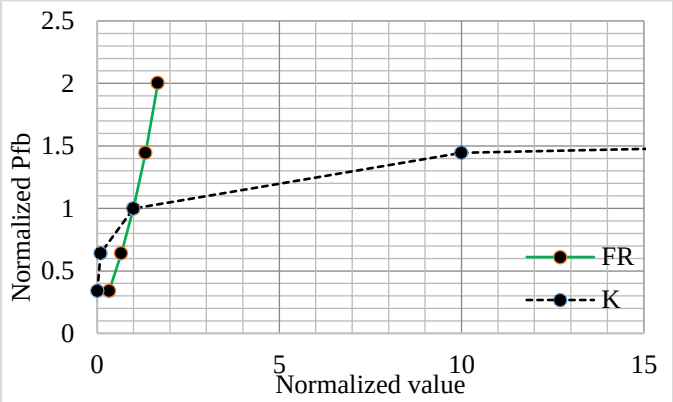

Figure 62. Sensitivity analysis of the equation

Evaluating the parameters sensitivities in equation (8) as shown in figure 58, the fracture breakdown pressure is more sensitive to filtrate reduction than initial permeability. This figure shows how effective using NPs and graphite is in reducing permeability in permeable sandstone. As expected, preventing pore pressure buildup is the best strategy to prevent wellbore instability and lost circulation problems caused by induced fractures.

5.1.3 A case study

The Hadrian-5 well in the United States Gulf of Mexico's canyon 919 block (Moyer et. al, 2012) was studied in this research to evaluate the effect of wellbore strengthening by using NPs. Reducing the cost of casings as well as the time required for the total casing run are desired especially in a deep water drilling operation. Besides the marine riser that connects the BOP to the semi-submersible drilling platform, 6 more casings and liners were used to provide a safe way to the target. As shown in Figure 63, a structural casing was placed at the depth of 7348 ft. A string of 22" conductor casing was landed at the depth of 9646 ft. The next section was drilled using a n isomeric olefin based synthetic fluid in the salt formation. The 13 5/8" casing was set at the depth of 12695 ft, approximately 500 ft below the top of salt formation. Three subsequent liners were set and cemented at the depths of 14753 ft, 16960 ft, and 18272 ft. Pore pressure was measured and recoded during the drilling operation.

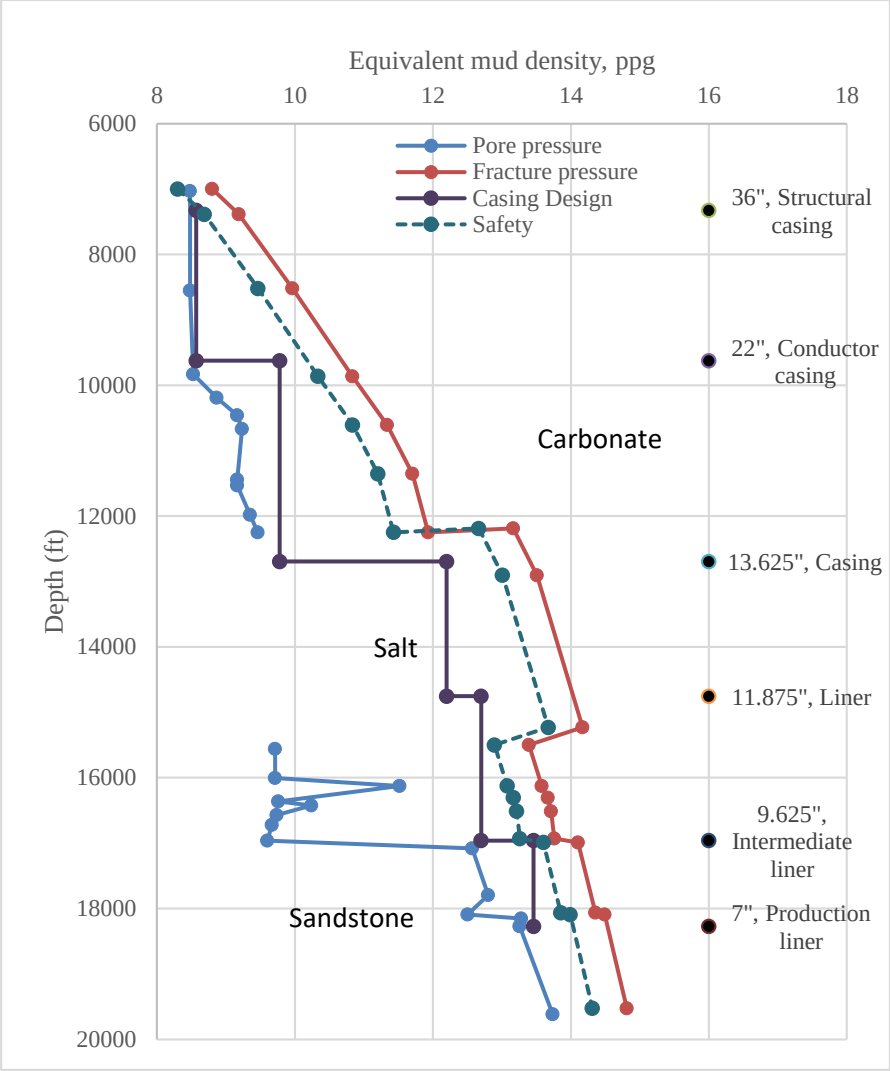

Figure 63. Actual pore pressure and casing depth

By substituting equation 22 in equation 26, it is possible to calculate the increase of fracture pressure. Figure 64 shows the casing design with wellbore strengthening when an average of a 15% filtration reduction is acquired by using barite NPs. Due to the very low permeability of the salt formation, filtration is negligible, and it was considered as a constant value. By decreasing the filtration, it was possible to reduce one liner size, and have a larger production liner at the depth of 18270 ft.

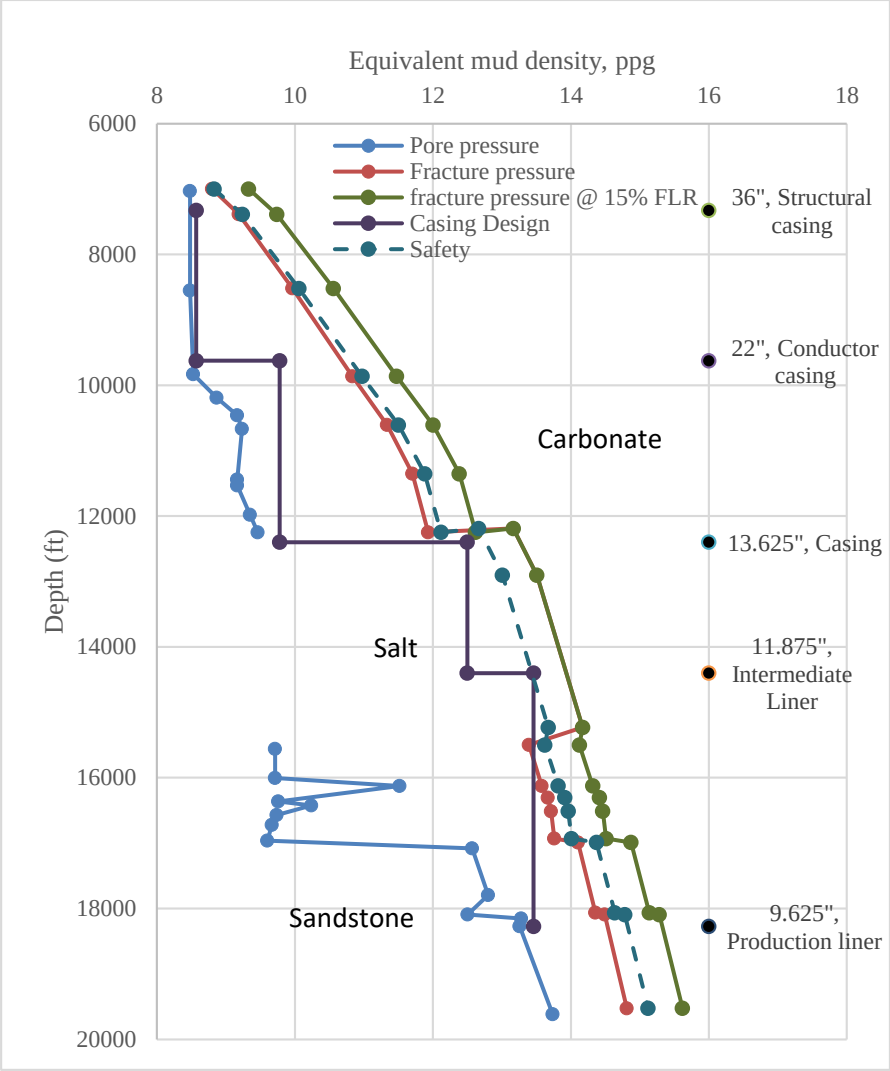

Figure 64. Casing design with wellbore strengthening

5.2 Machine learning

Microsoft Azure is a cloud computing service created by Microsoft. In this section, the statistical analyses to predict fluid loss reduction using Azure machine learning studio are presented. Two models were trained and used to predict fluid loss reduction based on the influencing parameters. Figure 65 shows the distribution of fluid loss reduction based on the data that was used in the modeling.

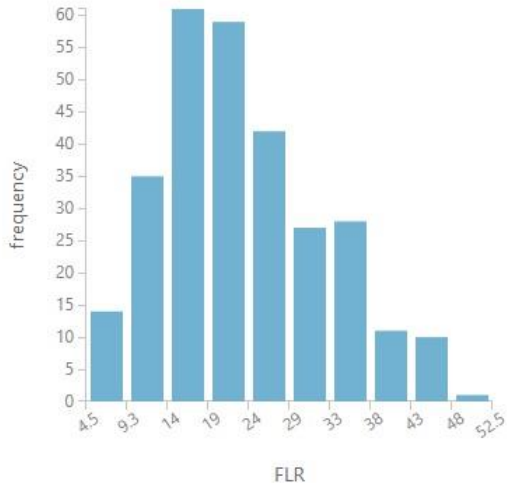

Figure 65. Fluid loss reduction distribution

5.2.1 Boosted Decision Tree Regressor

Decision tree learning uses a decision tree algorithm to predict the result values (leaves) from observations (branches). It is one of the predictive modeling approaches used in statistics and machine learning. In boosted decision tree regressor, each tree is dependent on prior trees and algorithm learns by fitting the residual of the previous trees.

By increasing maximum number of leaves per tree, the size of the tree possibly increases and provides better precision at the risk of overfitting. The user can define the minimum number of cases that are required to create any terminal node (leaf) in a tree. Therefore, by increasing the minimum leaf instances, the threshold for creating a new rule increases. The learning rate indicates the speed of learner convergence on the optimal solution. Very small learning rate causes training to take longer to converge on the optimal solution, while too big learning rate might end up missing the optimal solution. The number of trees constructed defines the total number of decisions to be created to find the optimal solution. In this study, the following settings were used to find the optimal solution to model fluid loss reduction based on the data from the previous chapter. Table 22 shows the setting for the boosted decision tree regression.

Table 22. Boosted decision tree regression

Setting	Value
Number Of Leaves	20
Minimum Leaf Instances	10
Learning Rate	0.2
Number Of Trees	100
Allow Unknown Levels	TRUE
Random Number Seed	

Twenty percent of the data were selected randomly and used as test data and the rest were used to train the predictive model. Figure 66 shows the schematic modeling process used to predict fluid loss reduction using boosted decision tree regressor.

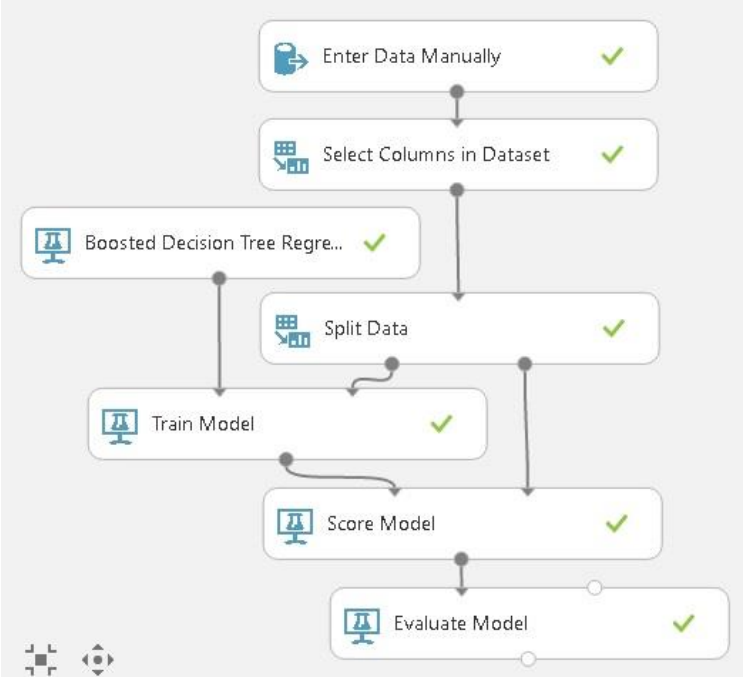

Figure 66. The schematic of modeling process used to predict fluid loss reduction using boosted decision tree regressor

Table 23 summarizes the evaluation results of the predictive boosted decision tree regressor, including the mean absolute error (MAE) and root mean squared error (RMSE).

Table 23. Model evaluation results

Metrics	
Mean Absolute Error	1.58228
Root Mean Squared Error	2.649264
Relative Absolute Error	0.163688
Relative Squared Error	0.047027
Coefficient of Determination (R^2)	0.952973

Using this model, the coefficient of determination (R^2) is higher than 0.95. Figure 67 shows an error histogram using boosted decision tree regressor over the data.

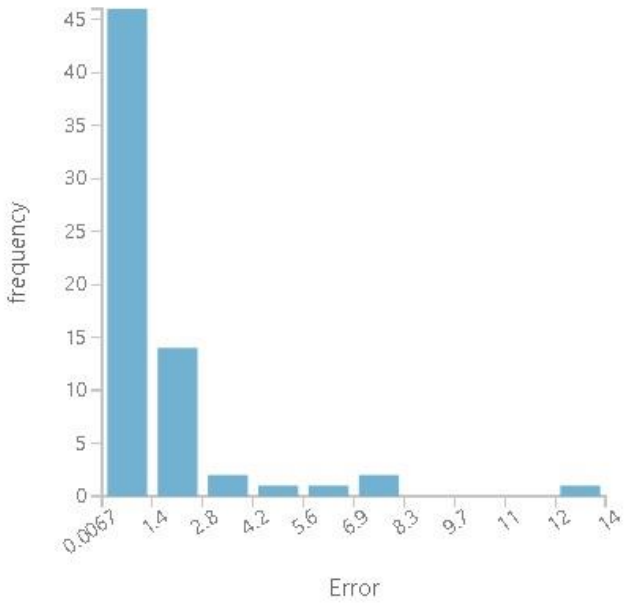

Figure 67. Error histogram for Boosted decision tree model

5.2.2 Neural Network Regression

In this study, the following settings for neural network regression were used to find the optimal solution to model fluid loss reduction based on the data from the previous chapter.

Table 24. Neural Network regression

Setting	Value
Loss Function	CrossEntropy
Learning Rate	0.005
Number Of Iterations	100
Initial Weights Diameter	0.01
Number of hidden nodes	1000
The initial learning weights diameter	0.01

Twenty percent of the data were selected randomly and used as test data and the rest were used to train the predictive model. Figure 68 shows the schematic of modeling process used to predict fluid loss reduction using Neural Network regression.

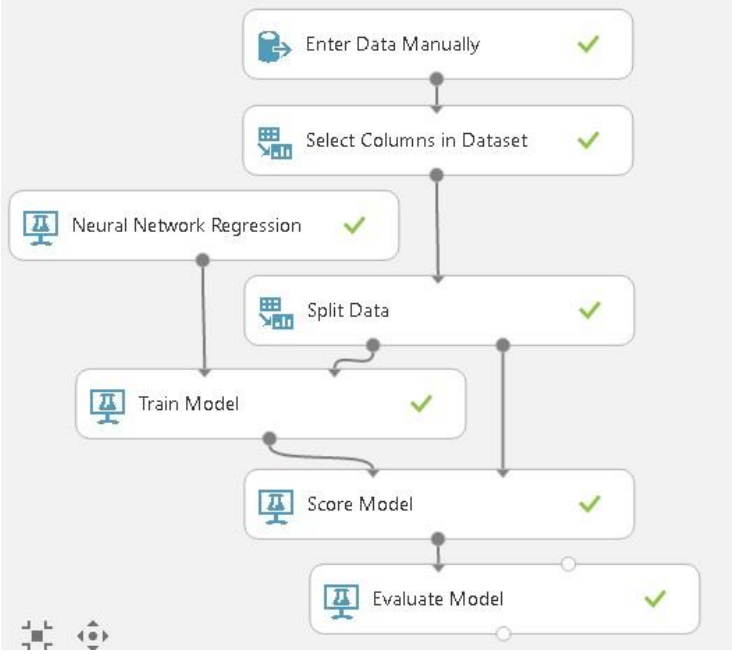

Figure 68. The schematic of modeling process using Neural network regression

Table 25 summerizes the evaluation results of the predictive Neural network regressor including the mean absolute error (MAE) and root mean squared error (RMSE). Using this model, the coefficient of determination (R^2) is higher than 0.88. Figure 66 shows error histogram using boosted decision tree regressor over the data.

Table 25. Model evaluation results

Metrics	
Mean Absolute Error	3.085551
Root Mean Squared Error	4.053305
Relative Absolute Error	0.319203
Relative Squared Error	0.110081
Coefficient of Determination	0.889919

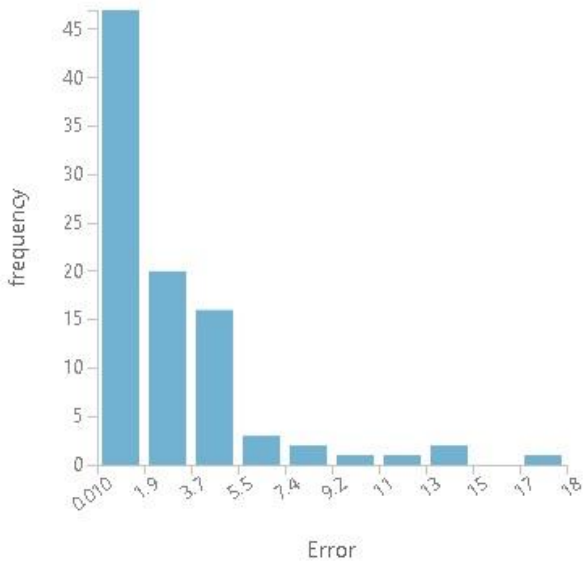

Figur 69. Error histogram for neural network regression

CHAPTER VI

CONCLUSIONS

The primary objective of this study was to investigate the optimal nanoparticle (NP) size distribution and concentration in different weighted water-based drilling fluid systems to minimize mud filtration into the different formations. Based on permeability and pore throat size, appropriate NPs size and concentration were studied and optimized. Hence, this study could be a key part of actual drilling fluid system pre-planning, especially in off-shore and deep-water drilling projects. The second objective was to develop a new correlation model between the permeability of different filter media as a function of time and filtrate flow when they come in contact with water-based drilling fluids containing NPs. The model includes the initial medium permeability and will predict permeability as filter-cake is being generated on the medium. The third objective was to develop a model to predict break down pressure as a function of permeability and fluid loss volume. This goal focuses on the wellbore strengthening criteria. Based on the presented wellbore strengthening model, it is possible to increase the fracture gradient at depth using a small concentration of barite NPs to generate a wider mud window. Having a wider mud window could result in a reduced number of casing strings required to complete a well that can reduce the total cost of drilling a well. The forth objective was to study the effect of combining NPs and LCM on sealing pressure. The results suggest that it is effective and adding NPs as well as other larger solid materials along with LCM improve the performance of water based mud to handle lost circulation situation.

The specific conclusions of this research are summarized as follows.

1. Various size barite NPs were prepared by ex-situ method and mechanically grinding and used in the water based drilling fluids.

2. Barite NPs addition to drilling fluids, even at low concentrations (1-5 wt%), improved water based drilling fluid performance in terms of fluid loss, lubricity, increasing fracture gradient pressure and wellbore strengthening.

3. Density and rheological properties of the drilling fluids remained unchanged after addition of barite NPs.

4. Adding barite NPs reduced CoF and enhanced the lubricity of the drilling fluid, enabling drilling operators to design and drill longer deviated or horizontal interval with the same hoisting capacity of drilling rig.

5. Parameters such as differential pressure show linear relationship to filtration, even with barite NPs, while temperature shows different levels of influence on filtration based on the composition of drilling fluid.

6. Adding a small amount of ex-situ NPs and grinded barite to the water based drilling fluid reduced the final LTLP fluid loss by 5-32 %, exhibited thin mud cake, and similar performance was obtained at HTHP filtration.

7. Adding barite NPs to the drilling fluid reduces cumulative fluid loss, prevents pore pressure build up, and increases fracture initiation pressure. Adding barite NPs to the water based drilling fluids is an effective way of wellbore strengthening.

8. Combining barite NPs and LCM in water based drilling increases sealing pressure and enable drilling operator to avoid running an excess casing string to deal with the lost circulation situation.

6.1 Original contributions to knowledge

1. Synthesizing and using barite NPs made both chemically and mechanically, as a weighing material in water based drilling, generally results in reducing fluid loss even in high permeable formations.

2. Barite NPs are effective if combined with other size solid materials in water-based mud.

3. Permeability reduction occurs if barite NPs are used with other solid material to create thin mud cake. Using low concentration of barite NPs (5% wt.) without other solid materials is not an effective method to reduce permeability in porous media.

4. Fluid loss reduction that is achievable using barite NPs , reduces pore pressure buildup and is an effective way to control fracture initiation pressure.

5. The fluid loss and fracture pressure models, developed in this study, can be used in well planning and cost reduction which is the main value in terms of engineering.

6.2 Recommendations for future research

The following recommendations are proposed for future studies:

1. Using other weighing materials such as $CaCO_3$ NPs in water based drilling
2. Dynamic filtration test for better understanding of barite NPs performance in water based drilling fluid.
3. Conducting more experiments using low concentration of NPs in water based drilling fluids and creating a bigger dataset.
4. Apply same test procedure to field cases to prove the value of the proposed modeling and potential cost savings for casing design.

REFERENCES

Abdo, J., and Haneef, D., "Nanoparticles: Promising solution to overcome stern drilling problems," N TI-Nanotech 2010, www.nsti.org, ISBN 978-1-4398-3415-2, Vol.3. (2010)

Akhtarmanesh, S., Al-saba M., Cedola, A.E., Qader, R., Caldarola, V.T., Hareland, G., and Nygaard, R., "Barite Nano-Micro Particles with LCM Seals Fractured Form Better in Weighted Water Based Drilling Fluids." American Rock Mechanics Association. (2016)

Al-Bazali, T.M., Zhang, J., Chenevert, M.E., and Sharma, M.M. "Factors Controlling the Membrane Efficiency of Shales when Interacting with Water-Based and Oil-Based Muds." SPE 100735-MS, Society of Petroleum Engineers, International Oil & Gas Conference and Exhibition in China, Beijing, China. (2006)

Al-saba, M.T., Nygaard, R., Saasen, A., and Nes. O.M., "Laboratory evaluation of sealing wide fractures using conventional lost circulation materials.", SPE 170576-MS, Society of Petroleum Engineers. (2014)

Alshubbar, G.D., Coryell, T.N., Atashnezhad, A., Akhtarmanesh, S., and Hareland, G., "The Effect of Barite Nanoparticles on the Friction Coefficient and Rheology of Water Based Mud." American Rock Mechanics Association. (2017)

Amanullah, M., Al-Arfaj, K. M, and Al-Abdullatif. Z, "Preliminary Test results of Nano-based Drilling Fluids for Oil and Gas Field Application", PE/AIDC 139534, 1-9. (2011)

Amanullah, M., and Al-Tahini, M. A., "Nano-Technology – Its Significance in Smart Fluid Development for Oil and Gas Field Application", SPE Saudi Arabia Section Technical Symposium, AlKhobar, Saudi Arabia. (2009)

Aston, M.S., Alberty, M.W., McLean, M.R., de Jong, H.J., and Armagost. K., "Drilling fluids for wellbore strengthening.", SPE 87130-MS, Society of Petroleum Engineers. (2004)

Bourgoyne, A.T. Jr., Millheim, K.K., Chenevert M.E., and Young F.S. Jr., "Applied Drilling Engineering", Society of Petroleum Engineers, Richardson, Texas. (1991)

Brady, M.E., Craster, B., Getliff, J.M., and Reid, P.I.., "Highly Inhibitive, Low-Salinity Glycol Water-Base Drilling Fluid For Shale Drilling In Environmentally Sensitive Locations.", SPE 46618-MS, Society of Petroleum Engineers. (1998)

Bruton, J.R., Ivan, C.D., and Heinz, T.J., "Lost circulation control: Evolving techniques and strategies to reduce downhole mud losses.", SPE 67735-MS, Society of Petroleum Engineers. (2001)

Caldarola, V.T., Akhtarmanesh, S., Cedola, A.E., Qader, R., and Hareland, G., "Potential Directional Drilling Benefits of Barite Nanoparticles in Weighted Water Based Drilling Fluids." American Rock Mechanics Association. (2016)

Ewy, R.T., and E.K. Morton, “Wellbore Stability Performance of Water Base Mud Additives”, SPE 116139, presented SPE Annual Technical Conference and Exhibition, 21-24 September, Denver, Colorado, USA. (2008)

Chenevert, M.E., and Sharma, M.M., “Maintaining shale stability by pore plugging,” US Patent 0314549, (2009)

Cai, J., Chenevert, M.E., Sharma, M.M., and Friedheim, J., “Decreasing Water Invasion Into Atoka Shale Using Nonmodified Silica Nanoparticles”, SPE 146979-PA, SPE Drill & Compl 27 (1): 103-112., (2012)

Cedola, A.E., Akhtarmanesh, S., Qader, R., Caldarola, V.T., Hareland, G., Nygaard, R., and Alsaba, M.T., “Nanoparticles in weighted water based drilling fluids increase loss gradient.”, ARMA 16-310, American Rock Mechanics Association. (2016)

Contreras, O., Hareland, G., Husein, M., Nygaard, R., and Alsaba. M.T., “Wellbore strengthening in sandstones by means of Nanoparticle-based drilling fluids.”, SPE 170263-MS, Society of Petroleum Engineers. (2014a)

Contreras, O., Hareland, G., Husein, M., Nygaard, R., and M. Alsaba M., “Experimental Investigation on Wellbore Strengthening In Shales by Means of Nanoparticle-Based Drilling Fluids”, SPE 170589-MS, presented at SPE Annual Technical Conference and Exhibition, 27-29 October, Amsterdam, Netherlands. (2014b)

Dewan, J. T., and Chenevert, M. E. “A model for filtration of water-base mud during drilling determination of mud cake parameters.” Petrophysics, vol. 42, no. 3, p. 237–250. (2001) Fraser, L.J., Harrington, B., Albarrazin, C., Snyder, G., and Donham, F., “Use of Mixed Metal Oxide fluid to combat losses in porous and fractured formations: two case histories,” AADE-03-NTCE-40. (2003)

Fuh, G.F., Morita, N., Boyd, P.A., and McGoffin, S.J., “A new approach to preventing lost circulation while drilling.”, SPE 24599-MS, Society of Petroleum Engineers. (1992)

Griffin, W. C., “Calculation of HLB values of Nonionic Surfactants”, J. Soc. Cosmet. Chem. 5, 249-256. (1954)

Growcock, F.B., Kaageson-Loe, N., Friedheim, J., Sanders, M.W., and Bruton, J., “Wellbore stability, stabilization and strengthening.”, OMC-2009-107, Offshore Mediterranean Conference. (2009)

Hettama, M., Horsrud, P., Taugbol, K., Friedheim, J., Huynh, H., Sanders, M.W., and Young, S., “Development of an innovative high-pressure testing device for the evaluation of drilling fluid systems and drilling fluid additives within fractured permeable zones.”, OMC-2007-082 Offshore Mediterranean Conference. (2007)

Husein, M.M., Rodil, E., Vera, J.H., “Preparation of AgBr Nanoparticles in Microemulsions Via Reaction of AgNO3 with CTAB Counterion”, Journal of Nanoparticle Research, Volume 9, Number 5, Page 787. (2007a)

Husein, M.M., Patruyo, L.G., Pereira, P., “In-Situ Removal of H2S(g) Using Ultradispersed Iron Oxide Nanoparticles”, AIChE annual meeting: Salt Palace Convention Center, Salt Lake City, Utah. (2007b)

Husein, M.M., and Nassar, N.N., “Nanoparticles Preparation using the single microemulsion scheme, “Current Nanoscience,4, pp 370-380. (2008)

Husein, M., Zakaria, M., and Hareland, G., “Novel nanoparticle-containing drilling fluids to mitigate fluid loss”, PCT Application: PCT/CA2012050075, (2012a)

Husein, M., Zakaria, M., and Hareland, G., “Use of nanoparticles as a lubricity additive in well fluids”, PCT Application: PCT/CA2012/050688, (2012b)

Khatib, Z.I., “Prediction of Formation Damage Due to Suspended Solids: Modeling Approach of Filter Cake Buildup in Injectors.”, MS 28488, Society of Petroleum Engineers, SPE Annual Technical Conference and Exhibition, New Orleans, Louisiana, (1994)

Kirsch, E.G.,“Die Theorie der Elastizität und die Bedürfnisse der Festigkeitslehre.”, Zeitschrift des Vereines deutscher Ingenieure, 42, 797–807. (1898)

Kostansek, E., “Emulsions.”, In: Kirk-Othmer encyclopedia of chemical technology, Wiley, Hoboken. (2003)

Kumar, A., and Savari, S., “Lost circulation control and wellbore strengthening: Looking beyond particle size distribution.”, AADE-11-NTCE-21, AADE National Technical Conference and Exhibition. (2011)

Lecolier, E., Herzhaft, B., Rousseau, L., Neau, L., Quillien, B., and Kieffer, J., “Development of a Nanocomposite gel for lost circulation treatment.”, SPE 94686-MS, Society of Petroleum Engineers. (2005)

Loggins, S.M.J., Cunningham, C., Akhtarmanesh, S., Gunter, B., & Hareland, G., “The Effect of Mechanically and Chemically Generated Barite Nanoparticles on the Reduction of Fluid Filtrate.” American Rock Mechanics Association, (2017)

Kanj, Y.M., Funk, J.J., and Al-Yousif, Z., “Nanofluid coreflood experiments in the Arab-D” SPE paper 12616, presented at the 2009 SPE Saudi Arabia Technical Symposium and Exhibition held in Saudi Arabia, Alkhobar, May 09-11, (2009)

Li, W., Kiser, C., Richard, Q., “Development of a filter cake permeability test methodology” American Filtration & Separations Society Conferences, 19 September, USA (2005)

Martinez, M.D., Mayne, J.D., Ortega, C., Trujillo, and Maestas, A. “The advantages of using a Multiple Leaf Filter System in a Chloride Separations Process.”, MAES International Symposium and Career Fair 25th Anniversary. (2000)

Mata, F., and Veiga, M., “Crosslinked cements solve lost circulation problems.”, SPE-90496-MS, Society of Petroleum Engineers. (2004)

MI-Swaco, “Drilling Fluids Handbook (Version 2.1)”, MI-Swaco, (2005)

Morita, N., Black, A.D., and Fuh, G.F., “Theory of lost circulation pressure.”, SPE 20409, Society of Petroleum Engineers. (1990)

Moyer, M.C., Lewis, S.B., Cotton, M.T., and Peroyea, M. “Challenges Associated With Drilling a Deepwater, Subsalt Exploration Well in the Gulf of Mexico: Hadrian Prospect.” Society of Petroleum Engineers. MS154928. (2012)

Nayberg, T.M., “Laboratory study of lost circulation materials for use in both oil-based and water-based drilling muds.”, SPE 14723-PA, Society of Petroleum Engineers. (1987)

Nwaoji, C.O., Hareland, G., Husein, M., Nygaard, R., and Zakaria, M.F., "Wellbore strengthening- nano-particle drilling fluid experimental design using hydraulic fracture apparatus." SPE 163434-MS, Society of Petroleum Engineers. (2013)

Osuji, C.E., Chenevert, M.E., and Sharma, M.M., "Effect of Porosity and Permeability on the Membrane Efficiency of Shales.", SPE 116306, Society of Petroleum Engineers, SPE Annual Technical Conference and Exhibition, Denver, Colorado, US, (2008)

Savari, S., Whiftill, D.L., Jamison, D.E., and Kumar, A., "A method to evaluate lost-circulation materials - Investigation of effective wellbore-strengthening applications.", SPE 167977-PA Society of Petroleum Engineers. (2014)

Sensoy, T., Chenevert, M. E., and Sharma, M. M., "Minimizing water invasion in shale using nanoparticles", PE 124429 presented at the 2009 SPE Annual Technical Conference and Exhibition, New Orleans, LA, 4-7 October, (2009)

Soroush, H., Sampaio, J.H.B., and Nakagawa, E.Y., "Investigation into strengthening methods for stabilizing wellbores in fractured formations.", SPE 101802-MS, Society of Petroleum Engineers. (2006)

Srivatsa, T. J., "An Experimental Investigation on Use of Nanoparticles as Fluid Loss Additives in a Surfactant–Polymer Based Drilling Fluid", Texas Tech University, M.Sc thesis, (2010)

Storn, R., and Price, K., "Differential evolution – A simple and efficient heuristic for global optimization over continuous spaces.", Journal of Global Optimization. 11: 341. doi:10.1023/A:1008202821328. (1997)

Tiller, F. M. and W. Li. "Theory and Particle of Solid/Liquid Separation" Fourth edition, 2002, university of Houston. (2002)

Van Oort, E., Hale, A.H., Mody, F.K. and Roy, S., "Transport in shales and the design of improved water-based shale drilling fluids", SPEDC, September, (1996)

Vidick, B., Yearwood, J.A., and Perthuis, H., "How to solve lost circulation problems.", SPE-17811-MS, Society of Petroleum Engineers. (1988)

Whitfill, D.L., Jamison, D.E., Wang, M., and Angove-Rogers, A., "Preventing lost circulation requires planning ahead." SPE-108647-MS, Society of Petroleum Engineers. (2007)

Withfill, D., and Miller, M.L., "Developing and testing lost circulation materials.", AADE-08-DF-HO-24, AADE Fluids Conference and Exhibition. (2008)

Zakaria, F. M, Mostafavi, V., Hareland, G., Husein, M., "Design and Application of Novel Nano Drilling Fluids to Mitigate Circulation Loss Problems during Oil Well Drilling Operations" presented at the World Nano Conference and Expo 2011 in Boston, Massachusetts, June 13-16. (2011)

APPENDICES

In this section, the details of filtration tests and the results were presented for each four drilling fluid cases. Appendix A contains the details of standard API LPLT Filter press tests for the drilling fluid case 1. Appendix B contains the details of filtration tests for the drilling fluid case 2. Appendix C contains the details of filtration tests for the drilling fluid case 3. Appendix D contains the details of filtration tests for the drilling fluid case 4. Appendix E contains the detail of statistical analysis SAS programming and Appendix F is the differential evolution method in MATLAB.

Appendix A: Standard API LPLT Filter press results for the drilling fluid case 1

Time	NPC	NPS	Perm	DP	Temp	Area	PV	YP	MW	Hmc	CFL	FLR
0	0	0	12	20	25	63.62	6	2	8.7	4	0	0.00
2											8	0.00
4											14.5	0.00
6											20	0.00
8											24	0.00
10											28	0.00
12											31	0.00
0	0	0	56	20	25	63.62	7	1	8.7	4	0	0.00
2											9	0.00
4											17	0.00
6											24	0.00
8											29.5	0.00
10											34	0.00
12											38	0.00
0	0	0	506	20	25	63.62	7	2	8.7	5	0	0.00
2											11	0.00
4											20	0.00
6											28	0.00
8											34.5	0.00
10											40.5	0.00
12											45	0.00
0	1	62	12	20	25	63.62	5	2	8.7	3	0	0.00
2											7	12.50
4											12	17.24
6											17	15.00
8											21	12.50
10											25	10.71

12											28	9.68
0	1	62	56	20	25	63.62	7	3	8.7	4	0	0.00
2											8	11.11
4											15	11.76
6											21	12.50
8											26	11.86
10											31	8.82
12											35	7.89
0	1	62	506	20	25	63.62	5	1	8.7	5	0	0.00
2											8	27.27
4											16	20.00
6											23	17.86
8											29	15.94
10											35	13.58
12											40	11.11
0	3	62	12	20	25	63.62	6	2	8.7	3	0	0.00
2											6	25.00
4											11	24.14
6											15	25.00
8											19	20.83
10											23	17.86
12											26	16.13
0	3	62	56	20	25	63.62	4	3	8.7	4	0	0.00
2											7	22.22
4											13	23.53
6											19	20.83
8											24	18.64
10											29	14.71
12											33	13.16

0	3	62	506	20	25	63.62	5	2	8.7	4	0	0.00
2											8	27.27
4											15	25.00
6											22	21.43
8											28	18.84
10											34	16.05
12											39	13.33
0	5	62	12	20	25	63.62	6	1	8.7	0	0	
2											9	
4											16	
6											22	
8											27	
10											31	
12											35	
0	5	62	56	20	25	63.62	4	2	8.7	0	0	
2											9	
4											17	
6											24	
8											31	
10											37	
12											43	
0	5	62	506	20	25	63.62	5	1	8.7	0	0	
2											12	
4											23	
6											33	
8											42	
10											50	
12											56	

Appendix B: Standard API LPLT & HPHT Filter press results for the drilling fluid case 2

Time	NPC	NPS	Perm	DP	Temp	PV	YP	MW	Hmc	CFL
0	0	0	12	100	25	40	50	11.6	2	0
5										4
10										6
15										7
20										7.8
25										8.6
30										9.1
0	0	0	56	100	25	44	52	11.6	3	0
5										10.8
10										14.8
15										17.6
20										19.2
25										20.8
30										22
0	0	0	506	100	25	43	55	11.6	4	0
5										16
10										20.8
15										24
20										26.4
25										28.8
30										30.4
0	1	744	12	100	25	39	49	11.6	1	0
5										3.2
10										4.8
15										6
20										6.7

25										7.3
30										7.8
0	1	744	56	100	25	40	51	11.6	3	0
5										9.5
10										13
15										15.5
20										17.5
25										19
30										20
0	1	744	506	100	25	37	48	11.6	3	0
5										13.5
10										18
15										21
20										23.5
25										25.5
30										27
0	2	744	12	100	25	38	49	11.6	1	0
5										2.4
10										4.2
15										5.4
20										6
25										6.6
30										7.2
0	2	744	56	100	25	41	52	11.6	2	0
5										7.8
10										11.4
15										13.8
20										15.6
25										16.8

30										18
0	2	744	506	100	25	39	47	11.6	3	0
5										12
10										17
15										20
20										22.5
25										24.5
30										26
0	4	744	12	100	25	34	48	11.6	1	0
5										1.9
10										3.8
15										5
20										5.6
25										6.3
30										6.9
0	4	744	56	100	25	36	47	11.6	2	0
5										7.5
10										10.5
15										13
20										14.7
25										16
30										17.2
0	4	744	506	100	25	35	45	11.6	3	0
5										10.6
10										16
15										19
20										21.4
25										23.2
30										25

0	1	62	506	100	25	39	49	11.6	3	0
5										11
10										17
15										20
20										22.5
25										25
30										26
0	3	744	56	100	25	36	49	11.6	2	0
5										7.5
10										11
15										13
20										14.8
25										16.2
30										17.5
0	3	62	56	100	25	37	48	11.6	2	0
5										5
10										7
15										8.5
20										9.5
25										10.5
30										11
0	3	1205	56	100	25	40	50	11.6	2	0
5										7
10										10
15										12
20										13.5
25										14.5
30										15
0	3	62	56	70	25	38	48	11.6	1	0

5										3.5
10										5
15										6.2
20										7
25										7.5
30										8
0	3	62	56	130	25	38	50	11.6	2	0
5										7
10										10
15										12
20										13
25										14
30										14.5
0	3	62	56	100	90	26	32	11.6	3	0
5										9
10										14
15										17
20										19.5
25										21.5
30										23
0	3	62	56	100	130	21	25	11.6	3	0
5										11
10										16
15										19
20										22
25										24
30										26
0	3	62	506	100	25	36	46	11.6	3	0
5										10.5

10										16.5
15										20
20										23
25										24.5
30										26
0	3	62	12	100	25	38	49	11.6	1	0
5										3
10										4.2
15										5.2
20										6
25										6.8
30										7.2
0	1	62	56	100	25	33	52	11.6	2	0
5										8
10										12
15										14.5
20										16
25										17
30										18
0	4	62	56	100	25	36	46	11.6	1	0
5										5
10										7
15										8
20										8.8
25										9.5
30										10

Appendix C: Standard API LPLT and HPHT Filter press results for the drilling fluid case 3

Time	NPC	NPS	Perm	DP	Temp	PV	YP	MW	Hmc	CFL
0	0	0	12	130	25	28	13	10.5	1	0
5										2
10										3
15										3.8
20										4.4
25										4.9
30										5.2
0	0	0	56	130	25	30	15	10.5	1	0
5										3.2
10										4.5
15										5.4
20										6
25										6.6
30										7.1
0	0	0	506	130	25	34	12	10.5	1	0
5										4
10										5.5
15										6.4
20										7
25										7.6
30										8.2
0	1	62	12	130	25	31	10	10.5	1	0
5										1.6
10										2.5
15										3.2
20										3.8

25										4.2
30										4.4
0	1	62	56	130	25	28	11	10.5	1	0
5										2.5
10										3.8
15										4.5
20										5.1
25										5.6
30										6
0	1	62	506	130	25	32	9	10.5	1	0
5										3.4
10										4.6
15										5.4
20										6
25										6.6
30										7.2
0	3	62	12	130	25	29	8	10.5	1	0
5										1.4
10										2.2
15										2.8
20										3.4
25										3.8
30										4
0	3	62	56	130	25	26	10	10.5	1	0
5										2
10										3.4
15										4.2
20										4.8
25										5.2

30									5.5
0	3	62	506	130	25	28	9	10.5	1	0
5										2.5
10										4
15										4.8
20										5.4
25										5.9
30										6.4
0	3	1205	12	130	25	29	10	10.5	1	0
5										1.8
10										2.8
15										3.6
20										4.2
25										4.6
30										4.9
0	3	1205	56	130	25	27	8	10.5	1	0
5										2.6
10										4
15										4.8
20										5.4
25										6
30										6.4
0	3	1205	506	130	25	26	10	10.5	1	0
5										3
10										4.5
15										5.2
20										5.8
25										6.4
30										7

0	0	0	12	500	120	30	11	10.5	2	0
5										7.5
10										11
15										14
20										16
25										18
30										19
0	0	0	12	500	120	29	10	10.5	2	0
5										8
10										12
15										14.5
20										16
25										17.5
30										18.5
0	0	0	12	500	93	28	12	10.5	2	0
5										9
10										13
15										16
20										17.5
25										19
30										20
0	1	62	12	500	120	28	9	10.5	2	0
5										6
10										9
15										11.5
20										13.5
25										15
30										16
0	1	62	12	500	120	26	10	10.5	2	0

5									6.5
10									9
15									11
20									12.5
25									14
30									15
0	1	62	12	500	93	25	9	10.5	2	0
5										7
10										9.5
15										12
20										14
25										15.5
30										16.5
0	3	62	12	500	120	26	9	10.5	2	0
5										5
10										7.5
15										9
20										10.5
25										12
30										13
0	3	62	12	500	120	27	8	10.5	2	0
5										5
10										7
15										9.5
20										11
25										12.5
30										13.5
0	3	62	12	500	93	25	8	10.5	2	0
5										5

10									8
15									10
20									11.5
25									13
30									14
0	3	1205	12	500	120	27	7	10.5	0
5									5
10									9
15									12
20									14
25									16
30									17.5
0	3	1205	12	500	120	25	9	10.5	0
5									5
10									9
15									12.5
20									15
25									16
30									17
0	3	1205	12	500	120	27	8	10.5	0
5									5
10									9
15									12.5
20									15
25									16.5
30									17.5
0	0	0	775	500	120	29	9	10.5	0
5									8.4
10									11.2

15										13
20										14.6
25										16
30										17
0	0	0	775	500	120	30	11	10.5	2	0
5										8
10										11
15										12.8
20										14
25										15.2
30										16
0	0	0	775	500	120	31	8	10.5	2	0
5										9
10										13.2
15										14.8
20										16
25										17
30										17.8
0	1	62	775	500	120	27	9	10.5	2	0
5										6
10										9
15										11
20										12.4
25										13.6
30										14.4
0	1	62	775	500	120	28	10	10.5	2	0
5										6
10										8.8
15										10.4

20									11.6
25									12.4
30									13
0	1	62	775	500	120	25	9	10.5	2	0
5										6
10										8.4
15										10.4
20										12
25										13.2
30										14
0	3	62	775	500	120	24	6	10.5	2	0
5										5.6
10										8
15										9.6
20										11
25										12
30										12.4
0	3	62	775	500	120	26	10	10.5	2	0
5										6
10										9.2
15										11
20										12
25										12.8
30										13.2
0	3	62	775	500	120	23	8	10.5	2	0
5										5.6
10										7.6
15										9
20										10.4

25										11.2
30										11.6
0	3	1205	775	500	120	26	5	10.5	2	0
5										7
10										9
15										10.8
20										12.4
25										13.2
30										14
0	3	1205	775	500	120	27	7	10.5	2	0
5										7.2
10										9.6
15										11.2
20										13
25										14
30										14.4
0	3	1205	775	500	120	25	9	10.5	2	0
5										6
10										8
15										9.6
20										11.2
25										12.8
30										13.6
0	3	62	56	100	25	29	8	10.5	1	0
5										1.5
10										2.4
15										3
20										3.6
25										4

30									4.2
0	3	62	12	100	25	27	8	10.5	1	0
5									1.2
10									2
15									2.4
20									2.8
25									3
30									3.1
0	3	62	506	100	25	26	10	10.5	1	0
5									2.8
10									4
15									4.8
20									5.4
25									5.8
30									6
0	1	62	56	100	25	31	10	10.5	1	0
5									2.8
10									4
15									4.6
20									5
25									5.5
30									5.8
0	4	62	56	100	25	30	9	10.5	1	0
5									1.5
10									2.2
15									2.8
20									3.2
25									3.5
30									3.8

0	3	744	56	100	25	26	10	10.5	1	0
5										2.8
10										3.8
15										4.5
20										5
25										5.3
30										5.5
0	3	1205	56	100	25	30	10	10.5	1	0
5										3
10										4.2
15										5
20										5.5
25										6
30										6.2
0	3	62	56	100	90	15	6	10.5	2	0
5										4.8
10										6.8
15										8
20										8.8
25										9.5
30										10
0	3	62	56	100	130	12	5	10.5	2	0
5										6
10										8.5
15										10
20										10.8
25										11.5
30										12
0	3	62	56	70	25	26	10	10.5	1	0

5										1.2
10										1.8
15										2.2
20										2.5
25										2.8
30										3
0	3	62	56	130	25	26	10	10.5	1	0
5										2.6
10										3.8
15										4.6
20										5.1
25										5.5
30										5.8
0	0	NA	12	100	25	32	12	10.5	1	0
5										1.8
10										2.6
15										3.2
20										3.6
25										3.8
30										4
0	0	NA	56	100	25	30	15	10.5	1	0
5										2.8
10										3.8
15										4.6
20										5.2
25										5.6
30										5.8
0	0	NA	56	100	25	34	12	10.5	1	0
5										2.5

10										3.6
15										4.5
20										5
25										5.4
30										5.5
0	0	NA	506	100	25	28	13	10.5	1	0
5										3
10										4.2
15										5
20										5.6
25										6
30										6.3

Appendix D: Filtration test for the drilling fluid case 4

Time	NPC	NPS	Perm	DP	Temp	PV	YP	MW	Hmc	CFL
0	0	0	12	100	25	23	2	10.1	1	0
5										3
10										4.2
15										5
20										5.6
25										6.2
30										6.6
0	0	0	56	100	25	20	5	10.1	1	0
5										3.2
10										4.5
15										5.4
20										6

25										6.5
30										7
0	1.5	62	12	100	25	19	7	10.1	1	0
5										1.7
10										2.8
15										3.7
20										4.4
25										5
30										5.6
0	1.5	62	12	100	25	19	5	10.1	1	0
5										1.8
10										3
15										3.8
20										4.6
25										5.2
30										5.8
0	3	62	12	100	25	17	6	10.1	1	0
5										1.7
10										2.8
15										3.7
20										4.4
25										5
30										5.4
0	3	62	12	100	25	16	7	10.1	1	0
5										1.8
10										3
15										3.8

20										4.6
25										5.2
30										5.6
0	1.5	1205	12	100	25	19	3	10.1	1	0
5										2.5
10										3.7
15										4.5
20										5.2
25										5.8
30										6.2
0	3	1205	12	100	25	18	5	10.1	1	0
5										2
10										3
15										3.9
20										4.7
25										5.2
30										5.6
0	3	62	56	100	25	20	3	10.1	1	0
5										4.2
10										6
15										7.2
20										8
25										8.6
30										9
0	3	744	56	100	25	19	2	10.1	2	0
5										5.5
10										7.5

15										9
20										10.5
25										11.4
30										12
0	3	1205	56	100	25	18	4	10.1	2	0
5										6
10										8.5
15										10
20										11
25										12
30										13
0	3	62	56	70	25	16	6	10.1	1	0
5										3.2
10										4.2
15										5
20										5.6
25										6.2
30										6.5
0	3	62	56	130	25	19	2	10.1	2	0
5										5.5
10										7.5
15										9
20										10
25										11
30										12
0	3	62	56	100	90	12	3	10.1	2	0
5										6.5

10										9
15										11
20										12
25										13
30										14
0	3	62	56	100	130	11	2	10.1	2	0
5										7.5
10										10
15										12.5
20										14
25										15
30										16
0	1	62	56	100	25	19	5	10.1	2	0
5										5
10										7
15										8.5
20										9.5
25										10.4
30										11
0	4	62	56	100	25	17	6	10.1	1	0
5										4
10										5.2
15										6.2
20										7
25										7.6
30										8
0	3	62	506	100	25	18	5	10.1	2	0

5										7
10										9.5
15										11
20										12
25										13
30										14

Appendix E: SAS file to analyze the data

```
data dataset;

/*Importing data from Excel file*/
proc import out=dataset
datafile='C:\Users\Sakhta\Desktop\dataset.xlsx'
dbms=excel replace;
run;

proc print data=dataset;
run;

* Descriptive Statistics;
proc means data = dataset;
var Time NPC NPS Perm DP Temp Area PV YP MW Hmc FLR;
run;

* Detailed descriptive Statistics;
proc univariate data = dataset
run;

* Correlations;
proc corr data = dataset;
var Time NPC NPS Perm DP Temp Area PV YP Mw Hmc FLR;
run;

*multiple linear regression;
proc reg data = dataset;
model  FLR = Time NPC NPS Perm DP Temp Area PV YP MW Hmc;
run;

* Robust Regression;
proc reg data = dataset;
  model FLR = Time NPC NPS Perm DP Temp Area PV YP MW Hmc;
  output out = t student=res cookd = cookd h = lev;
run;


data t; set t;
  resid_sq = res*res;
run;

proc sgplot data = t;
  scatter y = lev x = resid_sq / datalabel = FLR;
run;

data t2; set t;
  rabs = abs(res);
run;
```

```
proc sort data  = t2;
 by descending rabs;
run;

proc print data = t2 (obs=20);
run;

proc robustreg data=t2 method=m (wf=huber) ;
  model FLR = Time Npc Nps Perm DP Temp Area PV YP MW Hmc;
  output out = t3 weight=wgt;
run;
```

Appendix F: Differential evolution FLR, NPC, NPS, SG

```
clc
clear

NumOfVar = 4;
Dim=NumOfVar+1;
SwarmNum = 1000;
CR=0.85;
F=0.95;
Iteration = 1000;
load oscar

RandMat = rand(NumOfVar,SwarmNum);
Inipoints = zeros(NumOfVar,SwarmNum);

%%
%Variables ranges
%aa1
VarL(1)=-1000;VarU(1)=+1000;
%aa2
VarL(2)=0;VarU(2)=5;
%aa3
VarL(3)=0;VarU(3)=+4;
%aa4
VarL(4)=0;VarU(4)=+4;

%%
% initialization

aa1=size(1,SwarmNum);
aa2=size(1,SwarmNum);
aa3=size(1,SwarmNum);
aa4=size(1,SwarmNum);


for i=1:SwarmNum
```

```
   aa1(1,i)=rand*(VarU(1)-VarL(1))+VarL(1);
   aa2(1,i)=rand*(VarU(2)-VarL(2))+VarL(2);
   aa3(1,i)=rand*(VarU(3)-VarL(3))+VarL(3);
   aa4(1,i)=rand*(VarU(4)-VarL(4))+VarL(4);


end



%%Calc 1th Evaluate the constrains, conditions/Calculating the objF
fitness=size(1,SwarmNum);


 n(1,1)=aa1(1,1);
 n(2,1)=aa2(1,1);
 n(3,1)=aa3(1,1);
 n(4,1)=aa4(1,1);


 for i=1:SwarmNum

        fitness(i)=os1(aa1(1,i),aa2(1,i),aa3(1,i),aa4(1,i));

end

% y=randperm(SwarmNum);


inipoints(1,1:SwarmNum)=aa1(1,1:SwarmNum);
inipoints(2,1:SwarmNum)=aa2(1,1:SwarmNum);
inipoints(3,1:SwarmNum)=aa3(1,1:SwarmNum);
inipoints(4,1:SwarmNum)=aa4(1,1:SwarmNum);


inipoints(5,1:SwarmNum)=fitness(1,1:SwarmNum);




for ami=1:iteration
Y=zeros(3,SwarmNum);

for i=1:SwarmNum

    y1=round(rand*(SwarmNum-1)+1);
    y2=round(rand*(SwarmNum-1)+1);
    y3=round(rand*(SwarmNum-1)+1);

    while y1==i
        y1=round(rand*(SwarmNum-1)+1);
```

```
    end

    while y2==i | y2==y1
        y2=round(rand*(SwarmNum-1)+1);
    end

     while y3==i | y3==y1 | y3==y2
        y3=round(rand*(SwarmNum-1)+1);
     end

    Y(1,i)=y1;
    Y(2,i)=y2;
    Y(3,i)=y3;


end


WDV=size(3,SwarmNum);
for i=1:SwarmNum

    WDV(1,i)=(inipoints(1,Y(1,i))-inipoints(1,Y(2,i)))*F;
    WDV(2,i)=(inipoints(2,Y(1,i))-inipoints(2,Y(2,i)))*F;
    WDV(3,i)=(inipoints(3,Y(1,i))-inipoints(3,Y(2,i)))*F;
    WDV(4,i)=(inipoints(4,Y(1,i))-inipoints(4,Y(2,i)))*F;


end


NRV=size(3,SwarmNum);
for i=1:SwarmNum

    NRV(1,i)=(WDV(1,i)+inipoints(1,Y(3,i)));
    NRV(2,i)=(WDV(2,i)+inipoints(2,Y(3,i)));
    NRV(3,i)=(WDV(3,i)+inipoints(3,Y(3,i)));
    NRV(4,i)=(WDV(4,i)+inipoints(4,Y(3,i)));



end


TV=size(NumOfVar,SwarmNum);

for j=1:SwarmNum
    for i=1:NumOfVar
        a=rand;

    if a<CR
       TV(i,j)=NRV(i,j);
    else
```

```
        TV(i,j)=inipoints(i,j);

    end

    end
end
%%
%Filter TV by taking the upper and lowwer boundries into account

for i=1:SwarmNum

    if TV(1,i)<VarL(1)

        TV(1,i)=VarL(1);
    end

    if TV(1,i)>VarU(1)
        TV(1,i)=VarU(1);
    end

end

for i=1:SwarmNum

    if TV(2,i)<VarL(2)
        TV(2,i)=VarL(2);
    elseif TV(2,i)>VarU(2)
        TV(2,i)=VarU(2);
    end

end

for i=1:SwarmNum

    if TV(3,i)<VarL(3)
        TV(3,i)=VarL(3);
    elseif TV(3,i)>VarU(3)
        TV(3,i)=VarU(3);
    end

end

for i=1:SwarmNum

    if TV(4,i)<VarL(4)
        TV(4,i)=VarL(4);
    elseif TV(4,i)>VarU(4)
        TV(4,i)=VarU(4);
    end

end
```

```
%%
%calc
for i=1:SwarmNum

    %TV(3,i)=tan(sin(TV(1,i))*cos(TV(2,i)));
    TV(5,i)=os1(TV(1,i),TV(2,i),TV(3,i),TV(4,i));
end
%%
%replace if TV is better than inipoints

for i=1:SwarmNum

   if TV(5,i)<inipoints(5,i)
       inipoints(1:5,i)=TV(1:5,i);
   end

end
%%
%best global
subplot(3,3,1);
plot(inipoints(1,:))
xlabel ('Swarm Num')
ylabel ('a')
subplot(3,3,2);
plot(inipoints(2,:))
xlabel ('Swarm Num')
ylabel ('b')
subplot(3,3,3);
plot(inipoints(3,:))
xlabel ('Swarm Num')
ylabel ('c')
subplot(3,3,4);
plot(inipoints(4,:))
xlabel ('Swarm Num')
ylabel ('d')

BG(ami,1)=min(inipoints(5,1:SwarmNum));
subplot(3,3,5);
plot(BG)
xlabel ('Iteration num')
ylabel ('fittness=MSE')
pause(0.00001)


for j=1:SwarmNum


    if inipoints(5,j)==BG(ami,1)

       s=0;

       for i=1:42
```

```
data(i,14)=((inipoints(1,j)*((data(i,10)/8.33)^inipoints(2,j))*(data(i,
11)/data(i,3))^inipoints(3,j))*(data(i,1)^inipoints(4,j)));


        end

        j=SwarmNum;
        Bset(1:4,1)=inipoints(1:4,j);

    end


end



subplot(3,3,6);
plot(1:42,data(:,13))
hold on
plot(1:42,data(:,14))
hold off

xlabel ('data comparing')
ylabel ('Predicted  (%)')


Bset

BG(ami,1)
end






function o = os1(t1,t2,t3,t4)

load oscar
o=0;

for i=1:42


o=(((t1*((data(i,10)/8.33)^t2)*(data(i,11)/data(i,3))^t3)*(data(i,1)^t4
))-data(i,13))^2+o;

end


end
```

Differential evolution FLR, K and Pfb- MATLAB

```
clc
clear

NumOfVar=4;
Dim=NumOfVar+1;
SwarmNum=100;
CR=0.85;
F=0.95;
iteration=1000;
load oscar


RandMat=rand(NumOfVar,SwarmNum);
inipoints=zeros(NumOfVar,SwarmNum);

% Variables ranges
%aa1
VarL(1)=1;VarU(1)=50;
%aa2
VarL(2)=0.5;VarU(2)=5;
%aa3
VarL(3)=0;VarU(3)=2;
%aa4
VarL(4)=0;VarU(4)=1;



% Initialization

aa1=size(1,SwarmNum);
aa2=size(1,SwarmNum);
aa3=size(1,SwarmNum);
aa4=size(1,SwarmNum);

for i=1:SwarmNum

  aa1(1,i)=rand*(VarU(1)-VarL(1))+VarL(1);
  aa2(1,i)=rand*(VarU(2)-VarL(2))+VarL(2);
  aa3(1,i)=rand*(VarU(3)-VarL(3))+VarL(3);
  aa4(1,i)=rand*(VarU(4)-VarL(4))+VarL(4);


end
```

```
%% Fitness
fitness=size(1,SwarmNum);
  n(1,1)=aa1(1,1);
 n(2,1)=aa2(1,1);
 n(3,1)=aa3(1,1);
 n(4,1)=aa4(1,1);

for i=1:SwarmNum

    fitness(i)=os1(aa1(1,i),aa2(1,i),aa3(1,i),aa4(1,i));

end



inipoints(1,1:SwarmNum)=aa1(1,1:SwarmNum);
inipoints(2,1:SwarmNum)=aa2(1,1:SwarmNum);
inipoints(3,1:SwarmNum)=aa3(1,1:SwarmNum);
inipoints(4,1:SwarmNum)=aa4(1,1:SwarmNum);

inipoints(5,1:SwarmNum)=fitness(1,1:SwarmNum);


for ami=1:iteration
Y=zeros(3,SwarmNum);

for i=1:SwarmNum

    y1=round(rand*(SwarmNum-1)+1);
    y2=round(rand*(SwarmNum-1)+1);
    y3=round(rand*(SwarmNum-1)+1);

    while y1==i
        y1=round(rand*(SwarmNum-1)+1);
    end

    while y2==i | y2==y1
        y2=round(rand*(SwarmNum-1)+1);
    end

     while y3==i | y3==y1 | y3==y2
        y3=round(rand*(SwarmNum-1)+1);
     end

    Y(1,i)=y1;
    Y(2,i)=y2;
    Y(3,i)=y3;


end
```

```
WDV=size(3,SwarmNum);
for i=1:SwarmNum

   WDV(1,i)=(inipoints(1,Y(1,i))-inipoints(1,Y(2,i)))*F;
   WDV(2,i)=(inipoints(2,Y(1,i))-inipoints(2,Y(2,i)))*F;
   WDV(3,i)=(inipoints(3,Y(1,i))-inipoints(3,Y(2,i)))*F;
   WDV(4,i)=(inipoints(4,Y(1,i))-inipoints(4,Y(2,i)))*F;


end


NRV=size(3,SwarmNum);
for i=1:SwarmNum

   NRV(1,i)=(WDV(1,i)+inipoints(1,Y(3,i)));
   NRV(2,i)=(WDV(2,i)+inipoints(2,Y(3,i)));
   NRV(3,i)=(WDV(3,i)+inipoints(3,Y(3,i)));
   NRV(4,i)=(WDV(4,i)+inipoints(4,Y(3,i)));

end


TV=size(NumOfVar,SwarmNum);

for j=1:SwarmNum
   for i=1:NumOfVar
      a=rand;

   if a<CR
     TV(i,j)=NRV(i,j);
   else
     TV(i,j)=inipoints(i,j);

   end

   end
end


%Filter TV by taking the upper and lower boundaries into account

for i=1:SwarmNum

   if TV(1,i)<VarL(1)

     TV(1,i)=VarL(1);
   end

   if TV(1,i)>VarU(1)
```

```
      TV(1,i)=VarU(1);
   end

end

for i=1:SwarmNum

   if TV(2,i)<VarL(2)
      TV(2,i)=VarL(2);
   elseif TV(2,i)>VarU(2)
      TV(2,i)=VarU(2);
   end

end

for i=1:SwarmNum

   if TV(3,i)<VarL(3)
      TV(3,i)=VarL(3);
   elseif TV(3,i)>VarU(3)
      TV(3,i)=VarU(3);
   end

end

for i=1:SwarmNum

   if TV(4,i)<VarL(4)
      TV(4,i)=VarL(4);
   elseif TV(4,i)>VarU(4)
      TV(4,i)=VarU(4);
   end

end



%calc
for i=1:SwarmNum


   TV(5,i)=os1(TV(1,i),TV(2,i),TV(3,i),TV(4,i));
end

%replace if TV is better than inipoints

for i=1:SwarmNum

  if TV(5,i)<inipoints(5,i)
     inipoints(1:5,i)=TV(1:5,i);
  end
```

```
end
%%
%best global
subplot(3,3,1);
plot(inipoints(1,:))
xlabel ('Swarm Num')
ylabel ('a1')
subplot(3,3,2);
plot(inipoints(2,:))
xlabel ('Swarm Num')
ylabel ('a2')
subplot(3,3,3);
plot(inipoints(3,:))
xlabel ('Swarm Num')
ylabel ('a3')


BG(ami,1)=min(inipoints(5,1:SwarmNum));
subplot(3,3,5);
plot(BG)
xlabel ('Iteration num')
ylabel ('fittness=MSE')
pause(0.00001)

for j=1:SwarmNum

   if inipoints(5,j)==BG(ami,1)

      s=0;

      for i=1:11

         data(i,4)=(inipoints(1,j)*(data(i,1)^inipoints(2,j)))*...
        (data(i,2)^inipoints(3,j))+inipoints(4,j);

      end

      j=SwarmNum;
      Bset(1:4,1)=inipoints(1:4,j);

  end


end

subplot(3,3,6);
plot(1:11,data(:,3))
hold on
plot(1:11,data(:,4))
hold off
```

```
xlabel ('data comparing')
ylabel ('P_f_b Increase (%)')



Bset

BG(ami,1)
end
```

VITA

Saman Akhtarmanesh

Candidate for the Degree of

Doctor of Philosophy

Dissertation: IMPROVING PERFORMANCE OF WATER-BASED DRILLING FLUID BY OPTIMIZATION OF BARITE NANOPARTICLE SIZE AND CONCENTRATION

Major Field: Chemical Engineering

Biographical:

Education:

Completed the requirements for the Doctor of Philosophy in Chemical Engineering at Oklahoma State University, Stillwater, Oklahoma in May, 2018.

Completed the requirements for the Master of Science in Drilling and Production Engineering at Amirkabir University of Technology, Tehran, Iran in 2012.

Completed the requirements for the Bachelor of Science in Petroleum Engineering at Amirkabir University of Technology, Tehran, Iran in 2009.

Experience:

Professional Memberships: